US Army Corps of Engineers®
Engineer Research and Development Center

Coastal and Hydraulics Laboratory

Numerical Model Study of Potential Salinity Impacts Due to Proposed Navigation Improvements to the Sabine-Neches Waterway, TX

Volume 1: DRAFT Report

Gary L. Brown and Janelle Stokes

December 2009

Preface

As part of the continuing studies of the Sabine-Neches Waterway, TX, The U.S. Army Engineer District, Galveston (SWG), requested the U.S. Army Engineer Research and Development Center, Waterways Experiment Station (ERDC-WES) to perform a numerical model study of circulation and salinity impacts resulting from modification of the Sabine-Neches Waterway (SNWW) in Texas. The study included development of a two- and three-dimensional (3D) model of the system, validating the model, and performing long-term simulations of impacts due to different deepening and widening plans.

The Galveston District provided funding for this study. Mr. Gary Brown served as principal investigator of the project. Technical assistance and oversight was given by R. C. Berger and Joe Letter. The Hydraulic Analysis Group of CHL, led by Mr. Tim Fagerburg, undertook the field data collection efforts. Ms. Janelle Stokes, Mr. Baldev Mann provided pertinent data available at the Galveston District and the Modeling Workgroup of the SNWW Interagency Coordination Team (ICT) provided additional information on the study area.

The study was conducted under general supervision of Dr. Robert T. McAdory, Chief of the Estuarine Engineering Branch, and Mr. Thomas W. Richardson, Director, CHL.

At the time of this publication, Dr. James R. Houston was Director of ERDC, and COL Gary E. Johnston was Commander and Executive Director.

Table of Contents

INTRODUCTION **1**

BACKGROUND AND PROBLEM STATEMENT **1**
OVERVIEW OF CIRCULATION AND SALINITY IN THE SNWW **3**
OBJECTIVE AND APPROACH **3**

NUMERICAL MODEL DESCRIPTION **4**

FIELD DATA COLLECTION AND ANALYSIS **4**
HYDRODYNAMIC AND SALINITY MODELS **5**
Computational Mesh *5*
Mean Low Tide (MLT), ft *8*
Mean Lower Low Water (MLLW), ft *8*
NAVD 88, ft *8*
Boundary Conditions *9*
Vertical datum shift (ft) *10*

CALIBRATION AND VERIFICATION **17**

MODEL CALIBRATION **17**
MODEL VERIFICATION **17**
Water Surface Elevation Data *18*
ADCP Discharge Data *20*
Velocity Data *22*
Salinity Data *24*

MODEL ANALYSIS OF THE IMPACTS OF RELATIVE SEA LEVEL RISE AND PROPOSED CHANNEL DEEPENING **29**

DESCRIPTION OF THE "MOST LIKELY" RELATIVE SEA LEVEL RISE **29**
DESCRIPTION OF PROPOSED CHANNEL DEEPENING **30**
BOUNDARY CONDITIONS FOR ANALYSIS OF CHANNEL DEEPENING IMPACTS **31**
Salinity *31*
RESULTS: EFFECTS OF RELATIVE SEA LEVEL RISE **35**
Water Surface Elevation *35*
Salinity *35*
RESULTS: EFFECTS OF 48' CHANNEL IMPLEMENTATION **39**
Water Surface Elevation *39*
Salinity *39*
RESULTS: EFFECTS OF 45' CHANNEL IMPLEMENTATION **44**

MODEL ANALYSIS OF PROPOSED SALINITY MITIGATION ALTERNATIVES **53**

DESCRIPTION OF PROPOSED SALINITY MITIGATION ALTERNATIVES **53**
MODELING APPROACH: TABS-MDS AND DOWSMM **55**
RESULTS **56**
TABS-MDS results: General Observations *56*
Habitat Salinity Analysis *57*

CONCLUSIONS **60**

REFERENCES **63**

APPENDIX A TABS-MDS DESCRIPTION

APPENDIX B WATER SURFACE ELEVATION AND SALINITY RESULTS

APPENDIX C DREDGING ANALYSIS

Introduction

Background and Problem Statement

The Sabine-Neches Waterway is located on the border of Texas and Louisiana. The system consists of 6 major hydraulically significant features:

1) Sabine Pass, an artificially enlarged channel dredged between Sabine Lake and the Gulf of Mexico

2) The Sabine-Neches Canal and Port Arthur Canal, the artificial shipping channels dredged along the western shore of Sabine Lake, to link the Neches and Sabine Canals to Sabine Pass, and to provide shipping access for the ports of Port Arthur, Beaumont and Orange, Texas.

3) The Gulf Intracoastal Waterway (GIWW), which traverses the system and links it hydraulically with the Calcasieu Lake on the East, and Galveston Bay on the west.

4) The Sabine River, which empties into Sabine Pass via Sabine Lake and the Sabine – Neches Waterway

5) The Neches river, which empties into Sabine pass via Sabine Lake and the Sabine – Neches Waterway

6) Sabine Lake, a large, shallow (approximately 8 feet deep) estuary, receiving fresh water from the Sabine and Neches rivers, and salt water from Sabine Pass.

In addition, there are several sensitive and extensive wetland habitats within the system, including the Sabine National Wildlife Refuge, and McFaddin National Wildlife Refuge.

Figure 1 is a location map of the system..

Figure 1: Location Map

Overview of Circulation and Salinity in the SNWW

The SNWW system exhibits very complicated circulation and salinity patterns. Fresh water enters the system via several tributaries, including the Sabine River, the Neches River, and other smaller inflows. The Neches River flows directly into Sabine Lake and the Sabine –Neches Canal, whereas the Sabine River flows into Sabine Lake, the Sabine-Neches Wildlife Refuge, and into Calcasieu Lake via the GIWW.

The Sabine Neches canal acts as a flow pathway for both fresh water from the inflowing rivers, and saline water intruding via tidal propagation through Sabine Pass. This combination results in highly stratified conditions in the Sabine-Neches canal. This stratification contributes to salt water intrusion migrating up the Sabine-Neches canal and into the northwest corner of Sabine Lake and the lower reaches of the Neches River.

As a result of this intrusion, the observed salinity in Sabine Lake is highest at both the southern end (where the lake connects to Sabine Pass) and at the northern end (where the lake connects to the Sabine-Neches canal). The lowest salinities are observed in the central and eastern portions of the lake, which are furthest from the hydraulic connection to sources of saline water.

Objective and Approach

This report details the development of a numerical model hydrodynamics and salinity in the Sabine-Neches waterway. The development and validation of the model are detailed, and the results of the model evaluation of salinity impacts due to proposed navigation improvements are presented.

The tasks performed and described by this report are:

a. Development of a three-dimensional numerical model.
b. Validation of the model for hydrodynamics and salinity using field data gathered for this undertaking,
c. Evaluation of proposed plan conditions.
d. Comparison and analysis of results.

Numerical Model Description

The TABS-MDS code of ERDC-WES is used for computing hydrodynamics, plus salinity and sediment transport. The model was originally developed as RMA10 by Resource Management Associates (King, 1993) and extensively modified by ERDC-WES staff into its present configuration. In agreement with the original author, the ERDC version of the code was given the name TABS-MDS to distinguish it from RMA10. It is a finite element model, which gives it great flexibility in matching complex geometry. Through the solution of equations of conservation of mass and horizontal momentum, as well as the convective-diffusion equation for transport of salinity and heat, the code accounts for forcing due to tides, freshwater inflows, wind, Coriolis effects (where applicable), and density gradients due to salinity and temperature. It also considers evaporation and precipitation to complete an accurate description of the system under study. For further discussion of TABS-MDS, see Appendix A.

ERDC-WES personnel have used the code extensively over the last decade in a variety of field investigations with excellent results. Its proven effectiveness makes it well suited for this application.

Field Data Collection and Analysis

A numerical hydrodynamic and transport model requires adequate field data to perform calibration and verification of the model. For this study, the Hydraulic Analysis Group of CHL performed an intensive data collection effort. These data include time-series observations of the following parameters:

- 16 tide observation locations
- 16 salinity observation locations
- 10 velocity observation locations
- 10 Acoustic Doppler Current Profiler (ADCP) 25-hour flow transects

The time-series data were collected between 16 May, 2001, and 10 January, 2002. The full data report is given in Fagerburg, et. al. (2001). The locations of the time-series data are given in Figure 2.

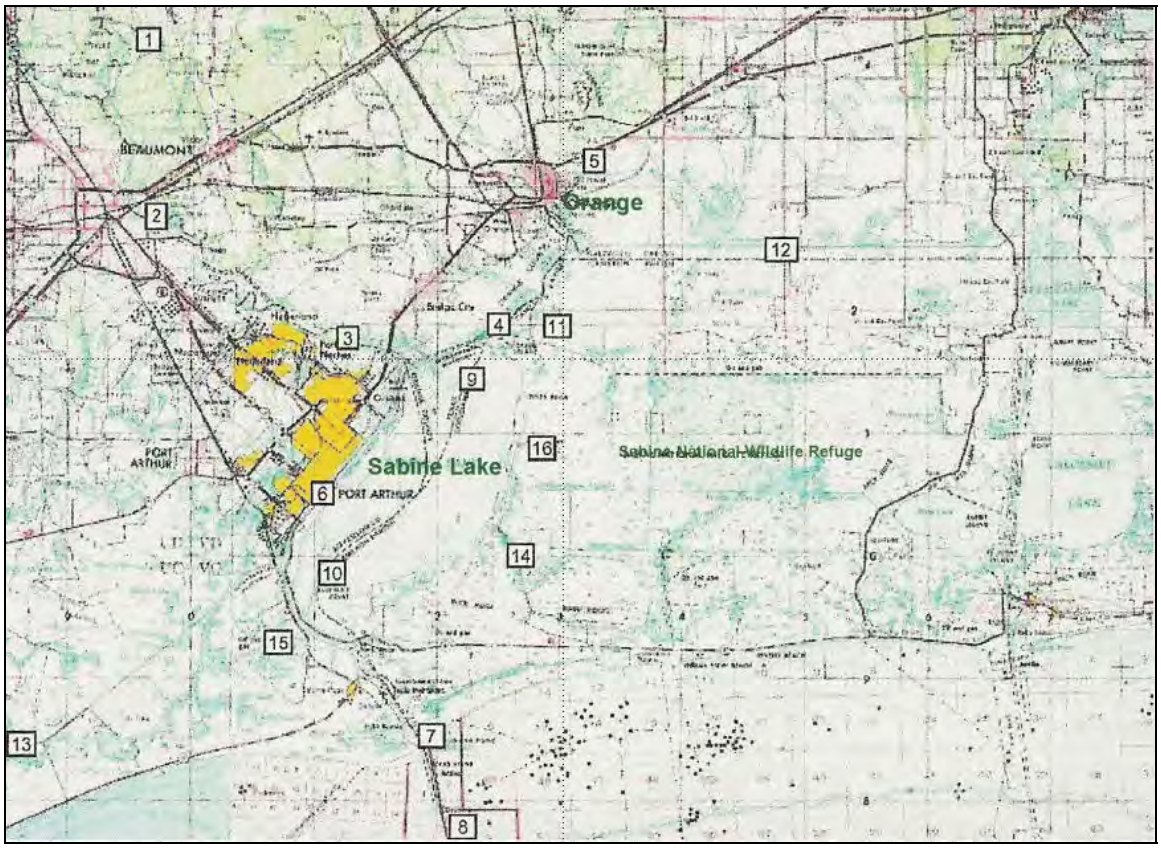

Figure 2: Instrument Location Map

Hydrodynamic and Salinity Models

Computational Mesh

The TABS-MDS code uses a computational mesh, as a mathematical representation of the physical environment under study. A mesh typically includes information on the shoreline geometry, the bathymetric features, and the bottom-type characteristics of the area involved. The extents of the model domain are given as follows:

- North to the Neches River at Evadale, TX, and the Sabine River at Ruliff, TX.
- East to a point approximately mid-way between the Sabine Lake and Calcasieu Lake, including approximately half of the Sabine-Neches Wildlife Refuge
- South approximately 55 miles into the Gulf of Mexico from the Gulf shoreline.
- West to a point approximately mid-way between Sabine Lake and Galveston Bay, including all of the McFaddin National Wildlife Refuge

The model mesh is given in Figure 3. It contains 33,321 surface nodes and 13,035 surface elements.

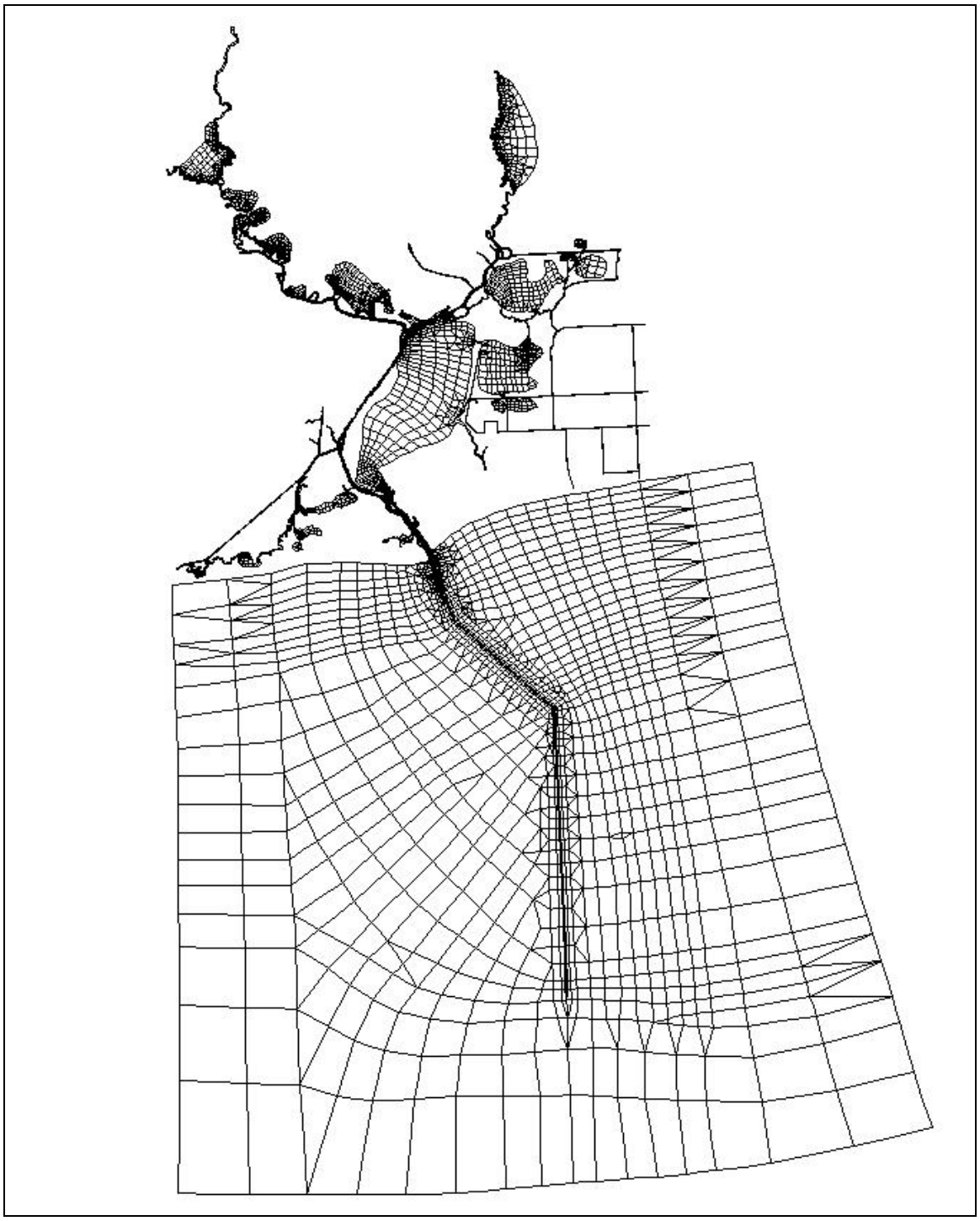

Figure 3: Model Mesh

The model mesh is assigned 3D resolution in all of the navigation channels and in Sabine Lake. This allows the model to simulate baroclinic forcing due to the density difference between salt water and fresh water. This resolution adds a significant computation burden to the model. The number of nodes and elements in the model with the 3D resolution included is 132,393 and 45,915, respectively.

The delineation of the shoreline in the model was accomplished with the use of National Oceanic and Atmospheric Administration (NOAA) charts, USGS Quad sheets, and of georeferenced satellite imagery provided by SWG. The bathymetry was taken from a variety of sources. Initially, the bathymetric data were taken from the NOAA charts of the region. The navigation channel bathymetry were taken from a comprehensive bathymetric survey provided by SWG. Additional bathymetric data was collected by SWG to confirm the accuracy of the bathymetric values taken from the NOAA charts for Sabine Lake.

The bathymetric data is given as Mean Low Tide (MLT). Table 1 gives the relationship between this datum and other commonly used datums, at Sabine Pass, TX.

Table 1. Referencing Table for Different Datums for Sabine Pass, Texas*

Mean Low Tide (MLT), ft		Mean Lower Low Water (MLLW), ft		NAVD 88, ft
0.0	=	-0.36	=	-0.78
0.36	=	0.0	=	-0.42
0.78	=	0.42	=	0.0
1.0	=	0.64	=	0.22
2.0	=	1.64	=	1.22
3.0	=	2.64	=	2.22
4.0	=	3.64	=	3.22

* This table provides the best estimate of equal elevations at the three datums but the relationships between the datums have not been fully field-verified.

Boundary Conditions

The applied boundary conditions and the data sources for each boundary condition are given in Figure 4.

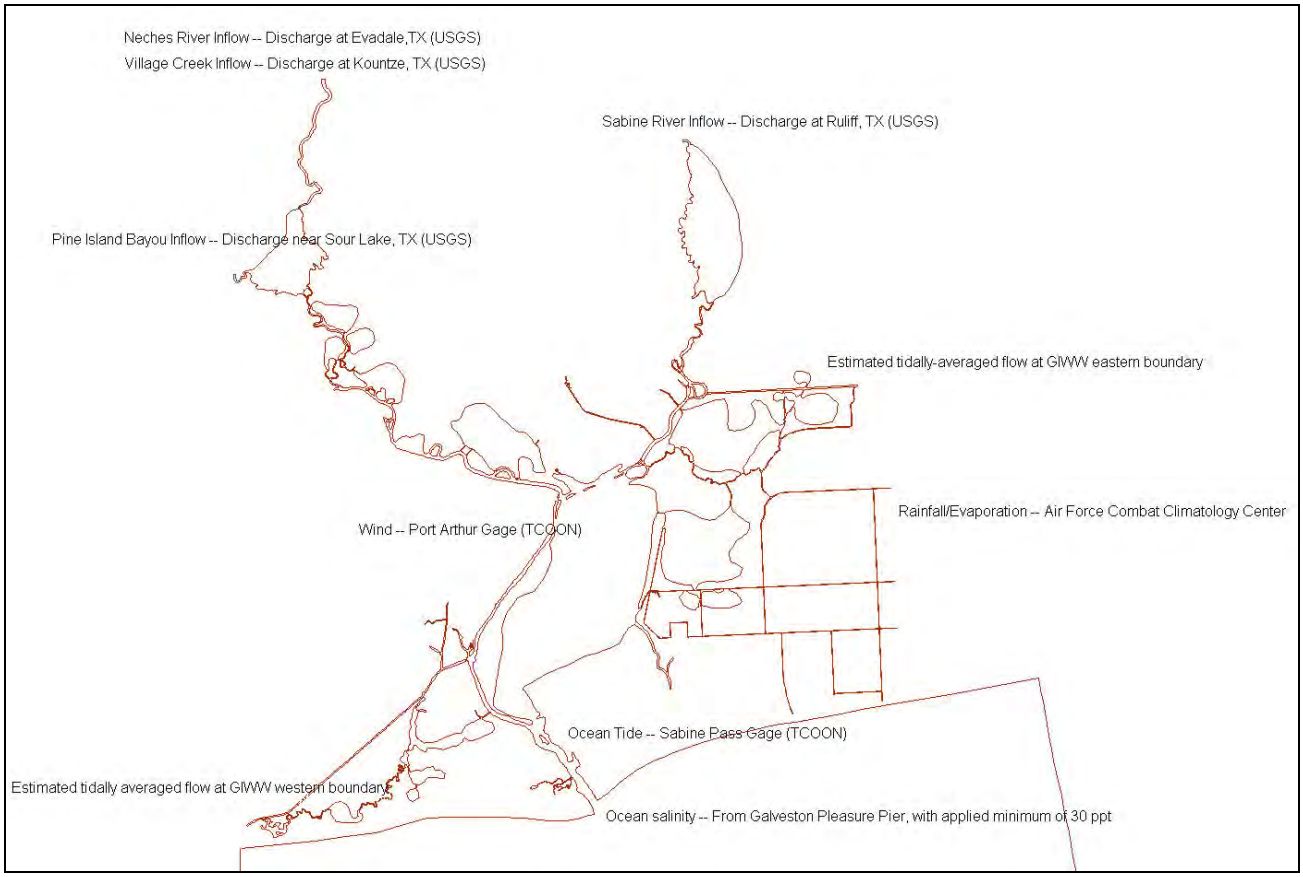

Figure 4: Applied Boundary Conditions

Ocean Tide – The tidal boundary condition applied at the ocean boundary was extrapolated from the observed tide at Sabine Pass. Since the tidal signal transforms dramatically between the offshore and Sabine Pass (due to nonlinear frictional effects) it was necessary to adjust the observed tidal signal such that the applied signal transformed into the observed signal at Sabine Pass as it propagated from the offshore inland. The signal was transformed by first decomposing it into several frequency bands (these bands were chosen to correspond roughly with the major tidal harmonic components), and then by adjusting the amplification factor and tidal plane adjustment of each frequency band consistent with observations of the model results. That is, model tides were extracted at both the offshore boundary and at Sabine Pass, the signals were decomposed, and the adjustment factors between each location were observed. These were applied to the model boundary, and the process was repeated until no further adjustment was required. The final adjustments are given in Table 2. A sample of the applied boundary tidal signal and the observed tidal signal as it propagates across the Sabine Pass gage are given in Figure 5.

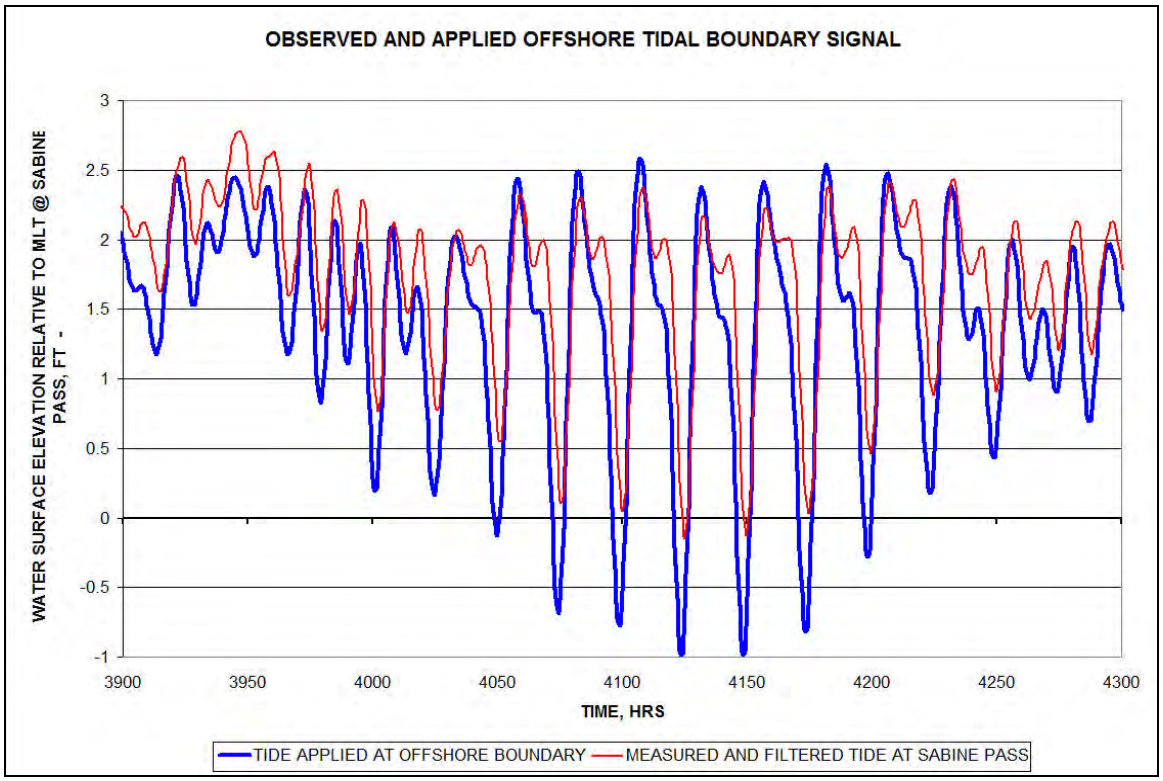

Figure 5: Observed and Applied Tidal Boundary

Table 2. Tidal boundary condition adjustment factors

Frequency Band (hrs)	Vertical datum shift (ft)	Phase shift (hrs)	Tidal amplitude multiplication factor
0-8	0.43	-1.0	0
8-16	0.43	-1.0	1.2
16-30	0.43	-1.0	1.5
>30	0.43	-1.0	1

Ocean Salinity – The salinity at the ocean boundaries was taken from the 30-year, monthly averaged salinity, measured offshore at Galveston, TX (Cochrane and Kelly, 1986). These salinities reflect the seasonal variability in near shore salinity along the Texas coast, influenced in large part by the Mississippi River. The salinity was adjusted such that the minimum applied salinity was 30 ppt. This adjustment was made because the model boundary is sufficiently far offshore (approximately 60 miles) that consistent salinity below 30 ppt is unlikely to occur. The applied ocean salinity is given in Figure 6.

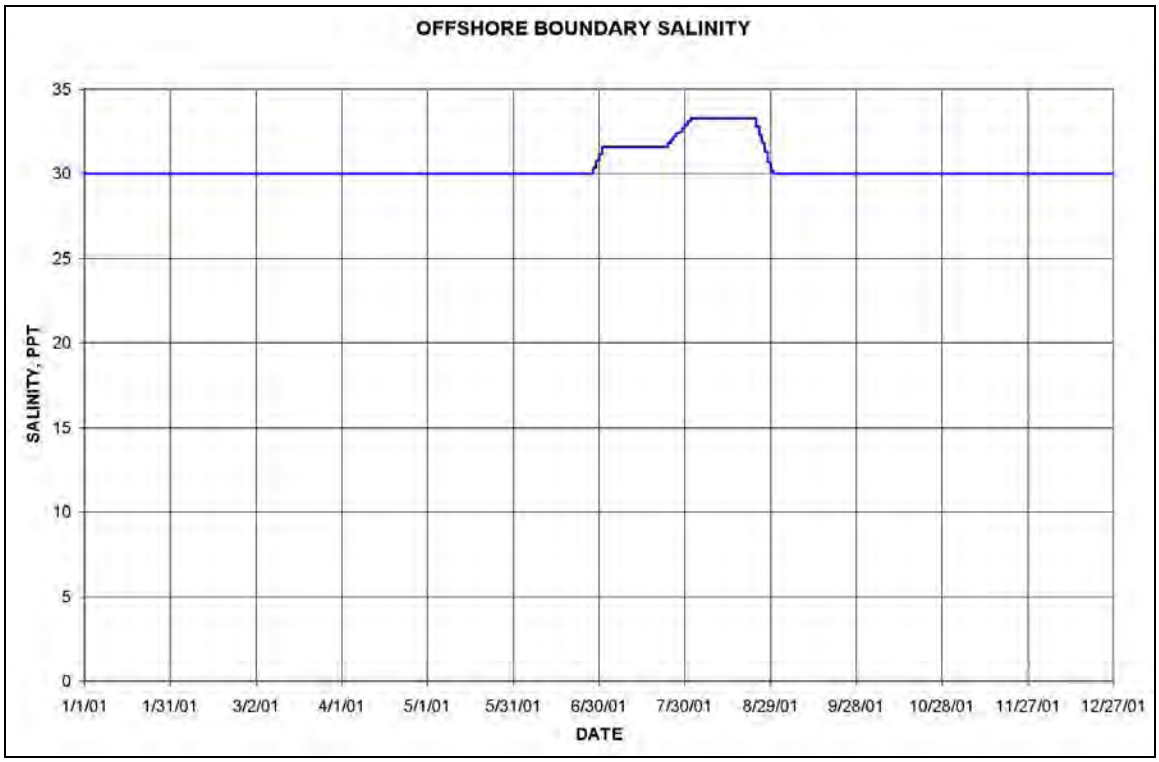

Figure 6: Applied Offshore Salt Boundary Condition

Wind – Hourly wind data were taken from the TCOON station at Port Arthur, TX. These were applied throughout the model domain. A plot of the applied wind magnitude and direction are given in Figure 7.

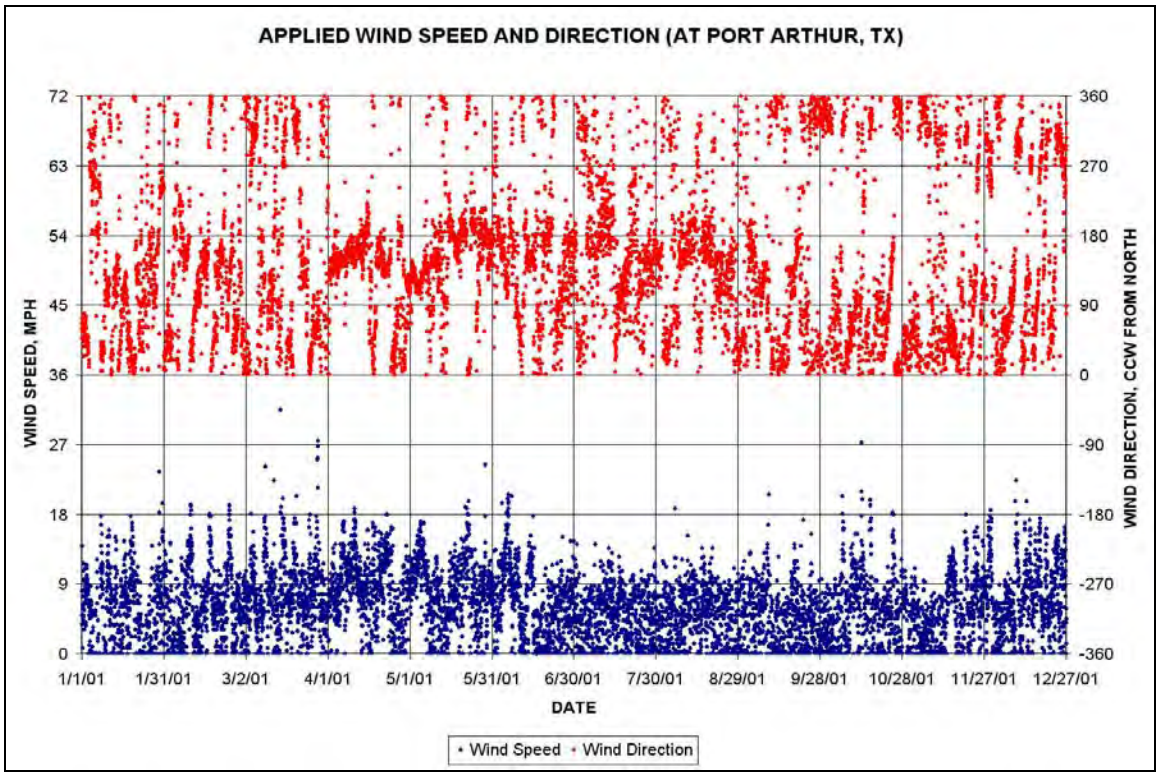

Figure 7: Applied Wind Speed and Direction

<u>Rainfall and evaporation</u> – Daily rainfall and evaporation values were taken from the Air Force Combat Climatology Center. These were applied throughout the model domain. The applied net precipitation (rainfall minus evaporation) is given in Figure 8.

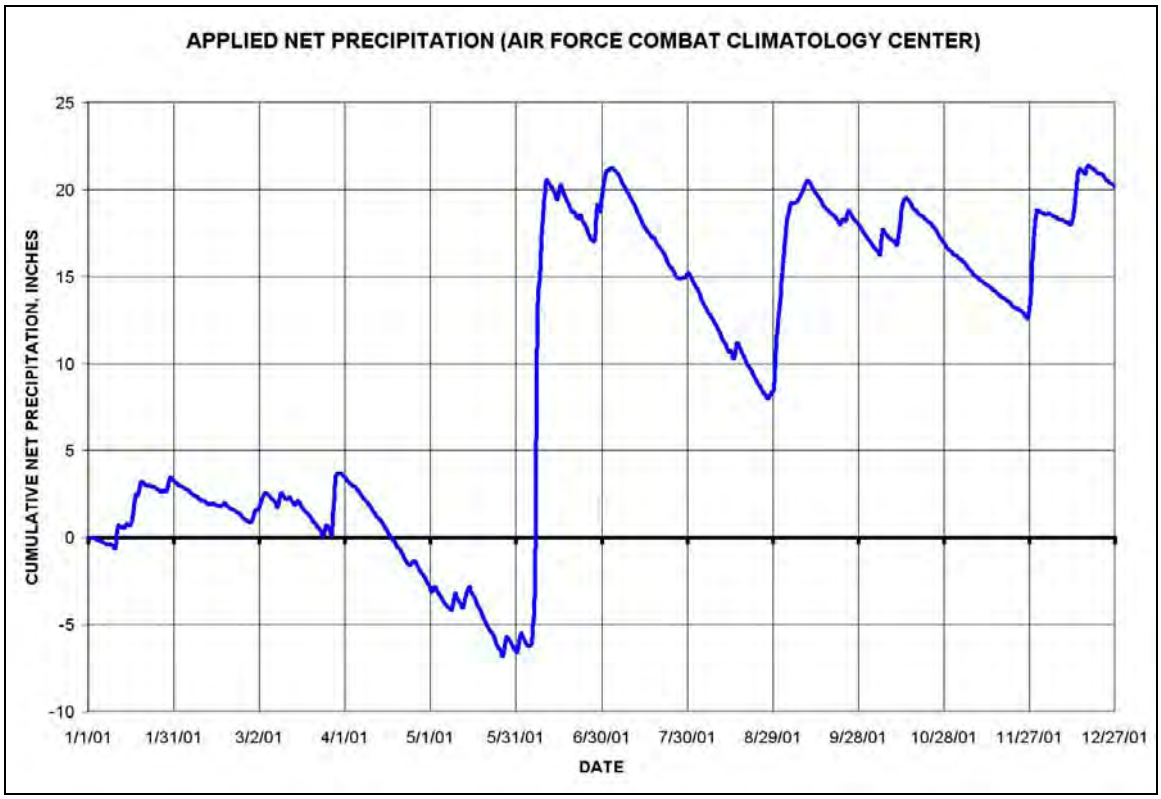

Figure 8: Applied Net Precipitation

River inflows – Daily river inflows for the 4 major freshwater sources to the system (The Sabine River, the Neches River, Village Creek, and Pine Island Bayou) were taken from USGS observations. The time series of these inflows for the model simulation period are given in Figure 9.

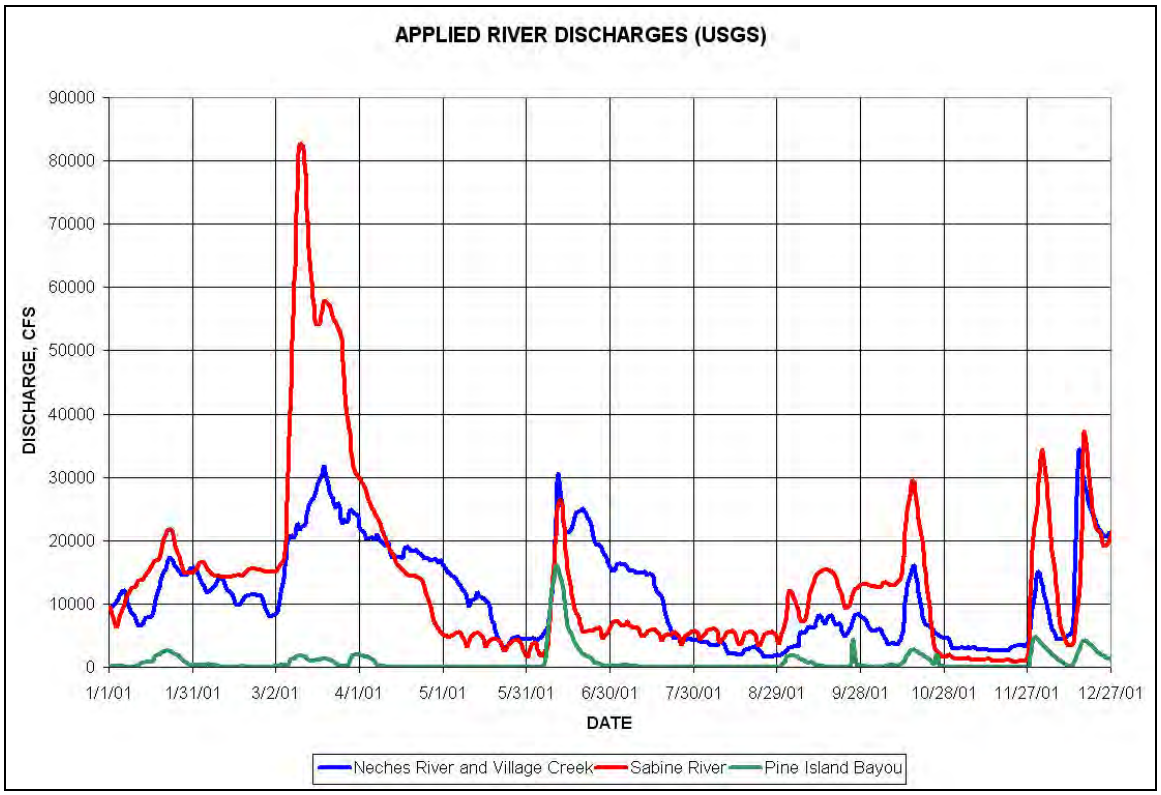

Figure 9: Applied River Discharges

GIWW eastern and western boundaries – Initially, both the GIWW eastern and western boundaries were modeled as no-flow boundaries. These boundaries were chosen such that their locations correspond to the typical locations of tidal nodes. Hence, the currents at these locations were presumed to be small. However, investigations by the Louisiana Department of Natural Resources (LDNR) indicate that there is net transport of Sabine River water to the east in the GIWW (LDNR, 2002). Hence, although the average tidal current may be near zero at this location, there is a net sub-tidal current that correlates with the discharge in the Sabine River.

The exact magnitude of this discharge is unknown. The field data collected for this study does include a 25-hour discharge transect observation at this location, but this observation is not of sufficient duration to generate a statistically significant correlation between the Sabine River discharge and the net GIWW flow.

Therefore, a functional relationship between river discharge and net GIWW flow was generated for both the eastern and western boundaries, using primarily engineering judgment. The resulting discharge was compared to the observed discharge at the GIWW east location, to ensure that they correspond. However, this only represents a correspondence for a specific 25-hour period, and therefore does not represent a verification of this correlation. The sensitivity of the model uncertainties in this relationship are discussed in the model verification section of this report.

There was no available data for comparison at the western GIWW boundary. However,

uncertainties at this boundary have little affect of the model results.

The functional relationships used to generate these flows are given in Equations 1 and 2. Plots of the discharges at these boundaries are given in Figures 10 and 11.

$$Q_{GIWW.E} = \frac{5}{11} Q_{SABINE} + 1000 \text{,with a maximum allowable outflow = 5000 cfs.....} \quad (1)$$

$$Q_{GIWW.W} = \frac{1}{10} Q_{NVPIB} \text{,with a maximum allowable outflow = 2000 cfs.....} \quad (2)$$

Where $Q_{GIWW.E}$ is the outflow at the GIWW eastern boundary, Q_{SABINE} is the Sabine River inflow, $Q_{GIWW.W}$ is the outflow at the GIWW western boundary, and Q_{NVPIB} is the combined inflow of the Neches River, Village Creek, and Pine Island Bayou.

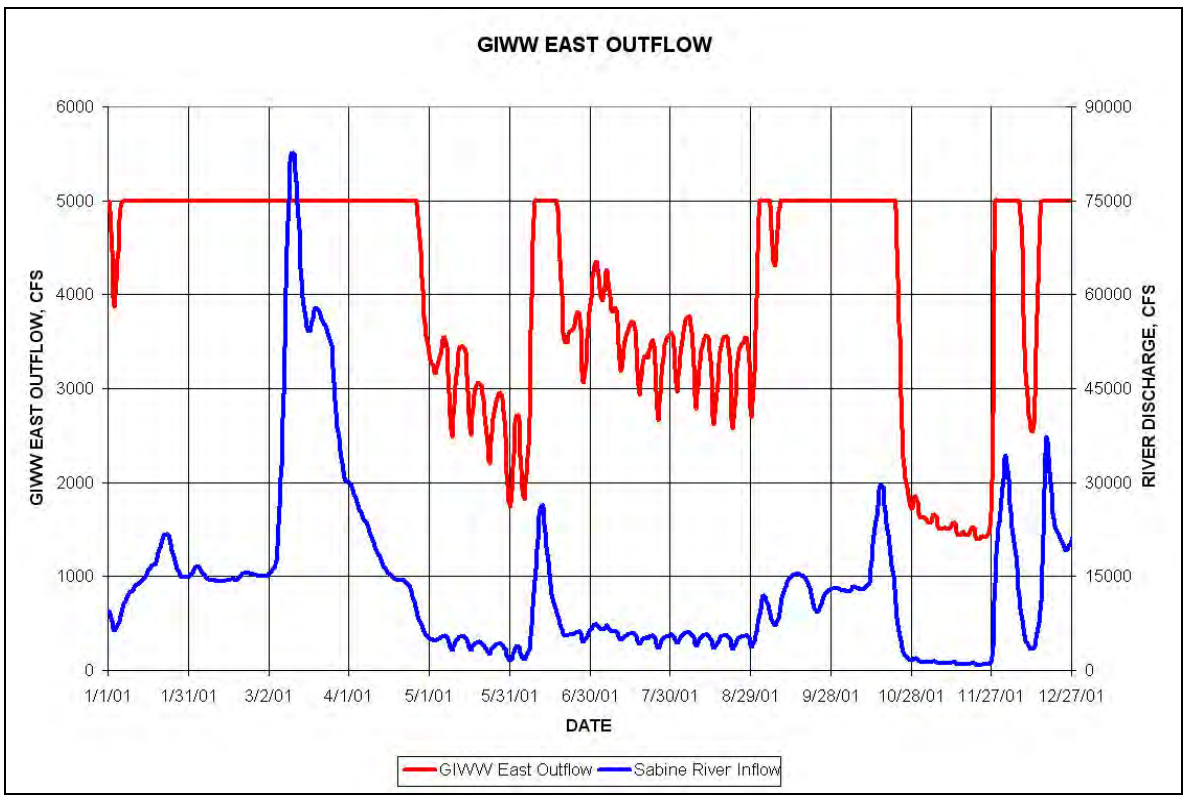

Figure 10: Applied GIWW East Outflow Boundary Condition

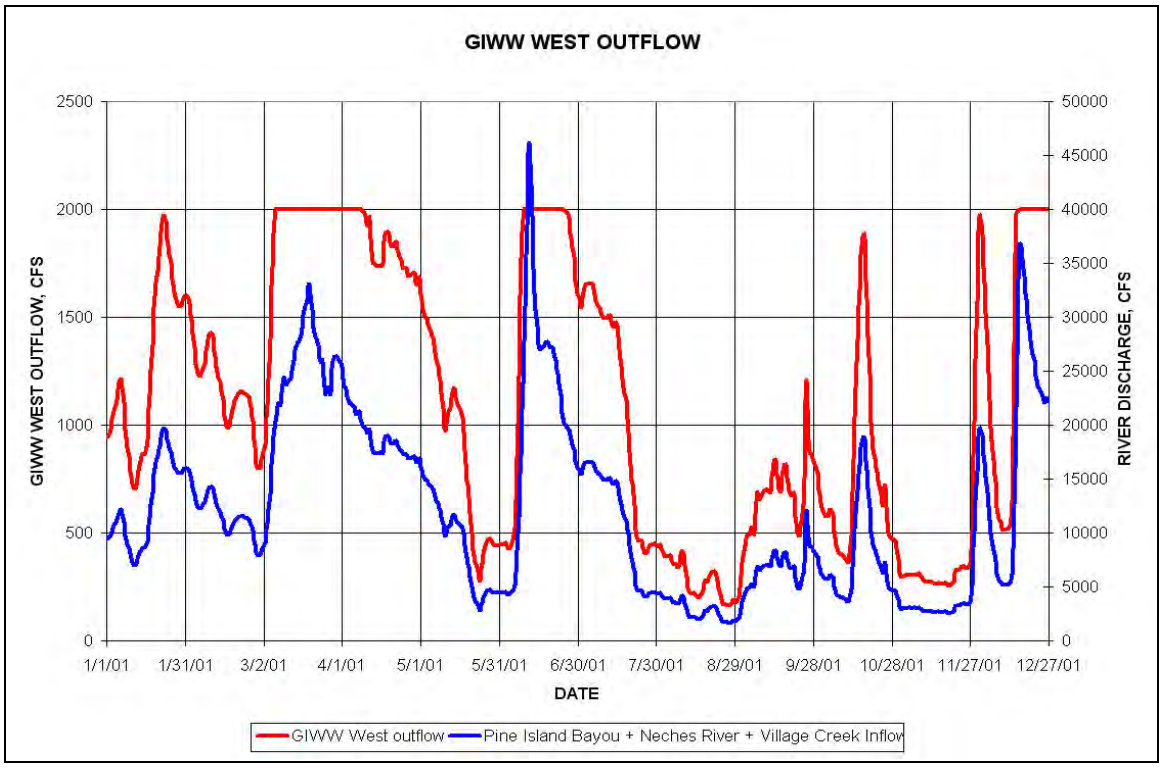

Figure 11: Applied GIWW West Outflow Boundary Condition

Power Plant Discharge at Bessie Heights– There is a constant intake of 5,000 cfs from Old River Cove, used as a coolant for a power plant. This water is then discharged into a channel that flows into Bessie Heights. This is represented in the model by an intake of 5,000 cfs at Old River Cove, at the local ambient salinity. This intake is discharged at this same salinity in Bessie Heights.

Calibration and Verification

The numerical model was calibrated and verified against the field data collected from June – December of 2001. The results of this effort are covered in this chapter. The specific data and procedures used for both calibration and verification are detailed.

Model Calibration

The model was calibrated against the 12 water surface elevation stations. The calibration period was chosen from June through July, 2001. The model was calibrated by making adjustments to the friction coefficient (Manning's n). Since the model relies on the Smagorinsky (1963) approximation for both horizontal turbulence closure and for horizontal salt diffusivity, these values were not adjusted as a calibration parameter. The Smagorinsky parameter was adjusted at specific locations within the domain, but this was done to provide numerical stability rather than to calibrate the model.

The discharge measurements and velocity measurements were not used for calibration per se. However, they were periodically inspected during the calibration process, in order to determine whether or not errors in the physical description of the system were present in the model

The model was not specifically calibrated for salinity, since the only parameters that could be used to calibrate for salinity (horizontal and vertical turbulent mixing) are constrained by the physics of the system. That is, turbulent mixing is a function of the velocities and velocity gradients present in the flow field, and as such dramatic adjustment of these parameters could result in a model that no longer obeys the proper physics. The results may match observations well, but not for the right reasons. This would result in a model that is unsuitable for use in the analysis of plan conditions, since the impacts of these changes could not be ascertained by a non-physics based model.

The Manning's n values used here are appropriate for a relatively smooth bay bottom with little or no vegetation (see Chow 1959). The values vary from 0.022 in the channel, to 0.03 in the shallows and wetlands (such as the Bessie Heights area). The system is generally homogeneous with respect to bottom roughness, except for the values assigned to the wetlands. Some of the eddy viscosity and turbulent diffusion values in regions of the domain adjacent to inflow and tidal boundaries were made artificially large, to ensure stability.

Model Verification

The model hydrodynamics were verified against 3 separate types of data: water surface elevation data (from August – December, 2001), ADCP 25-hour discharge data (from August 17th-18th, 2001), and velocity data (from June- December, 2001). The model salinities were verified against salinity data (from June- December, 2001). The following section contains a summary and discussion of these results.

Water Surface Elevation Data

A sample of the water surface elevation observations for both the model and the field for the verification period are given in Figure 12. The figure gives water surface elevations for a 28 day period (August 1st – August 28th). Since the field data are not referenced to a reliable vertical datum, the mean water surface elevation has been subtracted from the field data and the mean water surface elevation observed in the model has been added back in. This makes it easier to visually inspect the amplitude and phase comparisons between the model and the field.

Any of the field data that was obviously corrupted by bio-fouling of the sensor was omitted from this comparison and analysis. Also, the field data has been filtered to remove noise in the signal. Signals with a period of 6 hours or less were omitted from the data set.

The water surface elevation observations are given such that the gages in closest contact (hydraulically) with the ocean are shown at the top of the Figure. This is done so that the progression of the tide inland, and the consequent attenuation of the signal due to friction losses, can be readily observed for both the model and the field. The tide comparisons show that the model and field have good agreement with respect to the tidal signal, at all of the stations except for Station 5. This Station is far up the Sabine River, and shows that the model is overly dissipative in this reach. This increased attenuation could not be addressed by further reduction of friction coefficients, since the coefficients used are already representative of a relatively smooth bed.

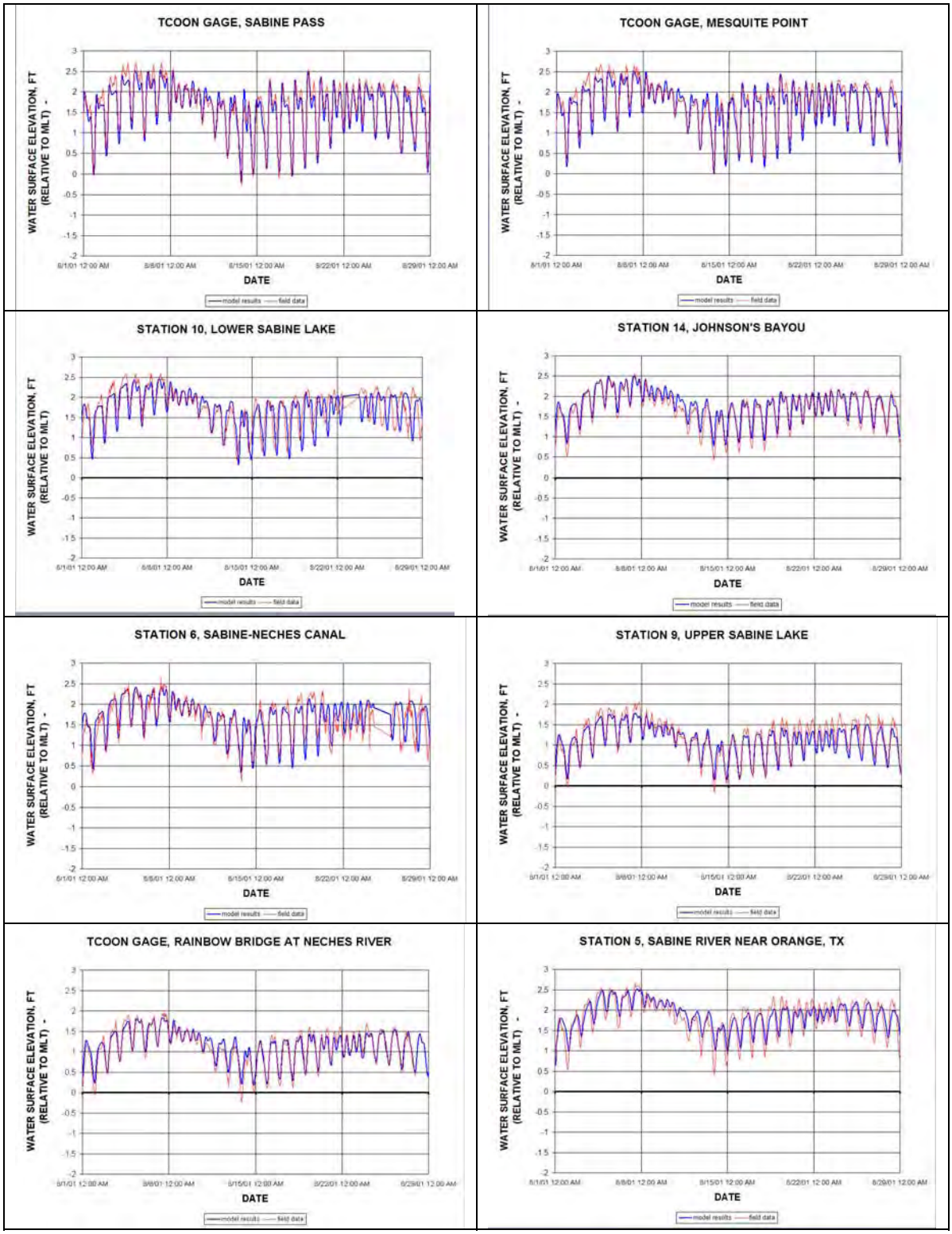

Figure 12: Tide Comparisons at Stations 5, 6, 9, 10, 14, and TCOON Gages at Sabine Pass, Mesquite Point, and Rainbow Bridge

ADCP Discharge Data

The discharge observations at all 10 transects given in the field data are plotted against model results in Figures 13-16. The locations of each range are shown in the figures. The major discrepancies between model and field observations occur at Ranges 6 and 7. The model depicts a somewhat larger tidal prism passing into the Neches River than the field observations show, and the phasing of the discharge though Range 7 is different than that observed in the field.

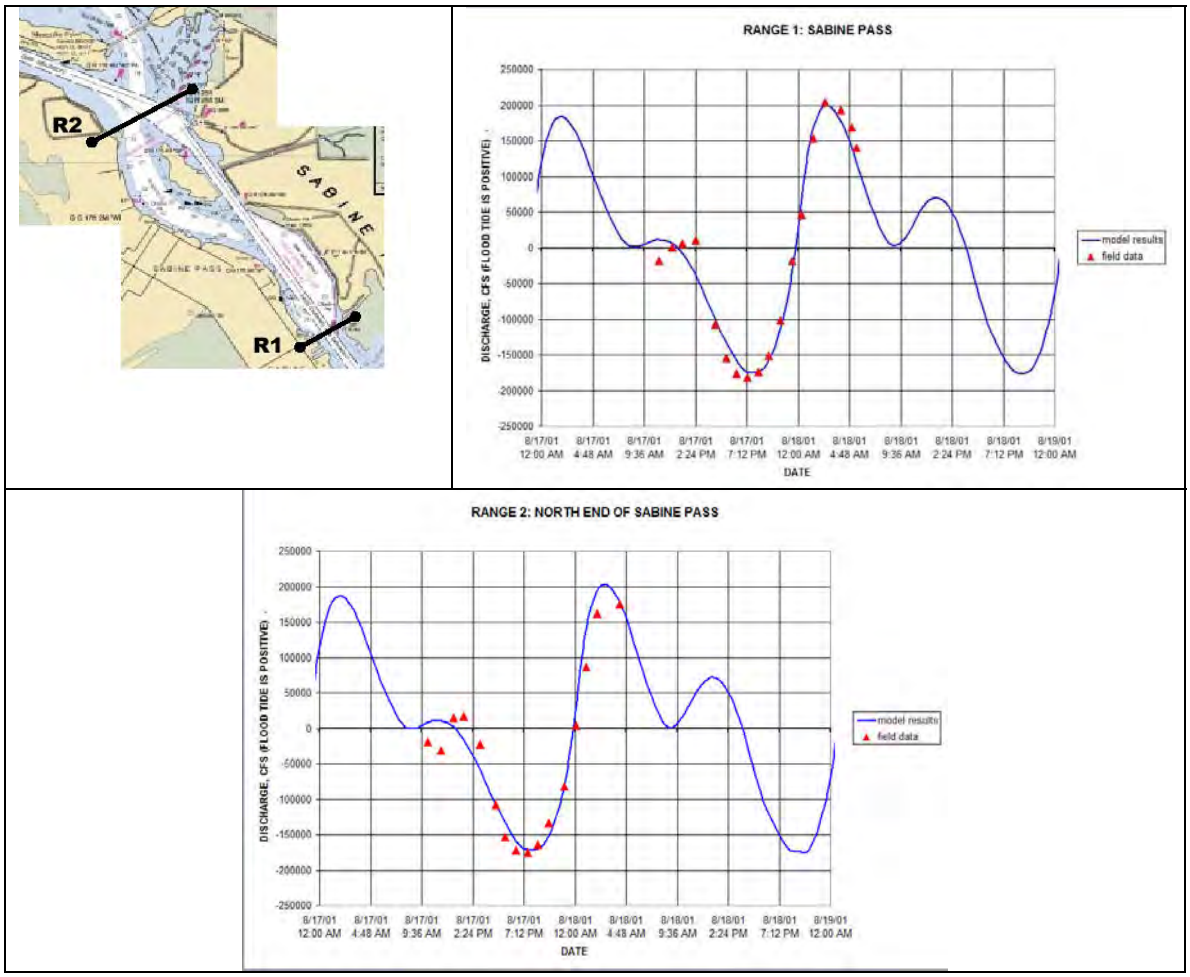

Figure 13: Discharge Comparisons at Ranges 1 and 2

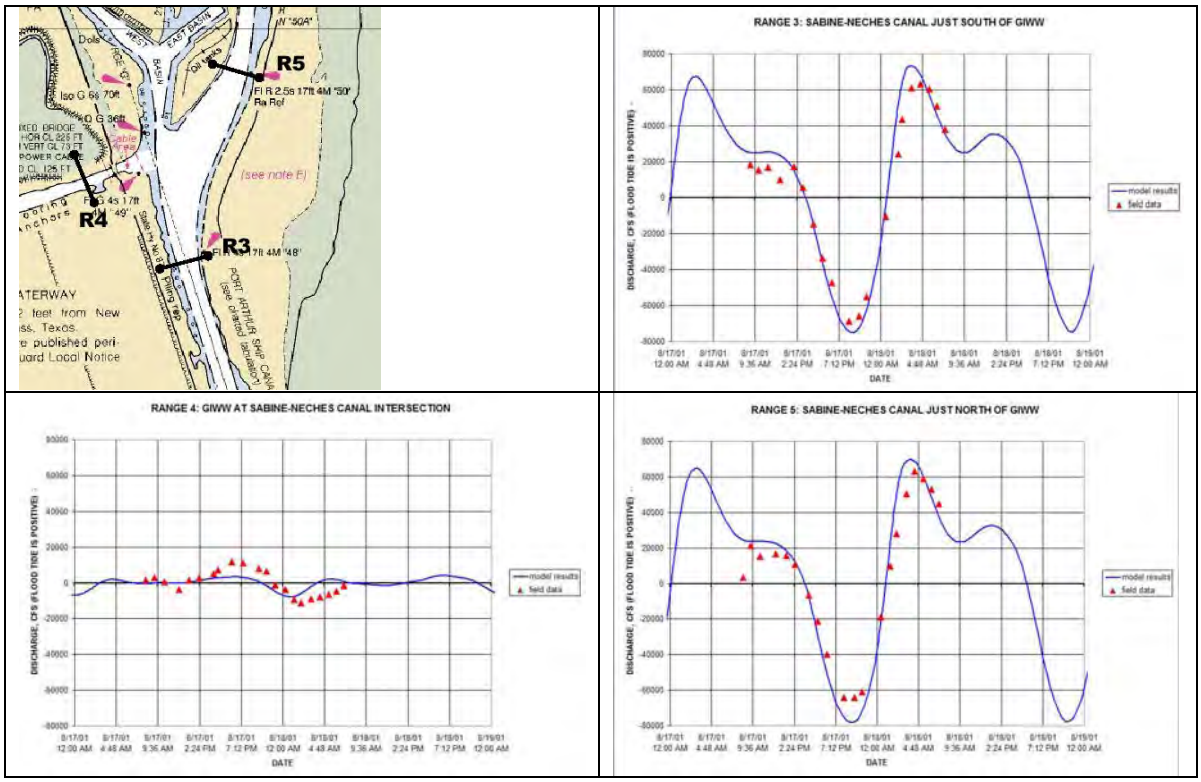

Figure 14: Discharge Comparisons at Ranges 3,4, and 5.

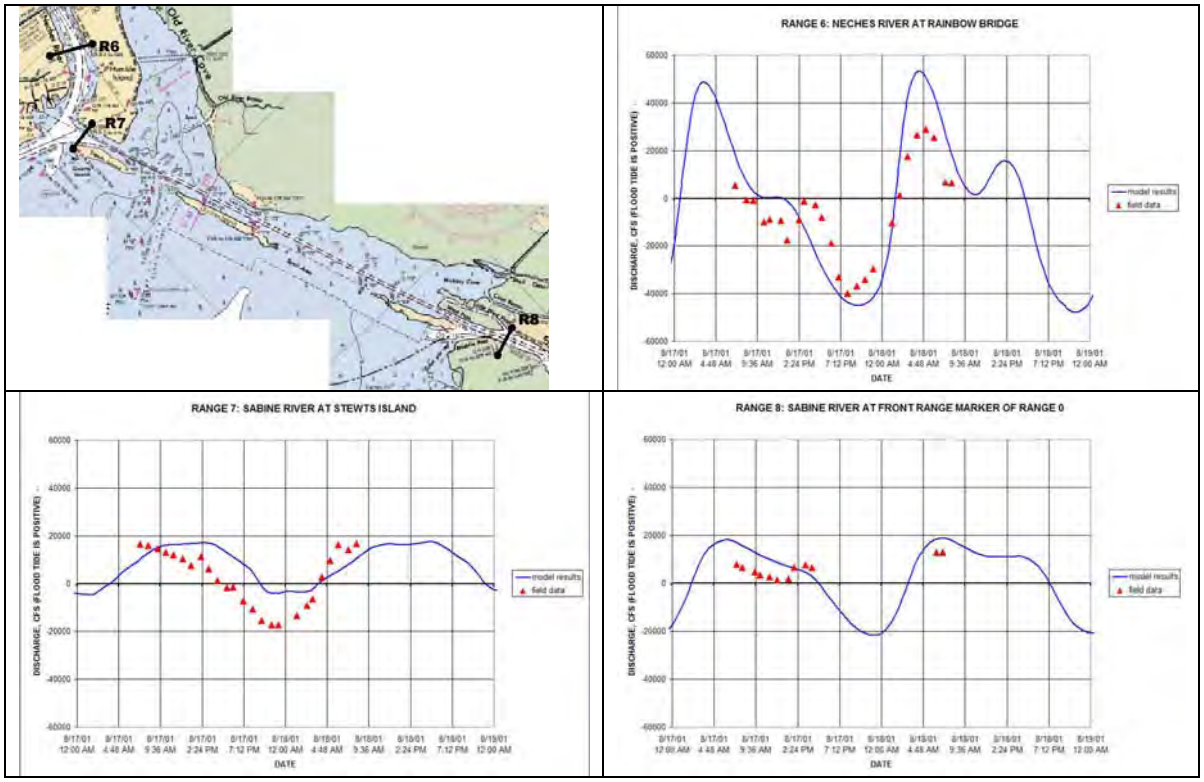

Figure 15: Discharge Comparisons at Ranges 6,7, and 8.

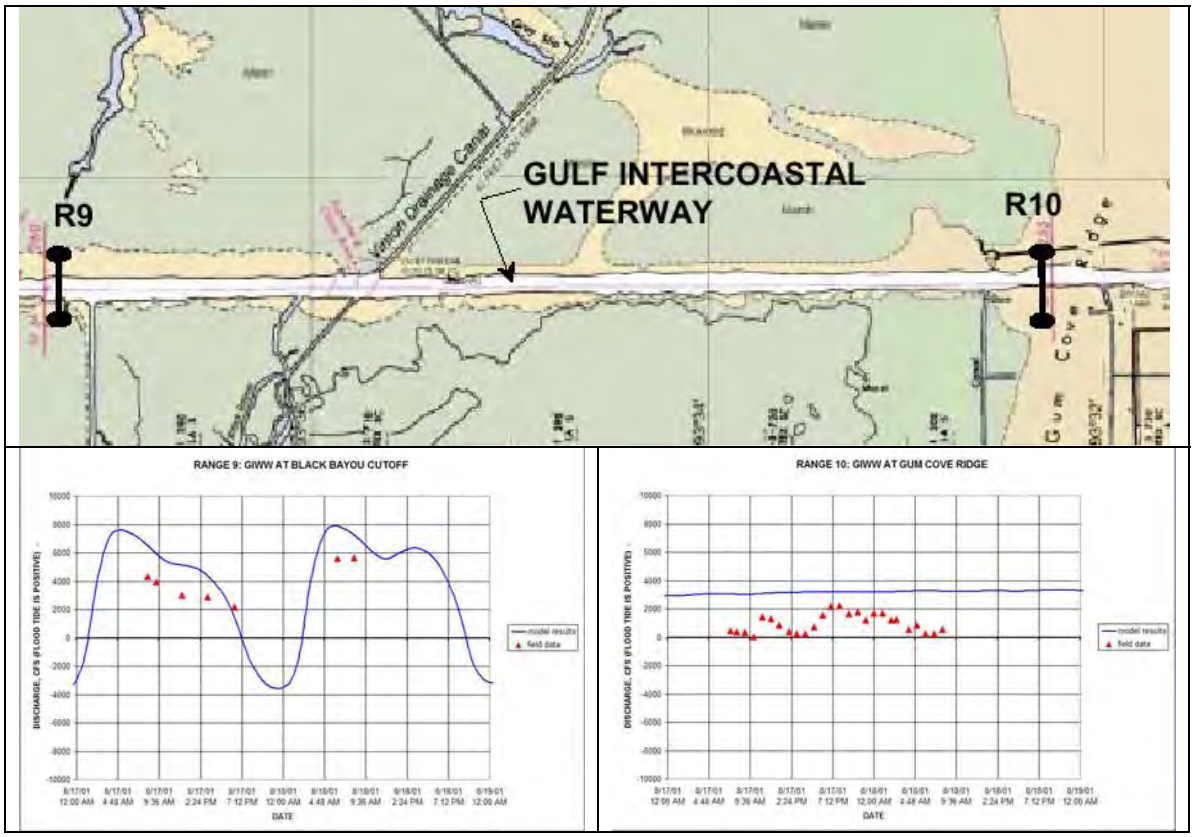

Figure 16: Discharge Comparisons at Ranges 9 and 10

Velocity Data

The velocity observations are given in Figures 17 and 18. They show good agreement at most of the gage locations. However, at Station 6 (in the Sabine-Neches Canal) there is a noticeable difference in the strength of the current in the model and the field. The current in the model is much stronger than that observed in the field. It is difficult to reconcile this with the generally good agreement in the discharge comparisons at this location. It is possible that the velocity measurement in the field was somehow obstructed, or subject to a local eddy with each tidal cycle. However, repeated attempts to confirm the cause of this discrepancy were unsuccessful.

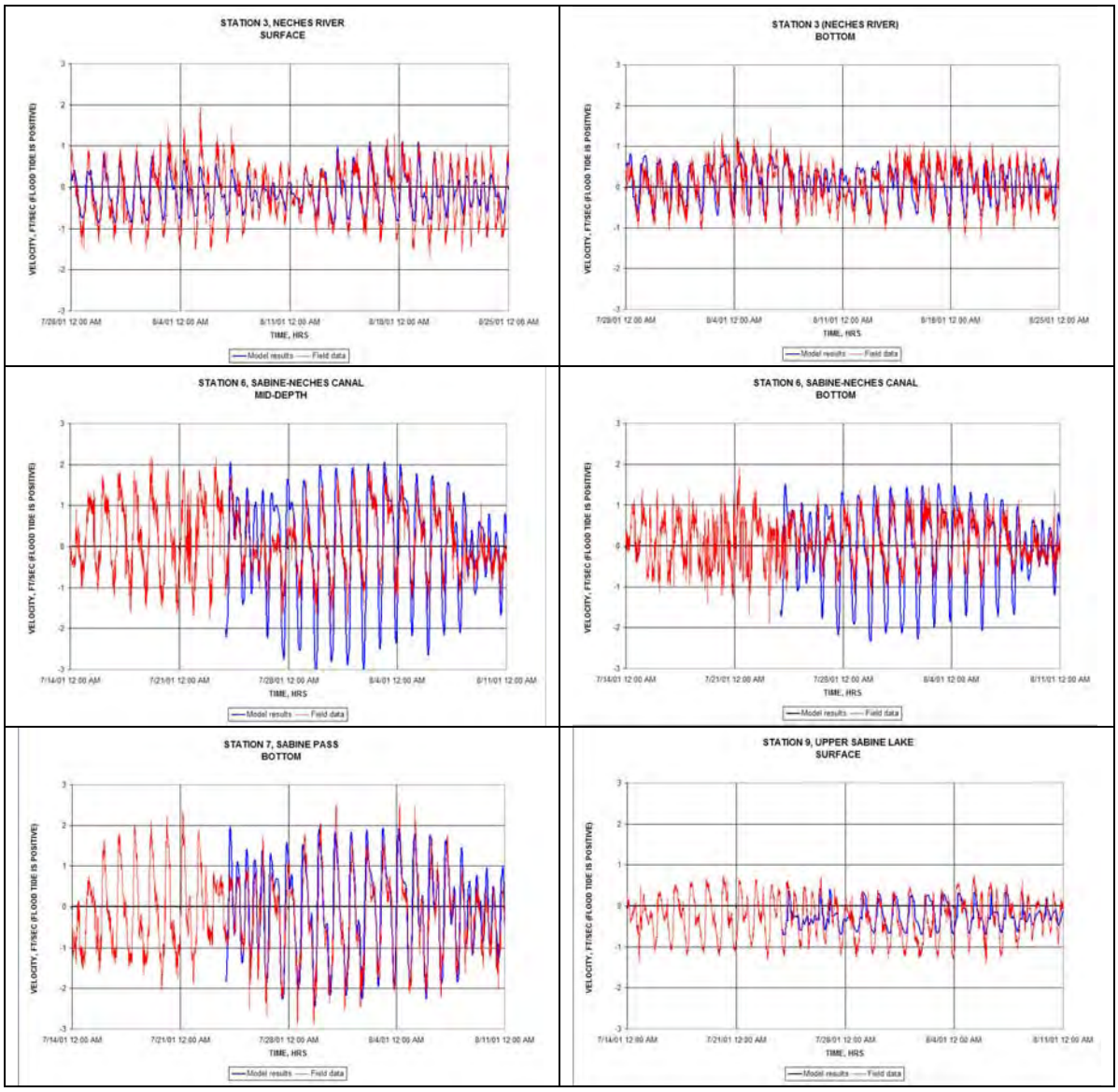

Figure 17 Velocities at Stations 3, 6, 7 and 9

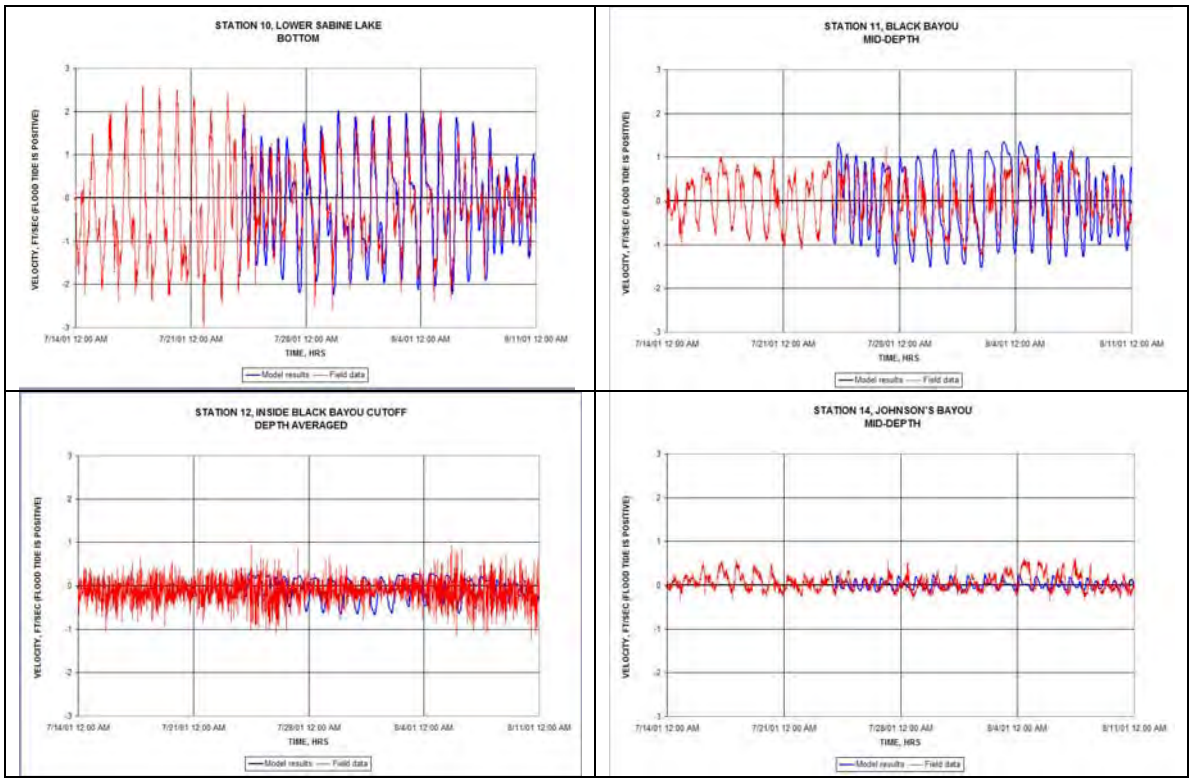

Figure 18: Velocities at Stations 10, 11, 12 and 14

Salinity Data

The salinity observations for both the model and the field for the verification period are given in Figures 19-21. Any of the field data that was obviously corrupted by bio-fouling of the sensor was omitted from this comparison and analysis. Also, the field data has been filtered to remove noise in the signal. Signals with a period of 6 hours or less were omitted from the data set.

The figures contain field data, and 2 different sets of model results. The results given in blue represent the results obtained from the model with the salinity initialized only once, at the beginning of the run. These results represent the true behavior of the model. The results given in green are results that are obtained from the model with the salinity initialized twice, during low flow events. The reason for including these results is discussed below.

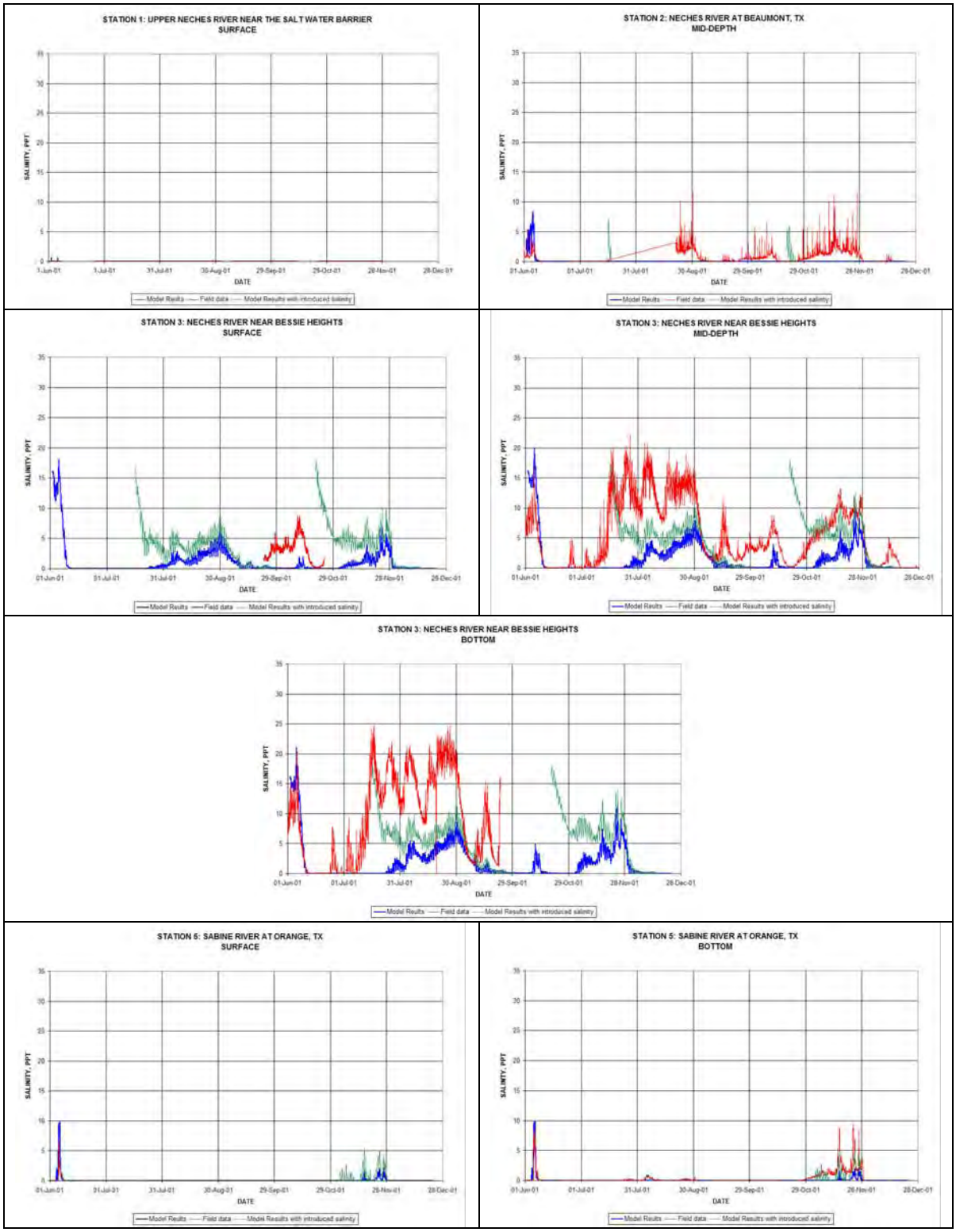

Figure 19: Salt Comparisons for Stations 1, 2, 3 and 5

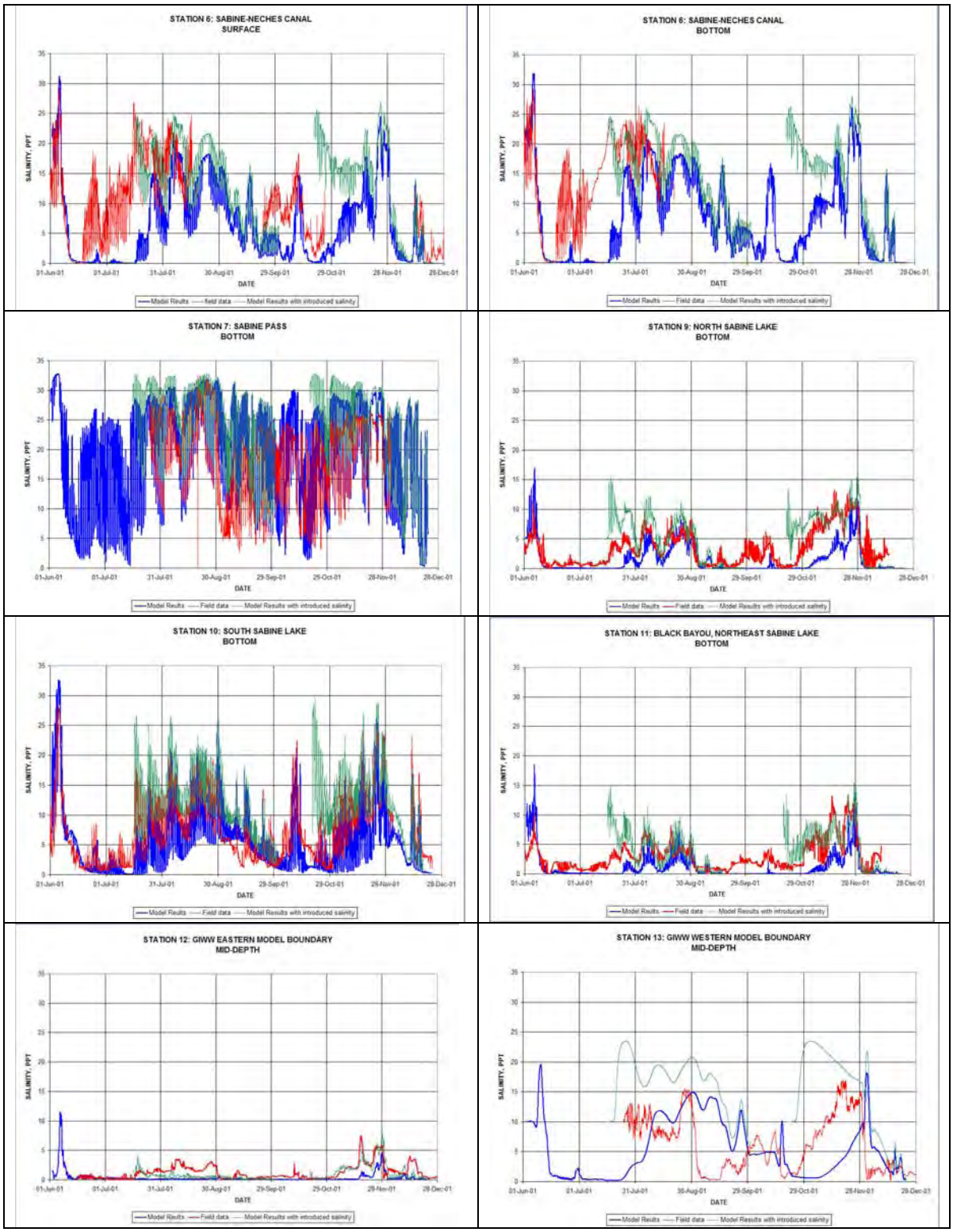

Figure 20: Salt Comparisons for Stations 6, 7, 9, 10, 11, 12, and 13

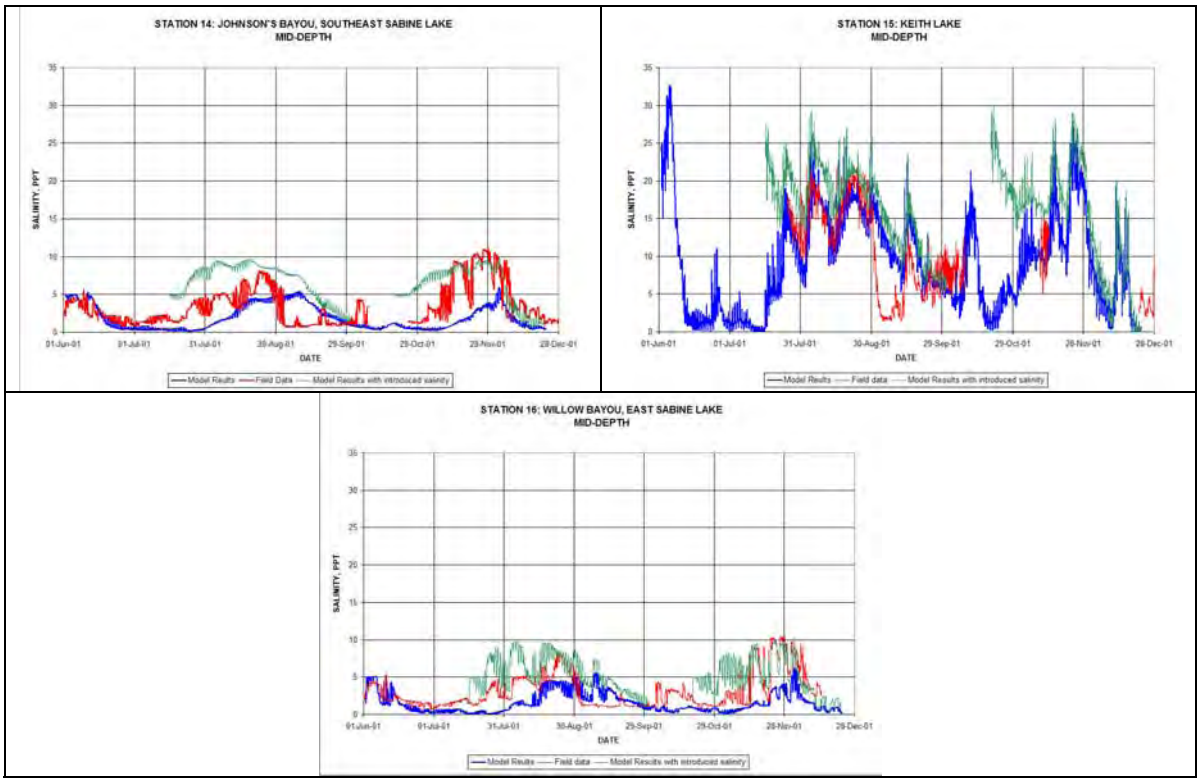

Figure 21: Salt Comparisons for Stations 14, 15, and 16

In general, the model duplicates the form of the salinity response well, but it often underpredicts the magnitude. This is especially true on the Neches River. The reason for the inability of the model to accurately simulate the salt transport into the system is not known with certainty. However, the two most likely factors are as follows:

- The model is overly diffusive with respect to the salinity stratification. The model does indeed simulate stratification, and the degree of stratification is on the order of that observed in the field (see Figure 23 for an example of the salinity stratification in the Neches River over one tidal cycle). However, the salt wedge interface is potentially much sharper in the field than in the model (i.e. the gradient occurs over a shorter vertical length). This, in turn, would result in a greater net upstream momentum of the salt wedge in the field than is observed in the model.

- The model does not drain as effectively as the actual system in the field. The hydraulic outlets available to flood waters in the field are far more numerous than those included in the model. Therefore, the fresh water inputs to the system would tend to have a greater impact on the salinity in the model than they do in the field. This is especially pertinent for the specific simulation period shown here. In early June of 2001, Tropical Storm Allison contributed over 2 feet of rain to the system, as well as significant flood flows in the rivers (see the rainfall and inflow boundary conditions). The consequent overland flooding that was observed in the field after this event is not represented in the model, since the land surface is not incorporated into the domain. In the model, all of this water must be contained in the defined flow pathways, and must exit the domain either through Sabine Pass, or through the GIWW East or West boundaries. Therefore, the potential exists for much higher residence times for this fresh water flood flows in the model than in the field, and this in turn serves to mitigate the salinity intrusion to a much greater

degree in the model than in the field.

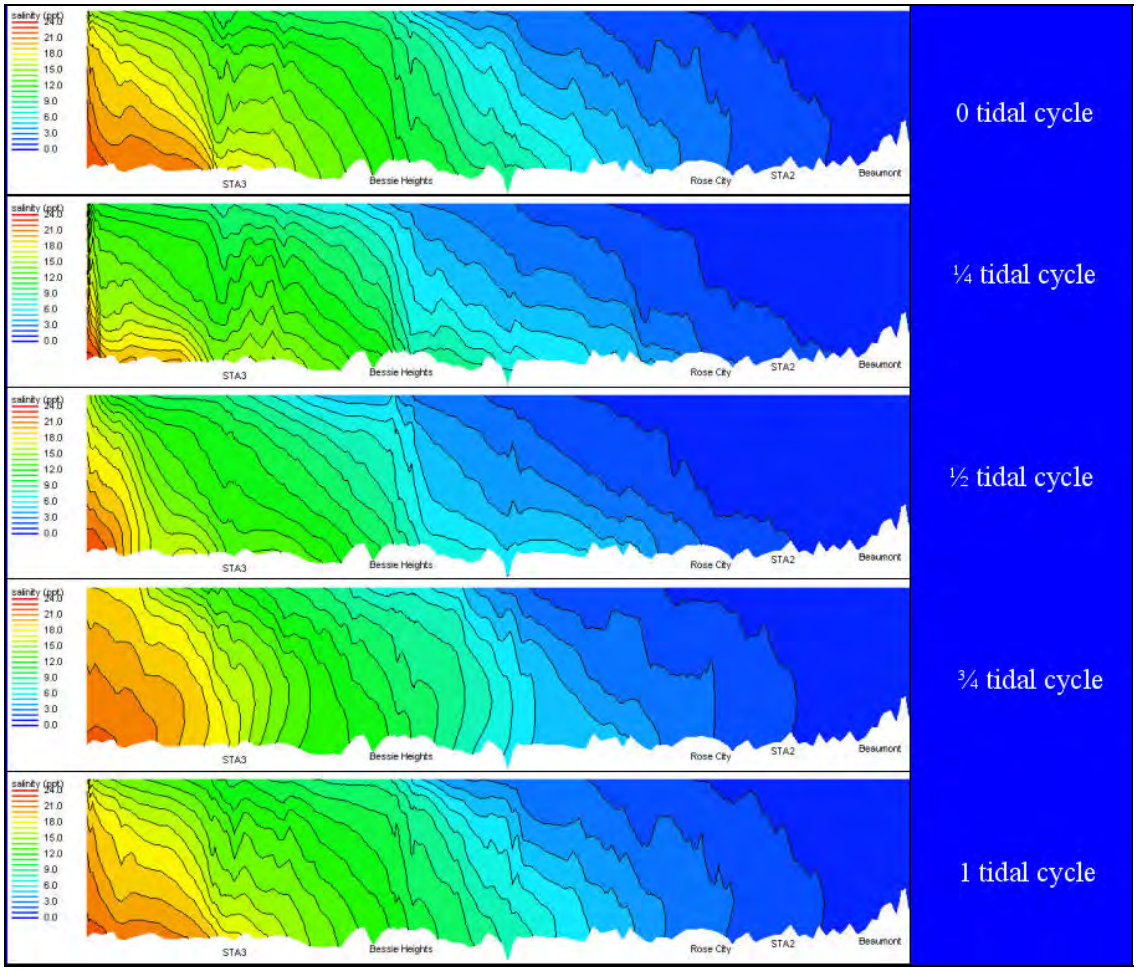

Figure 23: Plot of Salinity Stratification in the Neches River over 1 Tidal Cycle.

To investigate these phenomena, the model was simulated with the salinity initialized at 2 times where the inflows to the model were low. This is generally not good modeling practice, since it eliminates the "spin-up" time required to eliminate the effects of the initial salinity field. However, by introducing the salinity at low flow, it is possible to investigate how well the model behaves under conditions where the flow is not changing rapidly. Since the design flows employed in this project do not change rapidly, the behavior of the model under these conditions is of interest.

It can be seen that the model behaves better at most gages under these conditions. This may indicate that the model can simulate salinity intrusion, but it cannot respond as rapidly as the prototype due to problems such as the diffusion of the salt wedge. It may also indicate that alternate flow pathways exist in the prototype that allow the salt wedge to intrude more rapidly.

Model Analysis of the Impacts of Relative Sea Level Rise and Proposed Channel Deepening

This chapter contains the results of model simulations designed to assess impacts to salinity that would result from the occurrence of the "most likely" relative sea level rise at end of the design life do the project (2069) and the impacts of implementing a 48-foot channel deepening project.

Description of the "Most Likely" Relative Sea Level Rise

The channel deepening study for the Sabine-Neches Waterway had been updated to include the effects of Relative Sea-Level rise on the project impacts. In consultation with Corps Headquarters, these impacts were included by analyzing both the with and without project conditions for a single "most likely" future sea level rise condition.

Relative sea level rise consists of two components: global (eustatic) sea level rise, and local subsidence. The eustatic rate was taken from the National Research Council projections (NRC, 1987), as stipulated by Corps guidance (ER1105-2-100; Apr 2000). For the "most likely" case, the NRC Curve II was selected.

The projected rate of local subsidence was difficult to ascertain. Although tide records and direct observation of land based data indicate subsidence rates of 2-5 mm or higher, long-term data taken from basal peat analysis indicate rates that are an order of magnitude lower than this.

To date, there is no scientific consensus on what the local subsidence rate should be for future projections. The relative influence of historic anthropogenic activities, such as oil extraction and groundwater withdrawal, are difficult to quantify. If these activities have contributed significantly to recent observations of subsidence, then the cessation of these activities may result in a rapid deceleration of subsidence rates, returning them to the long-term average rates.

For the "most likely" condition, the lower rate of subsidence based on the basal peat analysis (0.5 mm/yr) was selected. This rate was chosen based on the assumption that the anthropogenic factors thought to contribute significantly to the local subsidence had largely ceased in the 1970's and 1980's and hence the subsidence may be expected to return to the slower long-term average rate.

Using this value of subsidence, together with the NRCII curve from 1987, and assuming a project year 0 = 2019, and a project year 50 = 2069, the value selected for the most likely sea level rise over the project life was 1.1ft.

Description of Proposed Channel Deepening

The recommended plan for the proposed SNWW 48-Foot project consists of deepening the existing navigation channel from 40 to 48 ft to the Port of Beaumont and extending the existing entrance channel into the Gulf of Mexico, Table 2 gives the proposed changes to the project depth. Figure 24 shows the extents of the modified channel.

TABLE 2 PROPOSED WATERWAY DIMENSIONS FOR 48' DEPTH

Reach	Section	Bottom Width (FT)	Side Slope	Project Depth (FT)	Proposed A.M. Increase (FT)	Allowable Overdepth (FT)	Total Design Depth (FT)
Sabine Bank Channel	1	700	1V/2H	50	2	2	54
Sabine Bank Channel	2	700	1V/2H	50	2	2	54
Outerbar Channel (0+000-18+000)	3	800	1V/10H	50	4	2	58
Sabine Pass Jetty Channel	4	500	1V/2H	48	5	2	52
Sabine Pass Channel (100+00-180+00)	5	500	1V/2H	48	3	2	55
Sabine Pass Channel (230+00-295+61)	6	500	1V/2H	48	2	2	57
Port Arthur Canal (0+00-290+00)	7	500	1V/2H	48	2	2	54
Port Arthur Junction + Taylors Bayou	8	500	1V/2H	48	5	2	57
Sabine Neches Canal	9	400	1V/2H	48	1	2	53
Neches River Channel	10	400	1V/2H	48	1	2	52
Neches River Channel	11	500		48	2	2	52
Neches River Channel	12	400		48	2	2	52
Neches River Channel	13	400	1V/2H	48	2	2	52
Neches River Channel	14	400	1V/2H	48	2	2	52
Neches River Channel (440+00-978+00)	15	400	1V/2H	48	2	2	54
Neches River Channel (440+00-978+00)	16	400	1V/2H	48	2	2	54
Neches River Channel (440+00-978+00)	17	400	1V/2H	48	2	2	54
Neches River Channel (440+00-978+00)	18	400	1V/2H	48	2	2	54

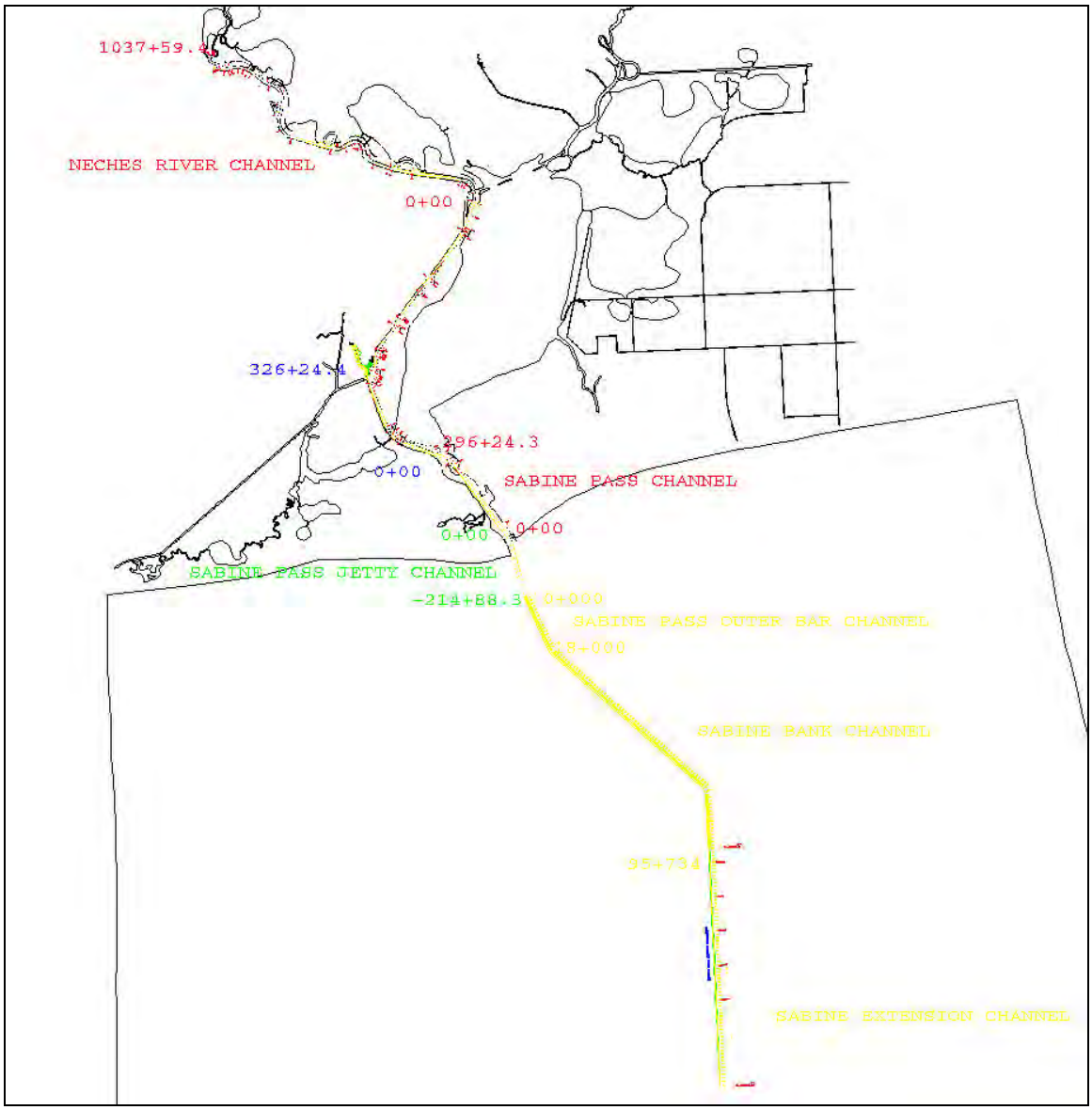

Figure 24: Proposed Extent of the Channel Deepening Project.

Boundary Conditions for Analysis of Channel Deepening Impacts

Salinity

Freshwater inflow for the SNWW HS model's future conditions was developed using model outputs from Run 8 of the Texas Commission on Environmental Quality (TCEQ) Water Availability Models (WAMs) for the lower Sabine and Neches Rivers. For existing conditions, "Run 8 uses modified diversion amounts (maximum use for the last 10 years), year 2000 area-capacity parameters for major reservoirs, and assumed return flows. It also includes term water rights and provides the most realistic assessment of current streamflow conditions" (TWDB, 2007: p. 363). The Texas Water Development Board (TWDB) has projected flows for the year

2060 by modifying Run 8 "to include projected increased demand from existing water rights, expected change to return flows, projected new strategies to come online before 2060, and estimated year 2060 storage capacities for major reservoir" (TWDB, 2007: p. 363) Figure 25 gives the inflows used for both the low flow and median flow cases.

The WAMs Run 8 for the year 2060 was developed using current patterns of precipitation and evaporation. USACE does not propose to modify the WAMs modeling runs to use future projections of precipitation or evaporation for the SNWW future conditions run. No attempt was made to project future precipitation because the Texas State Climatologist has recently concluded that it is impossible to predict with confidence what precipitation trends should be in Texas over the next half century (Nielsen-Gammon, 2009). Unlike precipitation, there is more consensus for a predicted temperature increase in Texas of close to 4°F by 2060. No attempt was made to change future temperatures in the 2060 WAMs model because resulting changes in evapotranspiration would be so small as to result in a negligible change in the modeling results.

Note that these forecasts of future water demand carry with them an inherent level of uncertainty. To limit the impacts of this uncertainty on the ability to asses project impacts, it is preferable that these inflows are utilized in the context of providing an approximate range of inflows against which to measure project impacts via model-to-model comparisons of results. This is best achieved by ensuring that the same inflows are used for all model runs, including the existing condition runs.

Although using the same set of inflows for all runs eliminates the possibility of ascertaining the impacts of future water use changes on the salinity of the system, it also eliminates the uncertainty assocaited with these impacts from the analysis. Since changes to inflows can have significant effects on salinity, these uncertainties can easily overwhelm other uncertainties in the analysis. Consider, for example, that the projected 10% inflow on the Neches is generally higher than the existing condition, and hence including these effects in the analysis would indicate zero or beneficial net salinity impacts of the project, relative to existing conditions. This may in fact be the case, but the inclusion of these results in the analysis would necessitate a formal analysis of the uncertainty associated with the projected inflows, which is difficult if impossible to quantify.
\

The low inflow runs were run for 5 months, with the first 2 months used as spin-up. The spin-up period is used to allow sufficient time for the system to reach dynamic equilibrium with respect to salinity concentration. It is not included in the analysis. Therefore, the low inflow analysis is conducted only for the final 3 months of the simulation period. This represents roughly the period from August though October.

The median inflow runs were run for 7 months, with the first month used as spin-up (i.e. 6 months are used for analysis). This represents roughly the period from April through September. The median flow runs only require 1 month of spin-up because the higher inflows result in lower average residence times in the system, which in turn correlates directly to the required spin-up time.

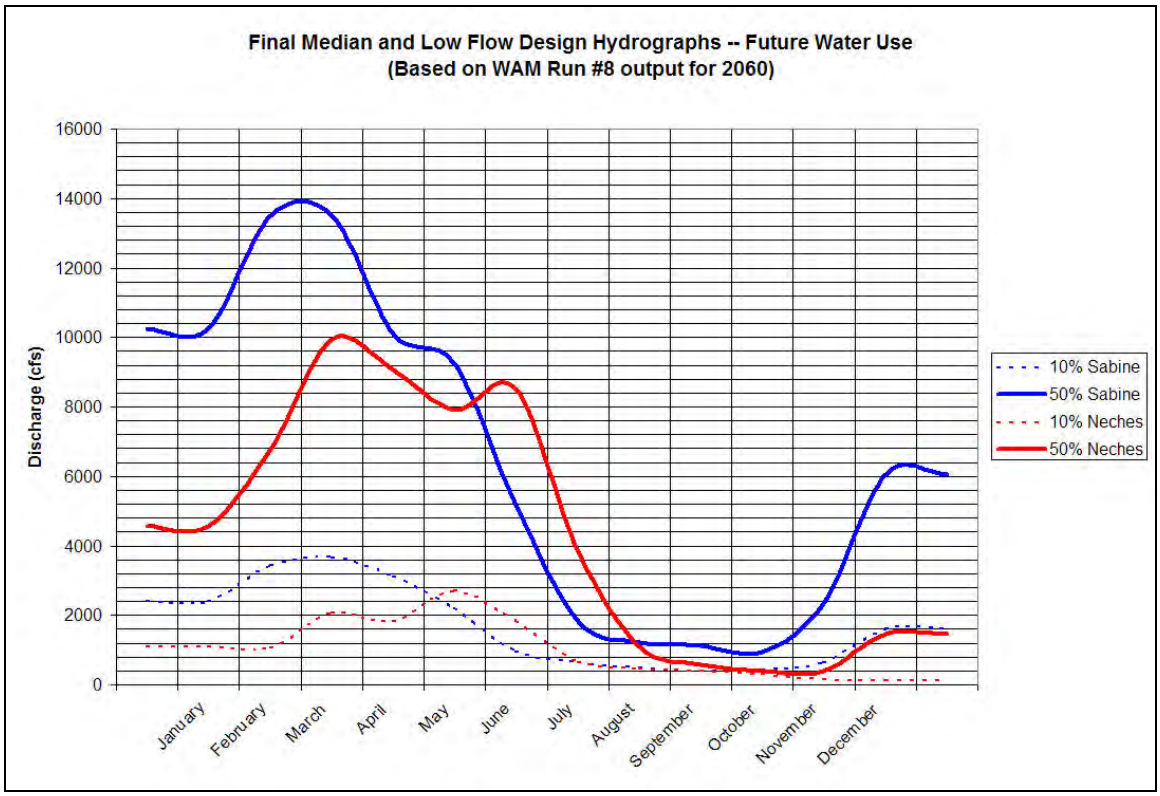

Figure 25: Low and Median Inflow Hydrographs

Statistical correlations were also used to generate applied rainfall and evaporation hydrographs for the low and median flow runs. These are given in Figures 26 and 27

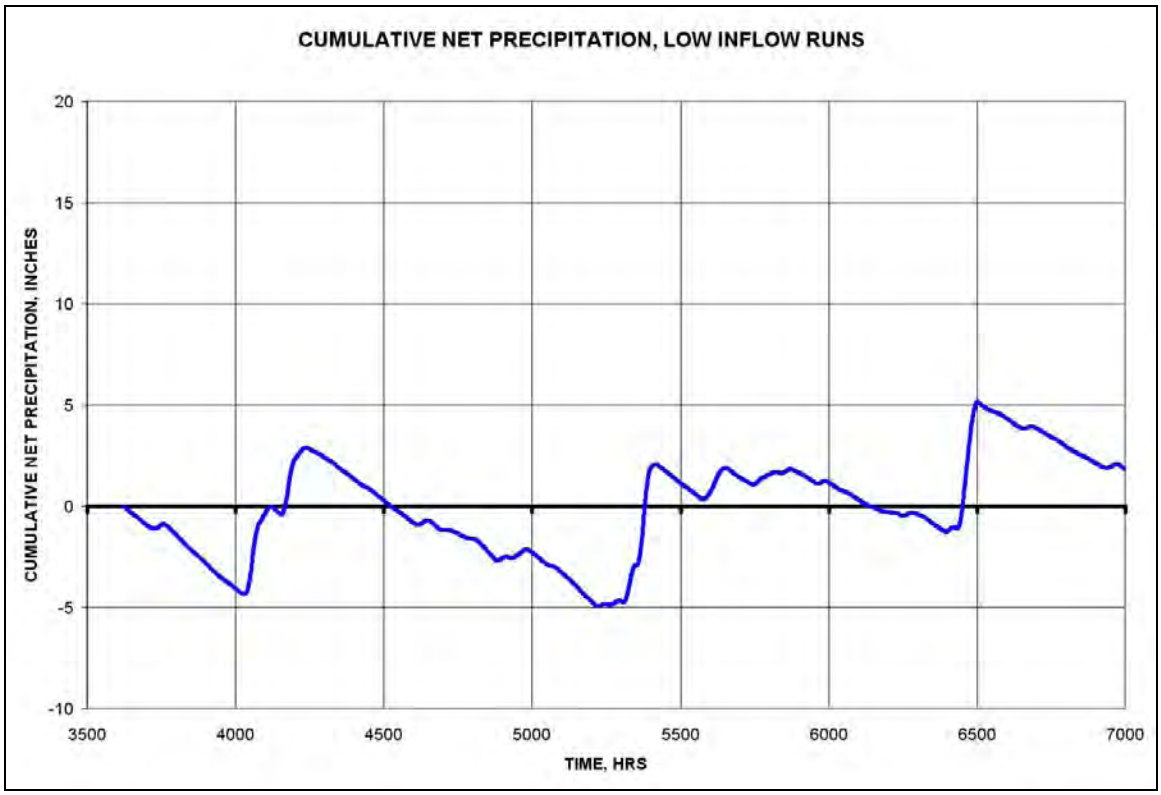

Figure 26: Low Inflow Cumulative Net Precipitation

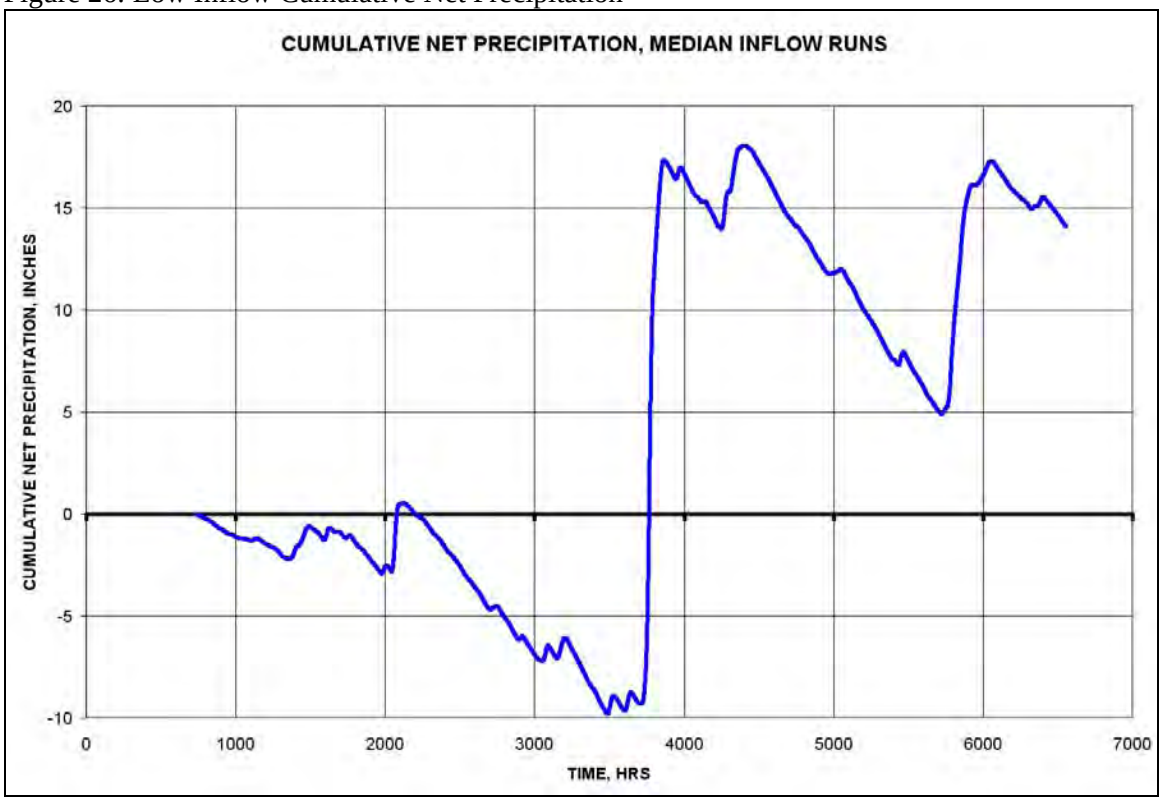

Figure 27: Median Inflow Cumulative Net Precipitation

The applied outflow at the GIWW East and West boundaries are governed by Equations 1 and 2.

using the low and median river inflows as input to the equations. The tide and wind conditions are the same as those used over the verification period.

Results: Effects of Relative Sea Level Rise

The effects of relative sea level rise alone were investigated by running the model wit the existing channel dimesions, both with and without the "most likely" relative sea level rise of 1.1 ft at the ocean boundary. The results of this analysis are discussed below.

Water Surface Elevation

The average water surface elevation through most of the study area increased by a value very close to the imposed value of 1.1 ft. This is due to the fact that the water surface slope is very mild through the system (on the order of 2X10-6) and hence the backwater effects that would serve to mitigate the sea level rise effect occur upstream of the study area. Water surface elevations both with and without relative sea level rise at several observation points throughout the study area are given in Appendix B.

Salinity

Figures 28 and 29 represent color contour plots of the average salinity values for both the with and without RLSR runs. Also, a plot of the salinity difference (plan minus base) is given.

Figure 30 represents a statistical analysis of the salinity differences between the with and without RLSR runs for the low flow case at each of the salinity sampling stations used for the calibration and verification of the model. Included in this analysis is an additional station (Station 17) which is located in the GIWW west of the Sabine-Neches Canal, just west of the Taylor Bayou outfall.

The salinity differences range between 0 and 3 ppt. They are most significant in the low flow case. The largest salinity differences are observed along the western shore of Sabine Lake, and in the Neches River near Bessie Heights. These differences are associated with the increased salinity intrusion both in the shp channel and through the southern connection between the channel and Sabine lake

For this system, this results in the highest salinity impacts in the following locations.

<u>Low Flow:</u>

- Neches River near Bessie Heights and Bessie Heights (approximately 2-2.5 ppt)
- Western Shore of Sabine Lake (approximately 1.5-2 ppt)

<u>Median Flow:</u>

- Neches River near Bessie Heights and Bessie Heights (approximately 1-1.5 ppt)
- Keith Lake Fish Pass (approximately 1.5-2 ppt)

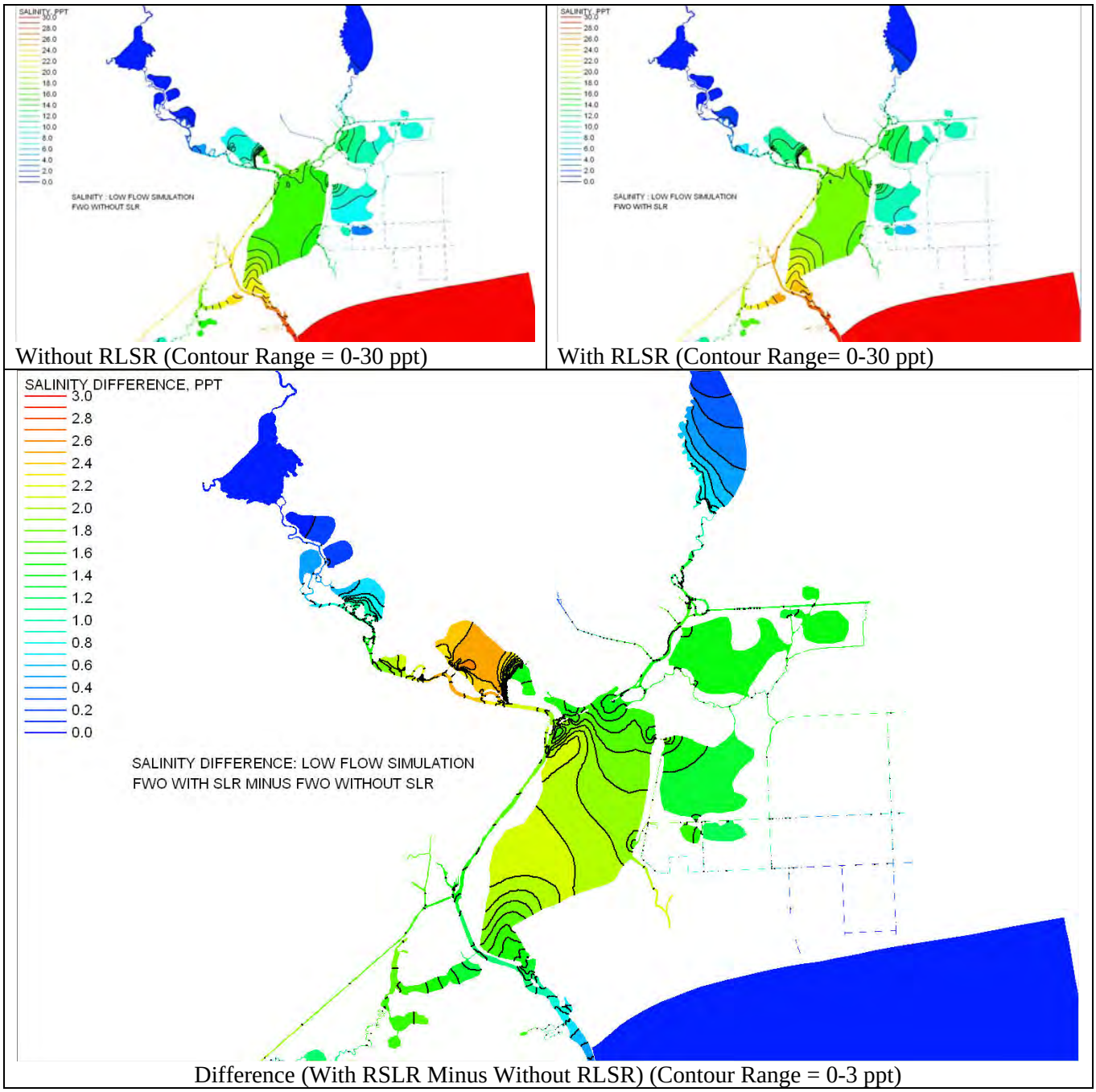

Without RLSR (Contour Range = 0-30 ppt)

With RLSR (Contour Range= 0-30 ppt)

Difference (With RSLR Minus Without RLSR) (Contour Range = 0-3 ppt)

Figure 28: Average Salinity Conditions Both With and Without Sea Level Rise, Low Flow Runs

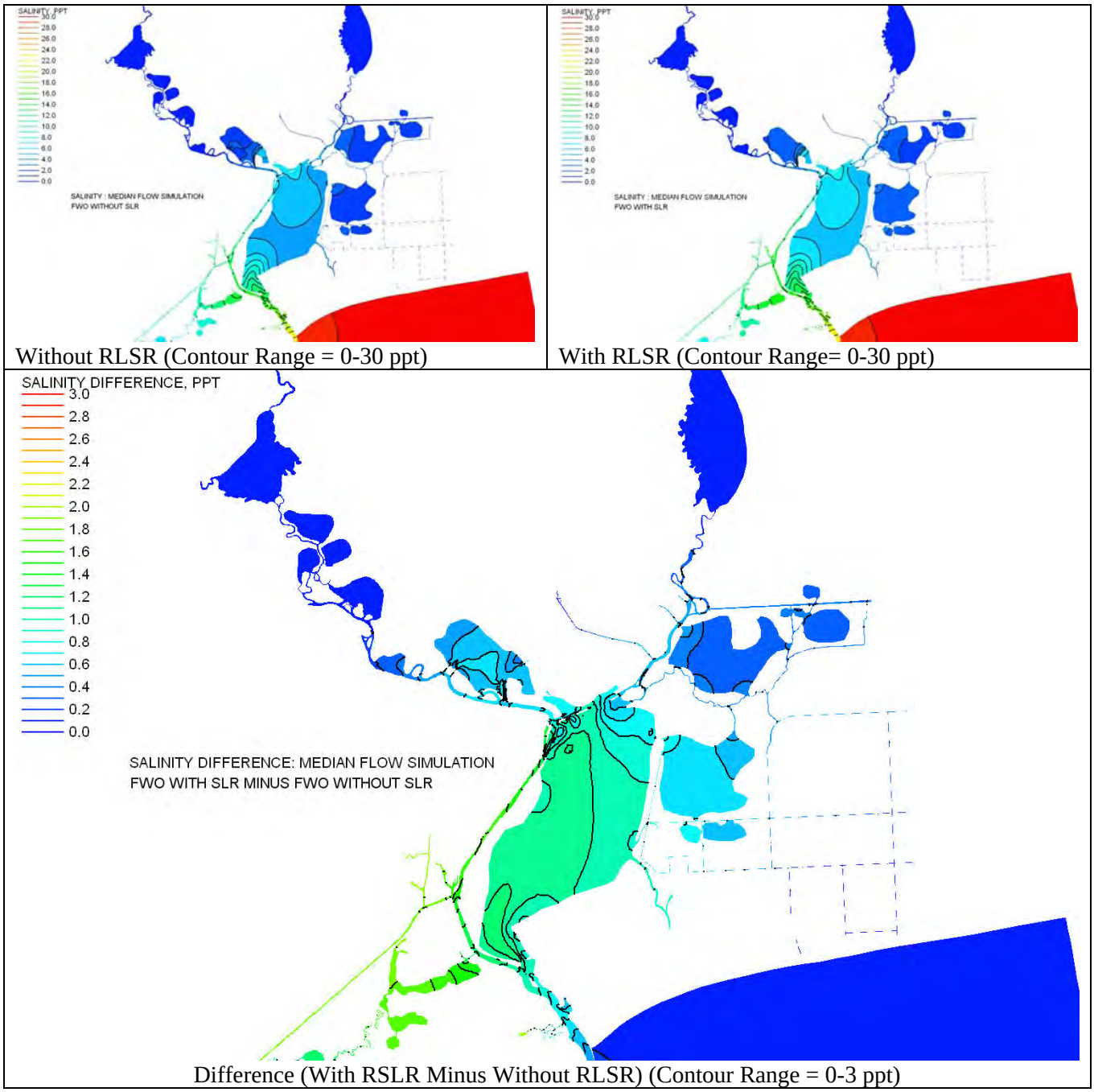

Without RLSR (Contour Range = 0-30 ppt)

With RLSR (Contour Range= 0-30 ppt)

Difference (With RSLR Minus Without RLSR) (Contour Range = 0-3 ppt)

Figure 29: Average Salinity Conditions Both With and Without Sea Level Rise, Median Flow Runs

LOW FLOW, FWO WITHOUT SLR AND FWO WITH SLR

AVERAGE DIFFERENCES

STATION #	1	2	3	5	6	7	9	10	11	14	15	16	17
SURFACE SALINITY	0.08	0.89	2.21	1.12	1.62	0.50	1.56	1.65	1.46	1.98	1.25	1.90	1.61
MIDDEPTH SALINITY	0.08	1.18	2.26	1.17	1.56	0.45	1.57	1.67	1.51	2.01	1.23		1.61
BOTTOM SALINITY	0.08	1.40	2.23	1.20	1.56	0.42	1.57	1.68	1.51	2.03	1.24		1.60

STANDARD DEVIATION OF THE DIFFERENCES

STATION #	1	2	3	5	6	7	9	10	11	14	15	16	17
SURFACE SALINITY	0.11	0.37	0.45	0.52	0.58	0.53	0.33	0.57	0.39	0.28	0.47	0.66	0.41
MIDDEPTH SALINITY	0.11	0.35	0.29	0.55	0.56	0.46	0.33	0.57	0.41	0.30	0.47		0.41
BOTTOM SALINITY	0.11	0.35	0.33	0.56	0.57	0.45	0.33	0.57	0.41	0.30	0.48		0.41

NOTE: statistics calculated after the spin-up period (hr 5088 - 7296)

Figure 30: Statistical Analysis of With and Without RSLR Differences for the Low Inflow Runs

Results: Effects of 48' Channel Implementation

The effects of the proposed 48' deepening were investigated by running the model with the both the existing channel dimensions (future without project condition) and the 48' channel dimensions. Both runs are run with the "most likely" relative sea level rise of 1.1 ft at the ocean boundary. The results of this analysis are discussed below.

Water Surface Elevation

The average water surface elevation through most of the study area was largely unaffected by the addition of the 48' channel. However, both the amplitude and the average elevation of the tide on the upper Neches River (near the saltwater barrier) exhibit a measurable increase with the 48' channel. A sample of the modeled tidal signal is given in Figure 31. This change in the tidal signal results in an average increase in water surface elevation of 0.067 ft, or 0.8 inches. Water surface elevations both with and without the 48' channel at several observation points throughout the study area are given in Appendix B.

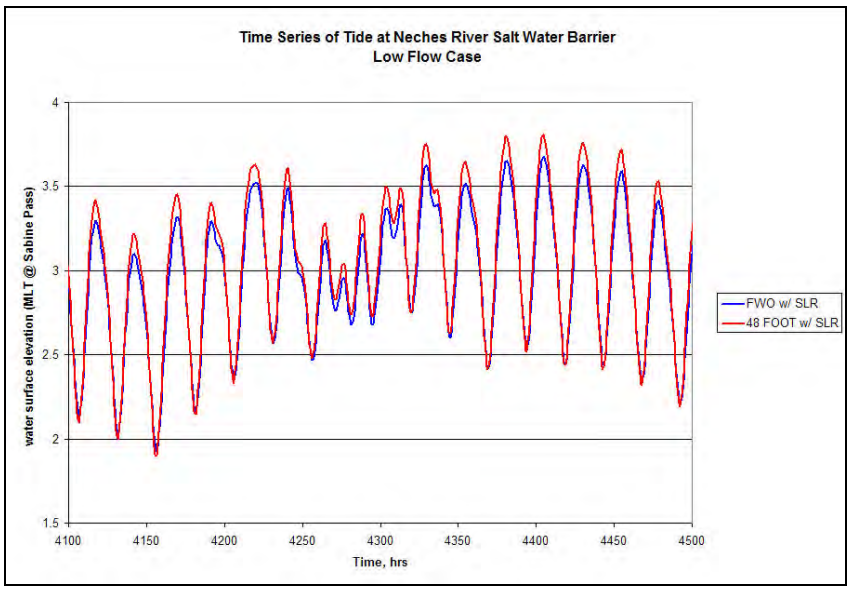

Figure 31: Sample of A Water Surface Elevation Time Series Both With and Without the 48' Channel

Salinity

Figures 42 amd 43 represent color contour plots of the average salinity values for both the with and without the 48' channel. Also, a plot of the salinity difference (plan minus base) is given.

Figures 44 and 45 represent a statistical analysis of the salinity differences between the with and

without 48’ channel runs for both the low and median flow cases at each of the salinity sampling stations used for the calibration and verification of the model. Included in this analysis is an additional station (Station 17) which is located in the GIWW west of the Sabine-Neches Canal, just west of the Taylor Bayou outfall.

The salinity differences range between 0 and 2 ppt. The largest salinity differences tend to conincide with the largest horizontal gradients of salinity. These occur at and just downstream of the leading edge of the salinity wedge in the channels, and along oligohaline-mesohaline transition zones. For the low flow case, these transition zones occur at or near Rose City on the Neches River, the Sabine River at Orange, Texas, and along the eastern shoreline of Sabine Lake. For the median flow case, the transition zones shift further downstream: at Bessie Height on the Neches River, at the GIWW and Keith Lake in the Sabine-Neches canal, and, again, along the eastern shore of Sabine Lake. The following is a sample of some of the highest salinity impacts.

Low Flow:

- Neches River near Rose City (0.7 ppt)
- Sabine River at Orange, Texas (0.9 ppt)
- Eastern Shore of Sabine Lake (1.0 ppt)

Median Flow:

- Neches River near Bessie Heights (1.8 ppt)
- Keith Lake Fish Pass (1.4 ppt)
- Eastern Shore of Sabine Lake (1.4 – 1.6 ppt)

Specific statistics were generated from the salinity analysis to support the Wetlands Value Assessment (WVA) ecological model (USFWS, 2002). The WVA requires input of “mean salinity” during the growing season for the assessment of impacts to brackish and saline habitats, and the "mean high salinity" statistic for impacts to fresh and intermediate habitats. The "mean high salinity" statistic is defined by the WVA as the average of the highest 33 percent consecutive salinity readings taken during a specified period of record. These statistics were provided to the Habitat Evaluation Workgroup of the SNWW ICT for use in predicting future-without project and future with-project conditions.

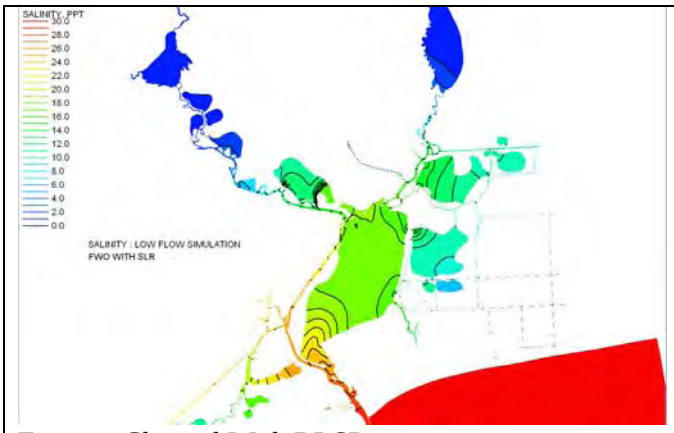

Existing Channel With RLSR
(Contour Range = 0-30 ppt)

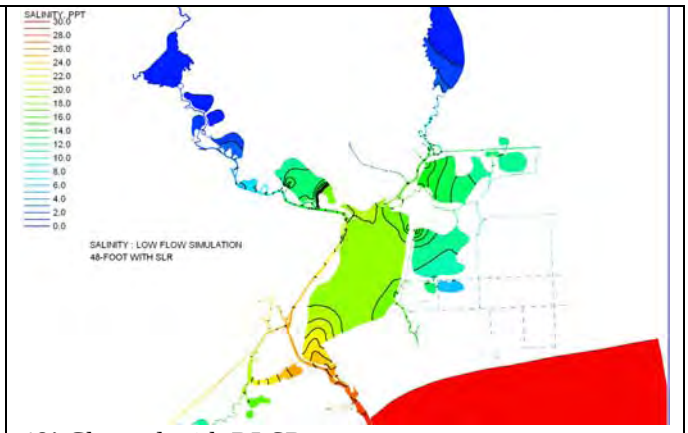

48' Channel with RLSR
(Contour Range= 0-30 ppt)

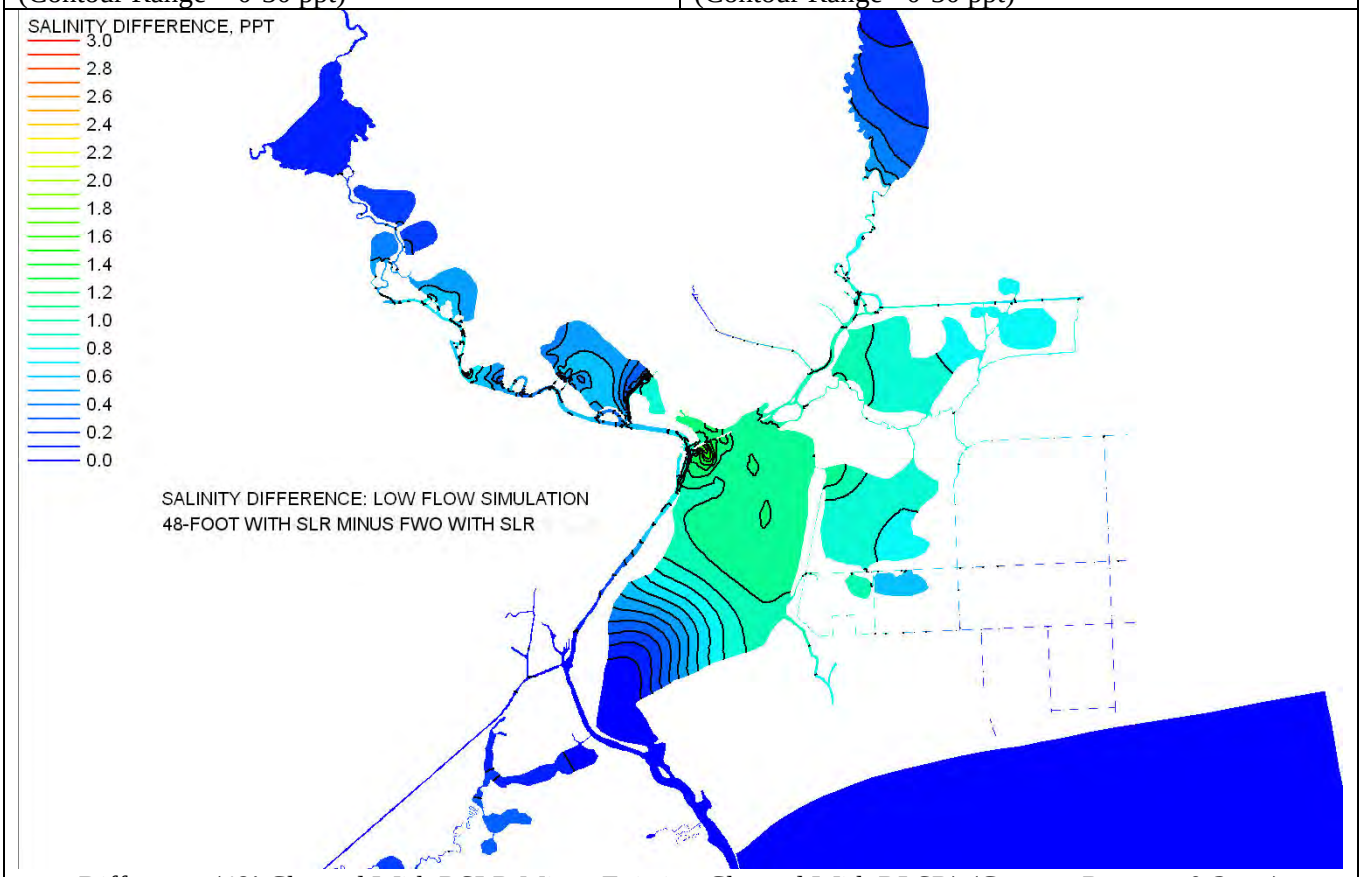

Difference (48' Channel With RSLR Minus Existing Channel With RLSR) (Contour Range = 0-3 ppt)

Figure 42: Average Salinity Conditions for the Existing Channel and the 48' Channel with RLSR, Low Flow Runs

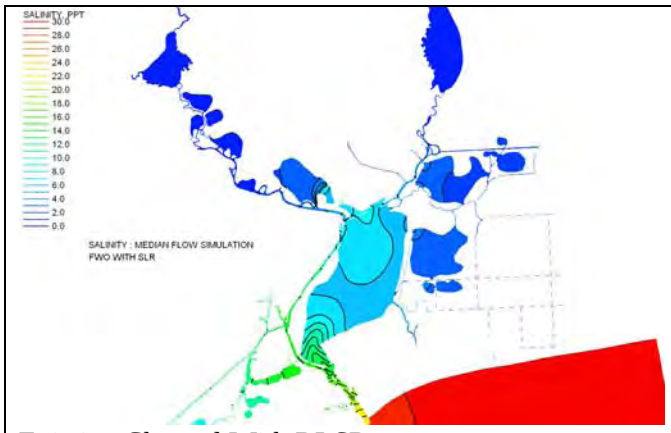

Existing Channel With RLSR
(Contour Range = 0-30 ppt)

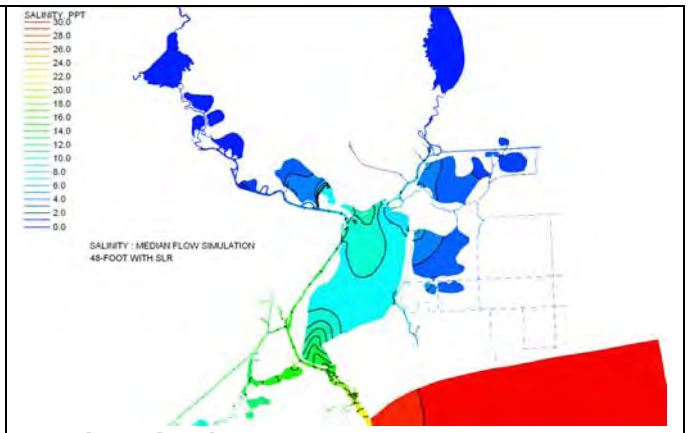

48' Channel with RLSR
(Contour Range= 0-30 ppt)

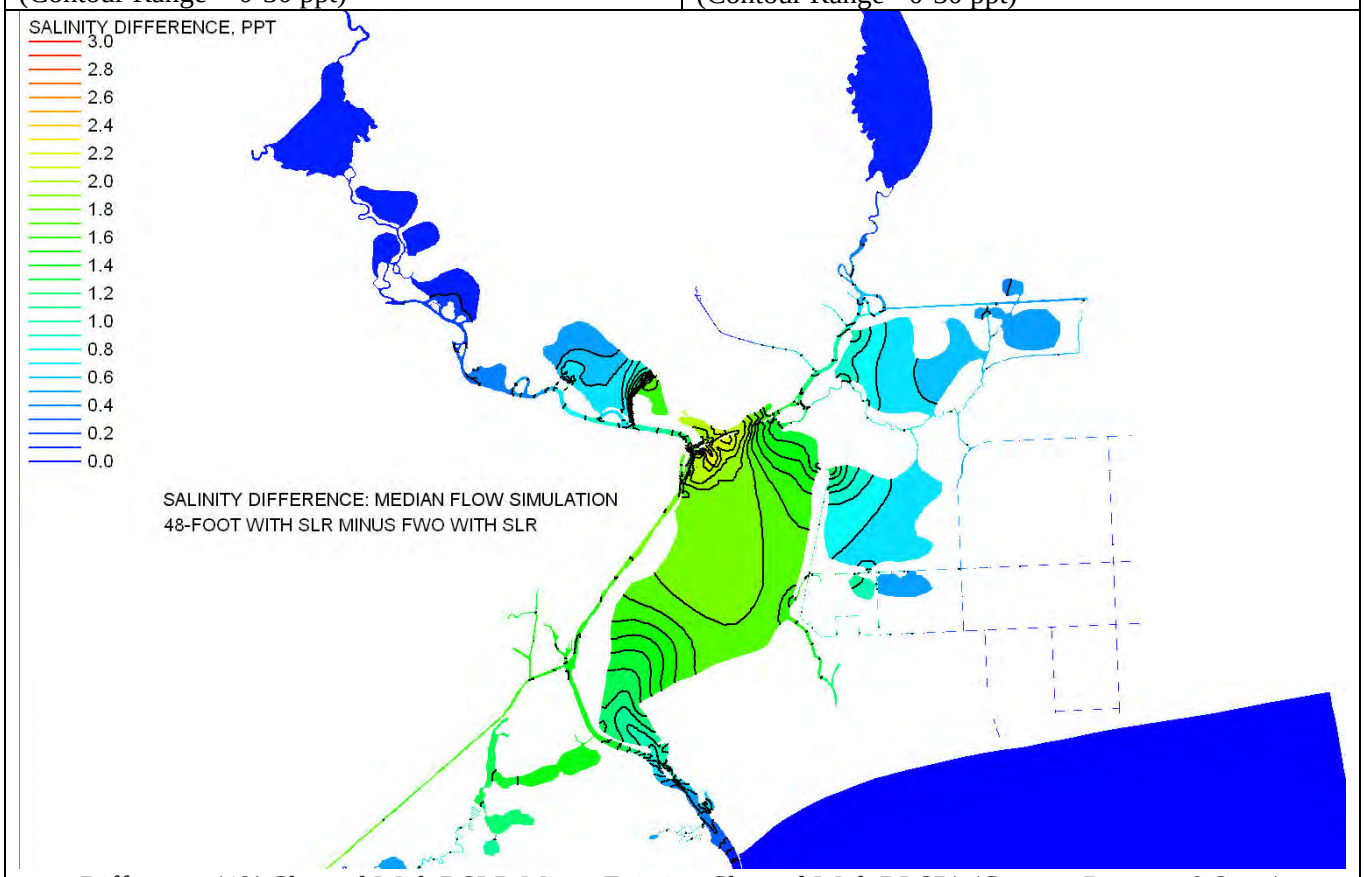

Difference (48' Channel With RSLR Minus Existing Channel With RLSR) (Contour Range = 0-3 ppt)

Figure 43: Average Salinity Conditions for the Existing Channel and the 48' Channel with RLSR, Median Flow Runs

LOW FLOW, FWO WITH SLR AND 48 FOOT CHANNEL WITH SLR

AVERAGE DIFFERENCES

STATION #	1	2	3	5	6	7	9	10	11	14	15	16	17
SURFACE SALINITY	0.14	0.68	0.41	0.89	0.08	-0.31	1.03	-0.10	1.01	0.96	-0.05	1.01	0.02
MIDDEPTH SALINITY	0.14	0.83	0.69	0.68	0.06	-0.25	1.03	-0.11	0.99	0.96	-0.04		0.01
BOTTOM SALINITY	0.14	0.85	0.55	0.58	0.00	-0.21	1.03	-0.12	0.99	0.97	-0.05		0.00

STANDARD DEVIATION OF THE DIFFERENCES

STATION #	1	2	3	5	6	7	9	10	11	14	15	16	17
SURFACE SALINITY	0.15	0.20	0.36	0.49	0.45	0.32	0.17	0.55	0.18	0.13	0.40	0.20	0.23
MIDDEPTH SALINITY	0.15	0.18	0.20	0.32	0.47	0.27	0.17	0.55	0.15	0.13	0.40		0.23
BOTTOM SALINITY	0.15	0.23	0.25	0.35	0.47	0.26	0.17	0.55	0.15	0.14	0.41		0.23

NOTE: statistics calculated after the spin-up period (hr 5088 - 7296)

Figure 44: Statistical Analysis of 48 Foot Channel and Existing Channel Differences for the Low Inflow Runs

MEDIAN FLOW, FWO WITH SLR AND 48 FOOT CHANNEL WITH SLR

AVERAGE DIFFERENCES

STATION #	1	2	3	5	6	7	9	10	11	14	15	16	17
SURFACE SALINITY	**0.00**	**0.13**	**0.79**	**0.23**	**1.60**	**0.11**	**1.37**	**1.18**	**1.09**	**1.61**	**1.41**	**1.38**	**1.62**
MIDDEPTH SALINITY	**0.00**	**0.16**	**1.18**	**0.22**	**1.78**	**0.25**	**1.37**	**1.16**	**1.11**	**1.62**	**1.42**		**1.60**
BOTTOM SALINITY	**0.00**	**0.26**	**1.18**	**0.21**	**1.70**	**0.29**	**1.38**	**1.12**	**1.11**	**1.62**	**1.41**		**1.58**

STANDARD DEVIATION OF THE DIFFERENCES

STATION #	1	2	3	5	6	7	9	10	11	14	15	16	17
SURFACE SALINITY	**0.01**	**0.22**	**0.64**	**0.44**	**1.20**	**1.01**	**0.73**	**0.90**	**0.73**	**0.59**	**0.88**	**0.61**	**0.83**
MIDDEPTH SALINITY	**0.01**	**0.28**	**0.69**	**0.38**	**1.24**	**0.98**	**0.73**	**0.92**	**0.73**	**0.59**	**0.92**		**0.83**
BOTTOM SALINITY	**0.01**	**0.43**	**0.63**	**0.37**	**1.26**	**0.95**	**0.73**	**0.97**	**0.73**	**0.60**	**0.97**		**0.83**

HIGHEST 10% OF DIFFERENCES

STATION #	1	2	3	5	6	7	9	10	11	14	15	16	17
SURFACE SALINITY	**0.01**	**0.55**	**1.63**	**0.91**	**3.04**	**1.53**	**2.26**	**2.14**	**2.01**	**2.42**	**2.47**	**2.24**	**2.79**
MIDDEPTH SALINITY	**0.01**	**0.68**	**1.92**	**0.89**	**3.33**	**1.63**	**2.26**	**2.15**	**2.00**	**2.44**	**2.51**		**2.78**
BOTTOM SALINITY	**0.01**	**1.03**	**1.87**	**0.84**	**3.26**	**1.65**	**2.26**	**2.14**	**2.00**	**2.47**	**2.51**		**2.78**

NOTE: statistics calculated after the spin-up period (hr 2136 - 6552)

Figure 45: Statistical Analysis of 48 Foot Channel and Existing Channel Differences for the Median Inflow Runs

Results: Effects of 45' Channel Implementation

In order to ascertain information concerning the relationship between the extent of deepening and the salinity impacts, a 45' channel deepening option was also run. Results for the median flow case are given in Appendix B. These results show the same general patterns at the 48' results except that the magnitude of the salinity change is the order of 0.2 o 0.4 ppt less.

Note that changing the design depth does not greatly influence the spatial distribution of the salinity change, but only the magnitude of the change. We can use this information to approximate salinity impacts for any design depth within the range already modeled (i.e. less than 48').

The procedure is as follows:

- At a given location, select the modeled salinity change for both the 48 foot and 45 foot conditions.

- Assume the salinity change is 0 for 0 deepening. This yields a third data point.

- Generate a quadratic equation from these three constants, as a function of the deepening. The equation can be easily generated using an EXCEL spreadsheet.

- This equation can be used to predict salinity at the location for which it is developed.

For example, for the median flow condition at the Bessie Heights location, the salinity change for the 48 foot deepening is 0.79 ppt, and for the 45' deepening it is 0.56 ppt. From these data, 3 pairs of deepening and salinity change data points can be generated.

Deepening (design plus average overdepth of 5')	Salinity increase (ppt)
13 (8+5)	0.79
10 (5+5)	0.56
0	0

From these data, the following quadratic equation can be derived.

$$S_I = 0.0016\left(D_C + 5\right)^2 + 0.0401\left(D_C + 5\right) \quad \text{..... (3)}$$

Where:
S_I = the salinity increase for the desired design depth.

D_C = the amount of deepening, in feet.

So, based on this equation, the salinity impact for the median flow condition associated with a deepening of 6' at Bessie Heights would be 0.63 ppt.

These equations should give reasonable estimates of the salinity impacts, without having to model each deepening scenario independently.

Storm Surge Analysis

In order to simulate the impact of the channel deepening project on storm-surge inundation, a boundary tidal signal was generated that was taken from the tidal signal recorded at Sabine Pass during Tropical Storm Frances, which hit the Texas Coast on September 11th, 1998. This signal is given in Figure 46. The rivers were assigned constant inflows, which represent moderate inflow conditions (4000 cfs on the Neches River, 5000 cfs on the Sabine River).

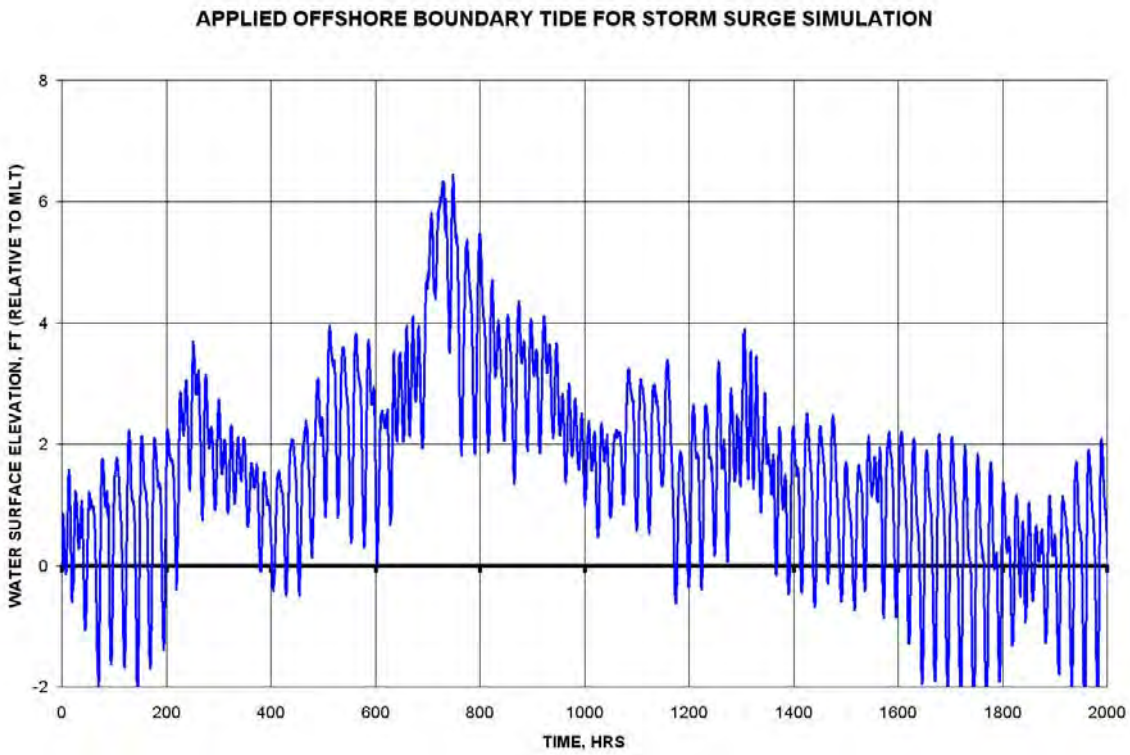

Figure 46: Applied Offshore Boundary tide for Storm Surge Simulation

Figure 47 depicts the maximum storm surge differences observed in the model runs. These occur at or near the peak storm surge, and vary between 0 and 0.4 ft increase in water surface elevation. The plan condition used to generate these storm surge runs included both deepening and widening of the channel, so there runs are conservative with respect to the predictions of impacts: i.e. the impacts should be less than those depicted here.

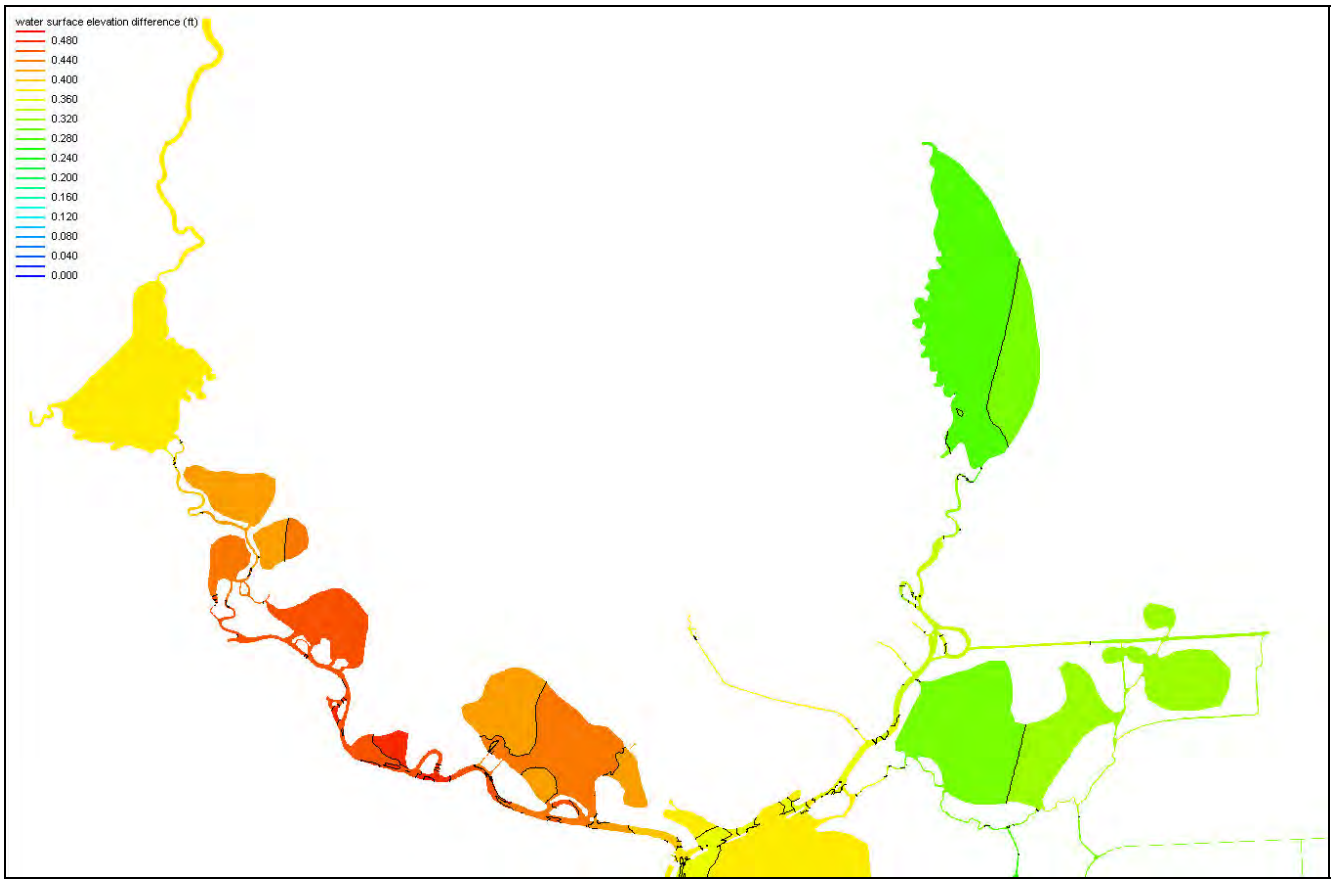

Figure 47: Maximum Water Surface Elevation Difference (Plan Minus Base) Observed at Peak Storm Surge (Contour Interval = 0-0.5 ft

Addendum for Relative Sea Level Rise Analysis: Addressing the Most Recent Corps guidance.

The channel deepening study for the Sabine-Neches Waterway has been updated to include the effects of Relative Sea-Level rise on the project impacts. In consultation with Corps Headquarters, these impacts were included by analyzing both the with and without project conditions for a single "most likely" future sea level rise condition.

Subsequent to the completion of this reanalysis, new Corps guidance has been released. The new Corps of Engineers guidance (EC 1165-2-211, July 2009) specifies the following procedures for incorporating relative sea level rise into the project impacts.

Evaluate alternatives using "low" "intermediate" and "high" rates of future sea-level change.

- Use the historic rate of local mean sea-level change as the "low" rate. (the guidance further states that historic rates of sea level rise are best determined by local tide records).

- Estimate the "intermediate" rate of local mean sea-level change using the modified NRC Curve I. Consider both the most recent IPCC projections and the NRC projections and add those to the local rate of vertical land movement

- Estimate the "high" rate of local mean sea-level change using the modified NRC Curve III Consider both the most recent IPCC projections and the NRC projections and add those to the local rate of vertical land movement

The Modified NRC curves are based on the curves published by the National Research Council in 1987 (NRC 1987) with modifications of the coefficients suggested in the Intergovernmental Panel on Climate Change (IPCC) 4th Assessment Report (AR4) (IPCC, 2007).

The Modified NRC equation is given below:

$$\eta(t) = (0.0017 + M)t + bt^2 \quad \text{.....} \quad (4)$$

Where
$\eta(t)$ = the relative sea level rise for year t (meters)
t = the elapsed time since the baseline year of 1986 (years)
M = the local rate of subsidence (+) or uplift (-) (meters/year)
b = the rate of acceleration of eustatic sea level rise (meters/year^2)

The values of b are chosen such that the sea level due to eustatic rise at year 2100 is equal to 0.5, 1.0, and 1.5 m respectively. These values are given below:

NRC Curve	**b (meters/year^2)**
NRC I	2.35611E-05
NRC II	6.20345E-05
NRC III	1.0051 E-04

This section is intended to address this new guidance, and the impact of this guidance on the study results.

Existing RSLR Analysis

Relative sea level rise consists of two components: global (eustatic) sea level rise, and local subsidence. The eustatic rate was taken from the National Research Council projections (NRC, 1987), as stipulated by Corps guidance (ER1105-2-100; Apr 2000). For the "most likely" case, the NRC Curve II was selected.

The projected rate of local subsidence was difficult to ascertain. Although NOAA tide records and direct observation of land based data indicate subsidence rates of 2-5 mm or higher, long-term data taken from basal peat analysis indicate rates that are an order of magnitude lower than this.

To date, there is no scientific consensus on what the local subsidence rate should be for future

projections. The relative influence of historic anthropogenic activities, such as oil extraction and groundwater withdrawal, are difficult to quantify. If these activities have contributed significantly to recent observations of subsidence, then the cessation of these activities may result in a rapid deceleration of subsidence rates, returning them to the long-term average rates.

For the "most likely" condition, the lower rate of subsidence based on the basal peat analysis (0.5 mm/yr) was selected (Tornqvist et al, 2006). This rate was chosen based on the assumption that the anthropogenic factors thought to contribute significantly to the local subsidence had largely ceased in the 1970's and 1980's and hence the subsidence may be expected to return to the slower long-term average rate.

Using this value of subsidence, together with the NRCII curve from 1987, and assuming a project year 0 = 2019, and a project year 50 = 2069, the value selected for the most likely sea level rise over the project life was 1.1ft.

New RSLR analysis as per the Updated Corps Guidance

According to the most recent guidance, the subsidence rate should be chosen based on the tidal record analysis. However, the regional scientific debate concerning the validity of these tidal records with respect to projection of future subsidence rates indicate that the basal peat rates should also be considered.

Figure 48 gives the computed sea level rise based on the new guidance, for the low (historic) rate, the intermediate (Modified NRC Curve I) rate, and the high (Modified NRC Curve III) rate. The rates are given for subsidence values that correspond to both the observed NOAA tidal gage values (rapid subsidence), and the observed basal peat values (moderate subsidence). For reference, the "most likely" sea level rise used in the model simulations of 1.1. feet is given as well.

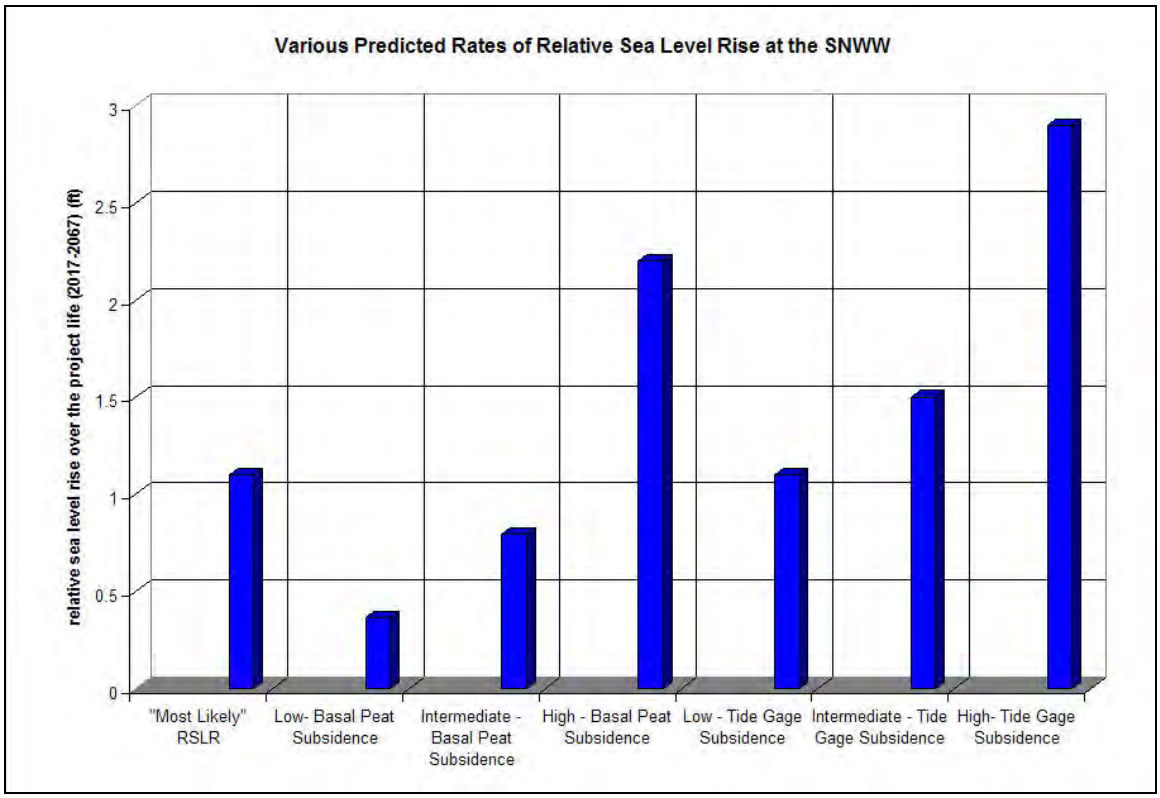

Figure 48: Various Predicted Rates of Relative Sea Level Rise

One can see that the modeled "most likely" rate is between the intermediate and high rates for the moderate subsidence case, and close to the low rate for the high subsidence case. Hence the "most likely" rate is within the range of the rates recommended for consideration in the most recent guidance.

In order to fully consider the impact of these various rates on the salinity modeling results, it would be necessary to model the impacts directly. However, some indication of the potential impacts of the various sea level rise scenarios can be inferred from the existing "most likely" model results, as well as other model results comparing different design deepening scenarios.

In the course of evaluating alternatives, the model was run for both the 45' deepened condition, and the 48' deepened condition. This analysis yields an indication of the relative impacts of deepening, as a function of the degree of deepening.

If one assumes that the impacts of deepening the channel from 45' to 48' are primarily a consequence of a change in the relative depth of the channel (i.e. the percent increase in depth over the existing depth), then one can make the assumption that, for a given design channel depth, the effect of decreasing the mean sea level should be qualitatively similar to the impacts of increasing the channel depth (since a decrease in mean sea level increases the percent change in channel depth).

Therefore, the effects of sea level rise on the project impacts can be qualitatively assessed with the results from the 2 channel deepening scenarios as follows:

- Calculate the difference in the salinity impacts of implementing the 48' channel and the 45' channel. In general, this is should be a salinity increase.
- Assume that this difference in salinity is similar to the difference in salinity one would find if one modeled the 48' channel with a a 3' difference in sea level. In this case, a positive difference would correspond to the lower sea level scenario, since a lower sea level implies a larger change in relative channel depth.
- Then, assuming this change in salinity impact varies linearly with the change in relative depth (and hence the change in sea level) one can generate a prediction of the difference in the salinity impact of the 48' foot project for each of the sea level rise scenarios.

Similarly, if we assume a linear relationship between the change in sea level and the change in salinity, we can generate estimated predictions of the salinity impacts of sea level rise alone (without project) by using the data from the "most likely" scenario to define the slope of the linear curve.

Using these methods, estimated salinity impacts can be generated for each of the sea level rise scenarios. Figure 49 gives the results of this analysis. The blue bars represent the impacts of sea level differences on the absolute salinity, and the green bars represent the impacts of sea level differences on the project impacts. The red bars represent the net impact on salinity, i.e. the sum of the blue and green bars.

For example, if one measured a 1ppt increase in absolute salinity for the "most likely" sea level rise condition (i.e. 1ppt increase including both sea level rise effects and deepening effects), and one wanted to estimate the difference in impact if the sea level rise had been given by the high estimate with tide gage subsidence, one would add 0.95 ppt to the estimated impact (given by the red bar for that sea level rise scenario), making a total estimated impact of 1.95 ppt.

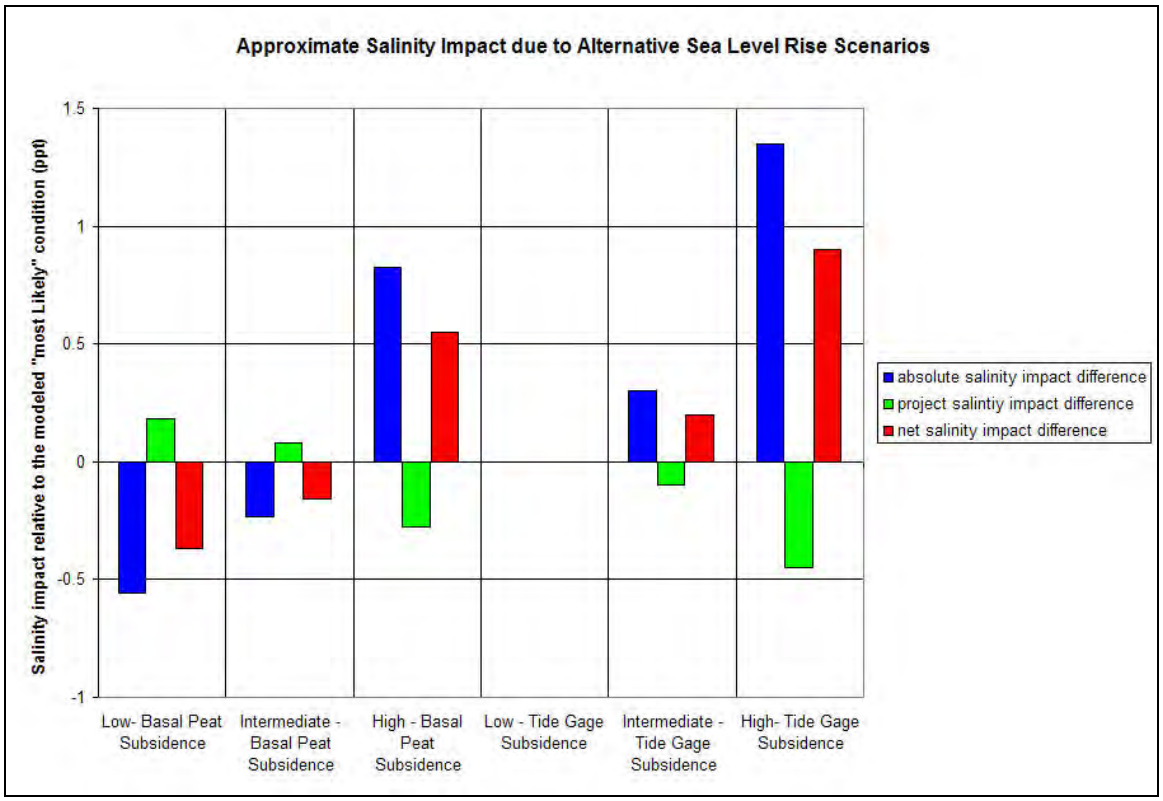

Figure 49: Approximate Effects on Salinity Assuming Alternate Relative Sea Level Rise Scenario.

It must be emphasized that this analysis is approximate, and can only be used to assess relative impacts of various sea level rise scenarios in a general sense. However, despite this constraint, the analysis is useful for estimating the general range of impacts to be expected for various sea level rise scenarios.

Model Analysis of Proposed Salinity Mitigation Alternatives

This chapter contains the results of model simulations design to assess the effectiveness of the proposed salinity mitigation measures.

Description of Proposed Salinity Mitigation Alternatives

Several options were proposed as potential measures to mitigate the impacts of increased salinity in the study area induced by the implementation of the plan channel. For the purposes of analysis, these mitigation measures were divided into 3 groups.

- Large-scale measures (H-S- Model Runs). These are measures that have the potential to impact the entire system.

- Small-scale measures (Desktop Model). that will have principally localized impacts. Many of these small scale measures represent changes to specific wetlands or inlets that are not resolved in the mesh, except as generalized marsh storage elements.

- Measures that do not require analysis with respect to salinity mitigation (Not Modeled) These are measures were not intended for salinity mitigation or it was not necessary to model them because their effect on salinity was prescribed. .

The following table gives a summary of each of these measures:

Table 3. Proposed Mitigation Measures

SNWW Mitigation Measures H-S Model Runs
1. Rose City & Bessie Heights West (Rose City West, TX 3-1 and TX 5-1) – low and median conditions; assume entire acreage of both removed from tidal prism by project yr 1. Total area affected – 1840 ac.
2. Rose City, Bessie Heights West, and Bessie Heights East (Rose City West, TX3-1, TX5-1, TX5-2); – low and median flow conditions; assume entire acreage of all removed from tidal prism by project yr 1.) Total area affected – 5019 acres.
3. Rose City, BHW, BHE and Old River Cove (Rose City West, TX3-1, TX5-1, TX5-2, TX6-1, and Old River Cove East); – low and median flow conditions; assume entire acreage of all removed from tidal prism by project yr 1.) Total area affected – 6670 acres.

SNWW Mitigation Measures Desk-top Model
1. TX8-1- assume logging canal plugged but natural Texas Bayou channel remains open. Median condition only since only affects brackish and saline marshes. Total area affected – 5224 ac.
2. TX8-1A - assume one weir at highway bridge that restricts flow to both the natural Texas Bayou channel and the logging canal. Median condition only since only affects brackish and saline marshes. Effective cross sectional area reduced to 40 x 6. Total area affected – 5224 ac.
3. TX8-1B - assume plugging of logging canal, filling behind canal (11 acres marsh), and a rock weir with 40 x 6 ft cross sectional opening in Texas bayou. Median condition only since only affects brackish and saline marshes. Total area effected – 5224 ac.
2. LA2-14 – 2 rock weirs with boat bays at Sabine Lake mouth of Willow Bayou (affects 11,185 ac) and Three Bayou (affects 6,650 ac); low flow condition only; primarily affects intermediate marsh. Total area affected –17835 ac.
3. LA2-15 – 2 rock weirs with boat bays (Greens Bayou and Right Prong of Black Bayou); low flow condition only, primarily affects intermediate marsh. Total area affected –18,332 ac.
4. LA3-2 – rock weir with boat bay at opening of natural trib just east of Raleigh's ditch on Black Bayou (#2) and plug at small trib opening on west Black Bayou (#6); low flow condition only, primarily affects intermediate marsh. Total area affected – 3056 ac.
5. LA3-3 – Rock liner at mouth of small stream leading south from Black Bayou (#5); low flow condition only, primarily affects intermediate marsh. Total area affected – 1233 ac.
6. LA3-4 – Rock weir with boat bay on small stream leading south from Black Bayou into Sterling Pond (#7); low flow condition only, primarily affects intermediate marsh. Total area affected – 955 ac.
7. LA3-5 – Rock weir at mouth of stream leading north from Black Bayou (#3); low flow condition only, primarily affects intermediate marsh. Total area affected – 321 ac.
8. LA3-7 – Rock liners at 4 large streams leading north from Black Bayou (#9a-9b); low flow condition only, primarily affects intermediate marsh. Total area affected – 1755 ac.
9. LA3-8 – Plug at oil field canal opening on west side of Black Bayou Cutoff Canal (#11); low flow condition only, primarily affects intermediate marsh. Total area affected – 1552 ac.

SNWW Measures Not Modeled
TX7-1 and 7-2 – North GIWW shoreline restoration
TX8-2 – Texas Point –berm and marsh fill behind jetty (acts as plug)
TX8-3 - Texas Point – filling logging canal
TX8-4 – Texas Point – unconfined marsh restoration behind TX8-2
TX8-5 thru 8-11 – Texas Point shoreline nourishment
TX12-1 – Blue Elbow South – plug of logging canal
LA2-1, 2-2 and 3-14 – marsh creation behind East Sabine Lake foreshore dike
LA2-7 – Willow and Three Bayous – adjustable control structures – assumed managed for specific salinity
LA2-8 – Greens Bayou and Right Prong of Black Bayou - adjustable control structures – assumed managed for specific salinity
LA2-16 thru 2-19, 2-ADD – Willow Bayou terracing or marsh restoration
LA2-11 thru 2-13, Willow Bayou – Unit 7 marsh restoration
LA3-1 – Black Bayou adjustable control structure - assumed managed for specific salinity
LA3-6 – Black Bayou sluice gates
LA3-9 thru 3-10, 3-15 thru 3-18 – Black Bayou marsh restoration
LA5-1/6-1, 5-2/6-2, 5-3 thru 5-6 – Louisiana Gulf shoreline nourishment
LATX1 –Sabine Island – plug pipeline canal
LATX2- Blue Elbow Swamp – plug logging canal

Note that the following mitigation measures were modeled using the 50 ft project mesh, and that results were reported to the Habitat Workgroup. These results will not be presented in this report because they were eliminated during preliminary screening.

- Purchasing freshwater flows in the Neches and Sabine Rivers
- Marsh islands separating the Sabine Neches Canal B from Sabine Lake
- Marshes constricting flow at the mouth of Sabine Lake
- Marsh constricting flow along the Port Arthur Canal
- Channel islands blocking flow from bayous emptying Rose City and Bessie Heights marshes
- Marsh restoration in Sabine Lake along the east shores of PA 8 and PA 11

Modeling Approach: TABS-MDS and DOWSMM

The large-scale measures were analyzed using the TABS-MDS model described in this report. The small-scale measures were analyzed using a simple desktop model developed for this project: The Desktop Off-channel Wetland Salinity Mitigation Model (DOWSMM). These small scale model results are given in the report associated with the first SNWW modeling effort, given here as Appendix ???.

Results

TABS-MDS results: General Observations

TABS-MDS Mitigation Runs: These runs feature the reclamation of wetlands in open water areas along the Neches River (mitigation measures 1-3).

Figure 46 contains plots of salinity differences between runs with both mitigation measures 1-3 and the 48' channel, and runs with the 48' channel only. The differences are only significant in the vicinity of the mitigation measures; i.e. in the Neches River.

Note that these runs result in a decrease in salinity in the Neches River. This decrease is due to the fact that the reclamation of the open-water areas along the Neches River effectively reduces the tidal prism that propagates up the river. Hence, the transport of salt water is decreased by decreasing the available storage area for tidal prism. Since there is only one connection to a salt source (the intersection of the Neches River and the Sabine-Neches Canal) the hydraulic behavior of this reach is relatively simple, and can be analyzed in this way.

There is a notable exception to this salinity decrease: a sharp increase in salinity in a portion of Bessie Heights. This is due to the reduction of the power plant discharge area. The power plant discharge is a constant 5000 cfs discharge into Bessie Heights at the ambient salinity of the water (that is, at the salinity of the intake at Old River Cove). Since the flow pathway of this water is constricted by the restored wetlands, the water cannot diffuse as freely and therefore shows a higher salt concentration. Note that this constriction is also the primary reason for the freshening in Bessie Heights in the region that is shielded from the salinity outfall.

Salinity Reduction (Mitigation Run Minus Plan Channel), Median Inflow Contour Interval = 0 to -2.5

Salinity Increase (Mitigation Run Minus Plan Channel), Median Inflow Contour Interval = 0 to 2.5

Figure 46: Salinity Difference Comparisons for the mitigation runs

Habitat Salinity Analysis

The Habitat Evaluation Workgroup will be provided with an extensive quantitative analysis of the model results, for use in evaluating the various mitigation alternatives. These data include the following:

- Percent exceedance plots of salinity (plan salinity, mitigation salinity, and salinity difference) at 34 locations throughout the project area
- Bar Charts of mean salinity at 34 locations throughout the project area
- Bar Charts of the mean value of the highest 33% of continuous salinity at 34 locations throughout the project area
- Salinity difference color contour maps of the TABS-MDS mitigation model runs

- Complete salinity statistics for the spatially averaged salinity for each of the DOWSMM small-scale model runs.
- Complete velocity statistics for the inlet velocity for each of the DOWSMM small-scale model runs.

A sample of both a typical percent exceedance plot and a plot of mean salinity is given in Figure 47. The complete set of mean salinity values and highest 33% continuous salinity values the model runs are given in Appendix B.

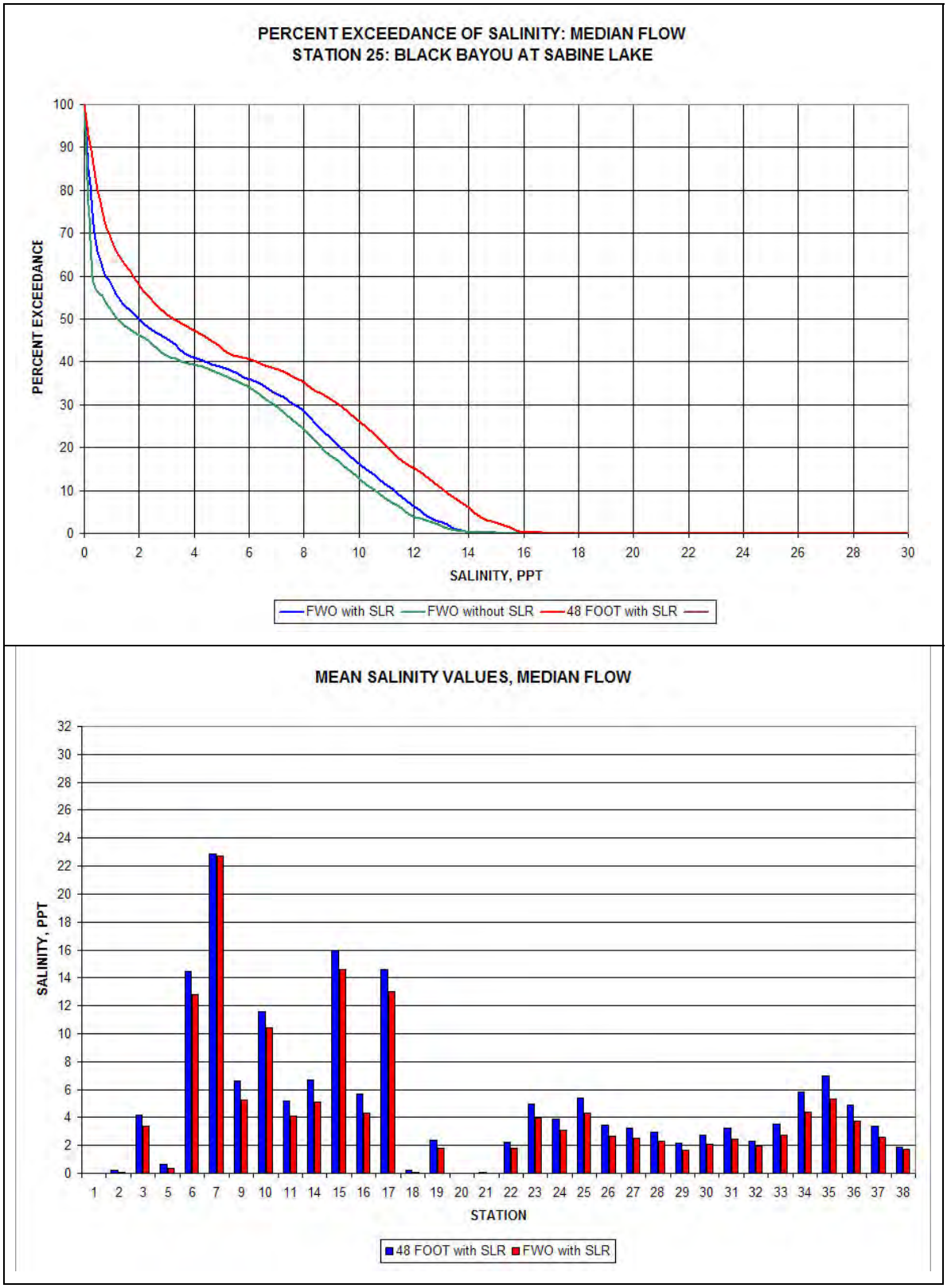

Figure 47: Samples of Habitat Salinity Analysis Data

Conclusions

- The following represents an overview of the conclusions found in this report.

- The TABS-MDS code of ERDC-WES is used for computing hydrodynamics and salinity transport for this study. It is a finite element model, which gives it great flexibility in matching complex geometry. It is capable of both 2D (vertically averaged) and 3D simulation. For this application, 3D resolution was used in the channels and Sabine Lake, and 2D resolution was used in the wetlands and shallow open-water areas.

- The extents of the model domain are given as follows:
    - North to the Neches River at Evadale, TX, and the Sabine River at Ruliff, TX.
    - East to a point approximately mid-way between the Sabine Lake and Calcasieu Lake, including half of the Sabine-Neches Wildlife Refuge
    - South approximately 60 miles into the Gulf of Mexico
    - West to a point approximately mid-way between Sabine Lake and Galveston Bay, including all of the McFaddin National Wildlife Refuge

- The model mesh contains 33,321 surface nodes and 13,035 surface elements.

- The tide comparisons show that the model and field have good agreement with respect to the tidal signal.

- The ADCP discharge comparisons show that the agreement is generally good. The major discrepancies between model and field observations occur at Ranges 6 and 7. The model depicts a somewhat larger tidal prism passing into the Neches River than the field observations show, and the phasing of the discharge though Range 7 is different than that observed in the field.

- The velocity observations show good agreement at most of the gage locations.

- In general, the model duplicates the form of the salinity response well, but it often underpredicts the magnitude. This is especially true on the Neches River. Additional simulations were run with salinity initialized at low flow, and these indicate that the model should perform better under conditions where the flushing and recovery are not especially rapid.

- The “most likely” relative sea level condition at the end of the project life (1069) was chosen as 1.1ft. The addition of this relative sea level rise results in the following locations with the highest salinity changes in the system.

Low Flow:

- Neches River near Bessie Heights and Bessie Heights (2-2.5 ppt)

- Western Shore of Sabine Lake (1.5-2 ppt)

Median Flow:

- Neches River near Bessie Heights and Bessie Heights (1-1.5 ppt)
- Keith Lake Fish Pass (1.5-2 ppt)

- For the proposed 48-foot plan channel condition, highest salinity impacts are found in the following locations.

Low Flow:

- Neches River near Rose City (0.7 ppt)
- Sabine River at Orange, Texas (0.9 ppt)
- Eastern Shore of Sabine Lake (1.0 ppt)

Median Flow:

- Neches River near Bessie Heights (1.8 ppt)
- Keith Lake Fish Pass (1.4 ppt)
- Eastern Shore of Sabine Lake (1.4 – 1.6 ppt)

- Each of these locations corresponds to sensitive environments. This is especially true of the cypress-tupelo swamps on the Neches and Sabine Rivers; the eastern side of Sabine Lake, where Willow Bayou and Johnson's Bayou link the Lake to the Sabine National Wildlife Refuge (SNWR); and Keith Lake Fish Pass which links the navigation channel to the J.D. Murphree Wildlife Management Area.
- Several options were proposed as potential measures to mitigate the impacts of increased salinity in the study area induced by the implementation of the project channel. For the purposes of analysis, these mitigation measures were divided into 3 groups.
    - Large-scale measures (H-S- Model Runs). These are measures that have the potential to impact the entire system.
    - Small-scale measures (Desktop Model). that will have principally localized impacts. Many of these small scale measures represent changes to specific wetlands or inlets that are not resolved in the mesh, except as generalized marsh storage elements.
    - Measures that do not require analysis with respect to salinity mitigation (Not Modeled) These are measures not expected to affect salinity.
- The large-scale measures were analyzed using the TABS-MDS model described in this report. The small-scale measures were analyzed using a simple desktop model developed for this project: The Desktop Off-channel Wetland Salinity Mitigation Model (DOWSMM). These results are described in Appendix ???.
- The mitigation runs results in a decrease in salinity in the Neches River. This decrease is due to the fact that the reclamation of the open-water areas along the Neches River effectively reduces the tidal prism that propagates up the river. Hence, the transport of

salt water is decreased by decreasing the available storage area for tidal prism. Since there is only one connection to a salt source (the intersection of the Neches River and the Sabine-Neches Canal) the hydraulic behavior of this reach is relatively simple, and can be analyzed in this way.

- The Habitat Evaluation Workgroup was provided with an extensive quantitative analysis of the model results, for use in evaluating the various mitigation alternatives.

References

Chow, V. T. (1959) "Open Channel Hydraulics". McGraw-Hill, New York.

Cochrane, J. D., and Kelly, F. J. (1986) "Low-frequency circulation on the Texas-Louisiana continental shelf" Journal of Geophysical Research 91(C9), 10645-1659.

Fagerburg, Tim. (2001) "Field Data Collection Summary Report for the Sabine-Neches Waterway Study" Memorandum For Record, submitted to SWG.

Gammill, S., Balkum, K., Duffy, K., Meselhe, E., Porthouse, J., Ramsey, E., and Walters, R., (2002) "Hydrologic Investigation of the Louisiana Chenier Plan", report prepared for the Louisiana Coastal Wetlands Conservation and Restoration Task Force, by the Louisiana Department of Natural Resources.

Intergovernmental Panel on Climate Change (IPCC). 2007. Climate Change 2007: Synthesis Report. Contribution of Working Groups I, II, and III to the Fourth Assessment Report of the Intergovernmental Panel on Climate Change [Core Writing Team Pachauri, R.K and Reisinger, A. (eds)]. IPCC, Geneva, Switzerland, 104 p.

King, I.P. (1988) "A Finite Element Model for Three-Dimensional Hydrodynamic System", report prepared by Resource Management Associates, Lafayette California, for U.S. Army Corps of Engineers, Waterways Experiment Station, Vicksburg, MS.

King, I.P. (1993). "RMA-10, a finite element model for three-dimensional density stratified flow," Department of Civil and Environmental Engineering, University of California, Davis.

National Research Council (NRC). 1987. Responding to changes in sea level: engineering implications. Commission of Engineering and Technical Systems, National Research Council, National Academy Press, Washington, D.C.

Smagorinsky, J. (1963). "General Circulation Experiments with the Primitive Equations." "Monthly Weather Review", Vol. 93, pp 99 – 165.

Törnqvist, T.E., Bick, S.J., van der Borg, K., and de Jong, A.F.M., 2006, How stable is the Mississippi Delta?: Geology, v. 34, p. 697–700, doi: 10.1130/ G22624.1.

Appendix A

TABS-MDS Introduction

TABS-MDS (Multi-Dimensional, Sediment) is a finite element, hydrodynamic model. It is based on RMA10, a model written by Ian King of Resource Management Associates (King, 1993). It is capable of modeling turbulent, sub-critical flows using 1-D, 2-D, and/or 3-D elements. It is also capable of modeling constituent transport. This includes modeling salinity, temperature, and/or fine-grained sediment. The model is capable of coupling the spatial density variation induced by concentration gradients in the constituent field to the hydrodynamic calculations. This enables the model to simulate phenomena such as saline wedges in estuaries. The model has features that permit the simulation of intermittently wetted regions of the domain, such as coastal wetlands.

TABS-MDS Theoretical Development

<u>3-D Equations</u>

We have 6 unknowns (u,v,w,h,s,ρ). Therefore, we require 6 equations.

The Navier-Stokes Equations (i.e. conservation of fluid momentum)

$$\rho\frac{\partial u}{\partial t}+\rho u\frac{\partial u}{\partial x}+\rho v\frac{\partial u}{\partial y}+\rho w\frac{\partial u}{\partial z}-\frac{\partial}{\partial x}\left(\varepsilon_{xx}\frac{\partial u}{\partial x}\right)-\frac{\partial}{\partial y}\left(\varepsilon_{xy}\frac{\partial u}{\partial y}\right)-\frac{\partial}{\partial z}\left(\varepsilon_{xz}\frac{\partial u}{\partial z}\right)+\frac{\partial p}{\partial x}-\tau_x=0 \quad \text{.....} \quad (1)$$

$$\rho\frac{\partial v}{\partial t}+\rho u\frac{\partial v}{\partial x}+\rho v\frac{\partial v}{\partial y}+\rho w\frac{\partial v}{\partial z}-\frac{\partial}{\partial x}\left(\varepsilon_{yx}\frac{\partial v}{\partial x}\right)-\frac{\partial}{\partial y}\left(\varepsilon_{yy}\frac{\partial v}{\partial y}\right)-\frac{\partial}{\partial z}\left(\varepsilon_{yz}\frac{\partial v}{\partial z}\right)+\frac{\partial p}{\partial y}-\tau_y=0 \quad \text{.....} \quad (2)$$

$$\rho\frac{\partial w}{\partial t}+\rho u\frac{\partial w}{\partial x}+\rho v\frac{\partial w}{\partial y}+\rho w\frac{\partial w}{\partial z}-\frac{\partial}{\partial x}\left(\varepsilon_{zx}\frac{\partial w}{\partial x}\right)-\frac{\partial}{\partial y}\left(\varepsilon_{zy}\frac{\partial w}{\partial y}\right)-\frac{\partial}{\partial z}\left(\varepsilon_{zz}\frac{\partial w}{\partial z}\right)+\frac{\partial p}{\partial z}+\rho g-\tau_z=0 \quad . \quad (3)$$

The Volume Continuity Equation

$$\frac{\partial u}{\partial x} + \frac{\partial v}{\partial y} + \frac{\partial w}{\partial z} = 0 \quad \text{.....} \quad (4)$$

The Advection-Diffusion Equation

$$\frac{\partial s}{\partial t} + u\frac{\partial s}{\partial x} + v\frac{\partial s}{\partial y} + w\frac{\partial s}{\partial z} - \frac{\partial}{\partial x}\left(D_x \frac{\partial s}{\partial x}\right) - \frac{\partial}{\partial y}\left(D_y \frac{\partial s}{\partial y}\right) - \frac{\partial}{\partial z}\left(D_z \frac{\partial s}{\partial z}\right) \quad \text{.....} \quad (5)$$
$$-\theta_s = 0$$

The Equation of State

$$\rho = F(s,t) \quad \text{.....} \quad (6)$$

where:

τ = applied forces (e.g. wind stress, bed shear stress, Coriolis force)

θ_s = salinity source/sink term

Now we reduce the number of unknowns requiring a simultaneous solution from 6 to 3.

Assuming that the influence of vertical momentum on the system is small and may be neglected, equation 3 reduces to the following equation:

$$\frac{\partial p}{\partial z} + \rho g = 0 \quad \text{.....} \quad (7)$$

Equation 7 is a statement that the vertical pressure distribution is hydrostatic.

Equation 4 may then be integrated in the vertical direction to yield the following equation:

$$\int_{a}^{a+h} \left(\frac{\partial u}{\partial x} + \frac{\partial v}{\partial y} \right) d\eta = - \int_{a}^{a+h} \frac{\partial w}{\partial z} d\eta = -w_s + w_b \quad \text{.....} \quad (8)$$

where:

w_s = the vertical velocity at the water surface

w_b = the vertical velocity at the bed

The surface velocity can be expressed as follows:

$$w_s = u_s \frac{\partial (z_b + h)}{\partial x} + v_s \frac{\partial (z_b + h)}{\partial y} + \frac{\partial (z_b + h)}{\partial t} \quad \text{.....} \quad (9)$$

Similarly, the bed velocity can be expressed as:

$$w_b = u_b \frac{\partial z_b}{\partial x} + v_b \frac{\partial z_b}{\partial y} + \frac{\partial z_b}{\partial t} \quad \text{.....} \quad (10)$$

where:

u_s, v_s = the surface horizontal velocity components

u_b, v_b = the near bed horizontal velocity components

z_b = the bed elevation

Note that by replacing equations 3 and 4 with 6 and 8, we recast the equations such that w is present only in the horizontal momentum equations and the advection diffusion equation. It can now be solved in a separate decoupled calculation using the original form of the continuity equation (equation 4). This is done by taking the derivative of equation 4 with respect to z and solving for w, applying w_s and w_b as boundary conditions.

We can further eliminate ρ from the list of unknowns requiring a simultaneous solution by solving the equation of state (equation 6) in a decoupled step.

Thus, we are left with 4 equations (1,2,8 and 5) and 4 unknowns (u,v,h and s) to be solved simultaneously. In practice, however, the solution is broken up into 2 steps: First the velocities and depth are solved simultaneously, and then the constituent concentration is solved. This method improves solution efficiency dramatically over the simultaneous solution of all 4 equations and unknowns.

Hence, the solution of a system of 4 equations and 4 unknowns becomes the solution of a system of 3 equations (1,2, and 8) and 3 unknowns (u,v, and h), followed by the solution of 1 equation (5) and 1 unknown (s).

Geometric transform

In order to use a fixed geometry to model a system with a time varying vertical dimension (depth) it is convenient to use a geometric transformation to map the system to a fixed geometry.

Time varying system

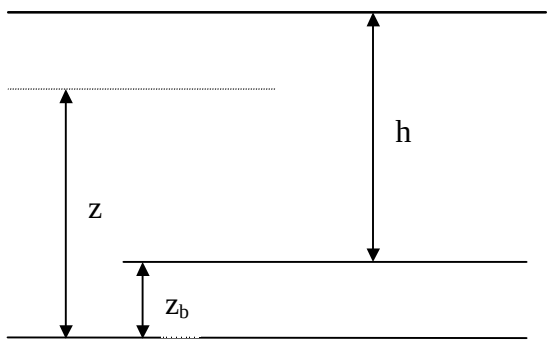

Fixed grid system

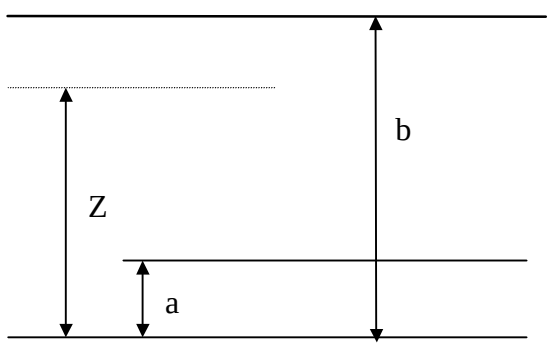

The transformation is based on the following relation:

$$\frac{h}{(z - z_b)} = \frac{(b - a)}{(Z - a)} \quad \text{.....} \quad (11)$$

$$z = \frac{(Z - a)}{(b - a)} h + z_b \quad \text{.....} \quad (12)$$

Hence:

$$U(x,y,z) = u\left(X, Y, \left(\left(\frac{Z-a}{b-a}\right)h + z_b\right)\right) \quad \text{.....} \quad (13)$$

After completing the transformation of the terms and simplifying, we arrive at the following transformed equations:

The Momentum Equations

$$\left\{\begin{array}{l} \rho\left[h\frac{\partial u}{\partial t} + hu\frac{\partial u}{\partial x} + hv\frac{\partial u}{\partial y} + \frac{\partial u}{\partial z}(b-a)\left(w - uT_x - vT_y - \frac{(z-a)}{(b-a)}\frac{\partial h}{\partial t} - \frac{\partial z_b}{\partial t}\right)\right] \\ -h\frac{\partial}{\partial x}\left(\varepsilon_{xx}\frac{\partial u}{\partial x}\right) - h\frac{\partial}{\partial y}\left(\varepsilon_{xy}\frac{\partial u}{\partial y}\right) - (b-a)\frac{\partial}{\partial z}\left(\varepsilon_{xz}\left(\frac{(b-a)}{h}\right)\frac{\partial u}{\partial z}\right) \\ +\rho gh\frac{\partial z_b}{\partial x} + \rho gh\frac{\partial h}{\partial x} + h\frac{\partial p}{\partial x} + \rho gh\frac{\partial h_D}{\partial x} - h\tau_x \end{array}\right\}\frac{1}{(b-a)} = 0 \quad (14)$$

$$\left\{\begin{array}{l} \rho\left[h\frac{\partial v}{\partial t} + hu\frac{\partial v}{\partial x} + hv\frac{\partial v}{\partial y} + \frac{\partial v}{\partial z}(b-a)\left(w - uT_x - vT_y - \frac{(z-a)}{(b-a)}\frac{\partial h}{\partial t} - \frac{\partial z_b}{\partial t}\right)\right] \\ -h\frac{\partial}{\partial x}\left(\varepsilon_{yx}\frac{\partial v}{\partial x}\right) - h\frac{\partial}{\partial y}\left(\varepsilon_{yy}\frac{\partial v}{\partial y}\right) - (b-a)\frac{\partial}{\partial z}\left(\varepsilon_{yz}\left(\frac{(b-a)}{h}\right)\frac{\partial v}{\partial z}\right) \\ +\rho gh\frac{\partial z_b}{\partial y} + \rho gh\frac{\partial h}{\partial y} + h\frac{\partial p}{\partial y} + \rho gh\frac{\partial h_D}{\partial y} - h\tau_y \end{array}\right\}\frac{1}{(b-a)} = 0 \quad (15)$$

Volume Continuity

$$\int_a^b \left[\frac{h}{(b-a)} \left(\frac{\partial u}{\partial x} + \frac{\partial v}{\partial y} \right) - \frac{\partial u}{\partial z} T_x - \frac{\partial v}{\partial z} T_y \right] dz$$

$$+ u_s \frac{\partial (z_b + h)}{\partial x} + v_s \frac{\partial (z_b + h)}{\partial y} + \frac{\partial (z_b + h)}{\partial t} - u_b \frac{\partial z_b}{\partial x} - v_b \frac{\partial z_b}{\partial y} - \frac{\partial z_b}{\partial t} = 0 \text{ .....} \qquad (16)$$

Advection-Diffusion Equation

$$\left\{ \begin{array}{l} h \frac{\partial s}{\partial t} + hu \frac{\partial s}{\partial x} + hv \frac{\partial s}{\partial y} + \frac{\partial s}{\partial z} (b-a) \left(w - uT_x - vT_y - \frac{(z-a)}{(b-a)} \frac{\partial h}{\partial t} - \frac{\partial z_b}{\partial t} \right) \\ - h \frac{\partial}{\partial x} \left(D_x \frac{\partial s}{\partial x} \right) - h \frac{\partial}{\partial y} \left(D_y \frac{\partial s}{\partial y} \right) - (b-a) \frac{\partial}{\partial z} \left(D_z \left(\frac{(b-a)}{h} \right) \frac{\partial s}{\partial z} \right) - h\theta_s \end{array} \right\} \frac{1}{(b-a)} = 0 \qquad (17)$$

where:

$$T_x = \frac{\partial z_b}{\partial x} + \frac{(z-a)}{(b-a)} \frac{\partial h}{\partial x} - \frac{h}{(b-a)} \frac{\partial a}{\partial x} + \frac{(z-a)}{(b-a)^2} h \frac{\partial a}{\partial x} \text{ .....} \qquad (18)$$

$$T_y = \frac{\partial z_b}{\partial y} + \frac{(z-a)}{(b-a)} \frac{\partial h}{\partial y} - \frac{h}{(b-a)} \frac{\partial a}{\partial y} + \frac{(z-a)}{(b-a)^2} h \frac{\partial a}{\partial y} \text{ .....} \qquad (19)$$

$$h_D = -\frac{(b-z)}{(b-a)} h \text{ .....} \qquad (20)$$

2-D Vertically Averaged Equations

If u,v,and s are assumed constant with respect to elevation (z), the 3-D equations can be integrated over depth to yield 2-D vertically averaged equations. For example, the X-momentum equation reduces to the following:

$$\left\{\begin{array}{l} \rho(b-a)\left[h\frac{\partial u}{\partial t}+hu\frac{\partial u}{\partial x}+hv\frac{\partial u}{\partial y}\right] \\ -h(b-a)\frac{\partial}{\partial x}\left(\varepsilon_{xx}\frac{\partial u}{\partial x}\right)-h(b-a)\frac{\partial}{\partial y}\left(\varepsilon_{xy}\frac{\partial u}{\partial y}\right) \\ +\rho gh(b-a)\left(\frac{\partial z_b}{\partial x}+\frac{\partial h}{\partial x}\right)+(b-a)\frac{gh^2}{2}\frac{\partial \rho}{\partial x}-h(b-a)\tau_x \end{array}\right\}\frac{1}{(b-a)}=0 \quad \text{.....} \qquad (21)$$

Similarly, the continuity equation reduces to:

$$h\left(\frac{\partial u}{\partial x}+\frac{\partial v}{\partial y}\right)+u\frac{\partial h}{\partial x}+v\frac{\partial h}{\partial y}+\frac{\partial h}{\partial t}=0 \quad \text{.....} \qquad (22)$$

And the advection-diffusion equation reduces to:

$$\left\{\begin{array}{l} h(b-a)\frac{\partial s}{\partial t}+h(b-a)u\frac{\partial s}{\partial x}+h(b-a)v\frac{\partial s}{\partial y} \\ -h(b-a)\frac{\partial}{\partial x}\left(D_x\frac{\partial s}{\partial x}\right)-h(b-a)\frac{\partial}{\partial y}\left(D_y\frac{\partial s}{\partial y}\right)-h(b-a)\theta_s \end{array}\right\}\frac{1}{(b-a)}=0 \quad \text{.....} \qquad (23)$$

2-D Laterally Averaged Equations

Lateral averaging eliminates the momentum equation in the direction normal to the dominant flow direction. The equations are integrated across the width of the channel. This operation requires that the channel width c is specified. For the purposes of TABS-MDS, the channel width in laterally averaged elements is constrained such that it is constant with respect to depth, but can vary with respect to x and y (i.e. along the channel length). For example, the X-momentum equation reduces to the following.

$$\left\{\begin{array}{l} \rho\left[h\frac{\partial u}{\partial t}+hu\frac{\partial u}{\partial x}+\frac{\partial u}{\partial z}(b-a)\left(w-uT_x-\frac{(z-a)}{(b-a)}\frac{\partial h}{\partial t}-\frac{\partial z_b}{\partial t}\right)\right] \\ -h\frac{\partial}{\partial x}\left(\varepsilon_{xx}\frac{\partial u}{\partial x}\right)-(b-a)\frac{\partial}{\partial z}\left(\varepsilon_{xz}\left(\frac{(b-a)}{h}\right)\frac{\partial u}{\partial z}\right) \\ +\rho gh\frac{\partial z_b}{\partial x}+\rho gh\frac{\partial h}{\partial x}+h\frac{\partial p}{\partial x}+\rho gh\frac{\partial h_D}{\partial x}-h\tau_x \end{array}\right\}\frac{c}{(b-a)}=0 \quad \text{.....} \qquad (24)$$

Similarly, the continuity equation reduces to:

$$\int_a^b\left[\frac{h}{(b-a)}\left(c\frac{\partial u}{\partial x}+u\frac{\partial c}{\partial x}\right)-c\frac{\partial u}{\partial z}T_x\right]dz$$

$$+cu_s\frac{\partial(z_b+h)}{\partial x}+\frac{\partial(z_b+h)}{\partial t}-cu_b\frac{\partial a}{\partial x}-\frac{\partial z_b}{\partial t}=0 \quad \text{.....} \qquad (25)$$

And the advection-diffusion equation reduces to:

$$\left\{\begin{array}{l} h\frac{\partial s}{\partial t}+hu\frac{\partial s}{\partial x}+\frac{\partial s}{\partial z}(b-a)\left(w-uT_x-\frac{(z-a)}{(b-a)}\frac{\partial h}{\partial t}-\frac{\partial z_b}{\partial t}\right) \\ -h\frac{\partial}{\partial x}\left(D_x\frac{\partial s}{\partial x}\right)-(b-a)\frac{\partial}{\partial z}\left(D_z\left(\frac{(b-a)}{h}\right)\frac{\partial s}{\partial z}\right)-h\theta_s \end{array}\right\}\frac{c}{(b-a)}=0 \quad \text{.....} \qquad (26)$$

1-D Equations

Under this approximation both vertical and lateral integration are applied. Hence, the form of the cross-section must be defined. In TABS-MDS, the cross section is assumed trapezoidal, with allowance made for off-channel storage.

For example, the X-momentum equation reduces to the following:

$$\left\{\begin{array}{l} \rho\left[A\frac{\partial u}{\partial t} + Au\frac{\partial u}{\partial x}\right] \\ -A\frac{\partial}{\partial x}\left(\varepsilon_{xx}\frac{\partial u}{\partial x}\right) \\ +\rho gA\frac{\partial z_b}{\partial x} + \rho gA\frac{\partial h}{\partial x} + \frac{gAh}{2}\frac{\partial \rho}{\partial x} - A\tau_x \end{array}\right\} = 0 \quad \text{.....} \qquad (27)$$

Similarly, the continuity equation reduces to:

$$A\left(\frac{\partial u}{\partial x}\right) + u\frac{\partial A}{\partial x} + \frac{\partial(A + A_{OC})}{\partial t} = 0 \quad \text{.....} \qquad (28)$$

And the advection diffusion equation reduces to:

$$\left\{(A + A_{OC})\frac{\partial s}{\partial t} + A\frac{\partial s}{\partial x} - A\frac{\partial}{\partial x}\left(D_x\frac{\partial s}{\partial x}\right) - A\theta_s\right\} = 0 \quad \text{.....} \qquad (29)$$

where:

A = The main channel cross-sectional area

A_{OC}= The off-channel storage cross-sectional area

Finite Element Formulation

In order to generate the finite element equations, we must integrate each of the equations over the element volume (for 3-D), area (for 2-D), or length (for 1-D), remembering to include the weight function in the integration (which, for the Galerkin method, is the same as the basis function).

In addition, we must recast the higher-order terms using integration by parts. This causes the boundary terms to drop out of the equations. For example,

Take the following pressure term, multiplied through by a weight function N.

$$N\frac{\rho gh}{(b-a)}\frac{\partial h}{\partial x} \quad \text{.....} \quad (30)$$

This can be rewritten as:

$$N\frac{\rho g}{2(b-a)}\frac{\partial h^2}{\partial x} \quad \text{.....} \quad (31)$$

Then , it can be integrated by parts:

$$\begin{aligned} N\frac{\rho g}{2(b-a)}\frac{\partial h^2}{\partial x} &= \frac{\partial}{\partial x}\left(N\frac{\rho gh^2}{2(b-a)}\right) - \frac{\partial N}{\partial x}\left(\frac{\rho gh^2}{2(b-a)}\right) \\ &- N\frac{gh^2}{2(b-a)}\frac{\partial \rho}{\partial x} - N\frac{\rho gh^2}{2(b-a)^2}\frac{\partial a}{\partial x} \end{aligned} \quad \text{.....} \quad (32)$$

Note that the first term on the right hand side of the equation can be evaluated as an area integral via the Gauss Divergence Theorem. Hence, it becomes a boundary term.

Time Derivative Solution Method

The time derivative is approximated with a simple, fully-implicit finite difference formulation. I.e.,

$$\frac{\partial \beta_t}{\partial t} = \frac{(\beta_t - \beta_{t-\Delta t})}{\Delta t} \quad \text{.....} \quad (33)$$

where:

β_t = any of the unknown variables at time t.

Δt = the time step

Newton-Rhapson Implementation

Once the finite element equations are built, they are solved using the Newton-Rhapson iterative method. In order to do this, partial derivatives with respect to each of the unknown variables must be derived for each system equation. These derivatives compose the stiffness matrix, and are used to drive the residual (i.e. the integral of each equation across an element) to 0.

$$\begin{bmatrix} X_u Y_u Z_u \\ X_v Y_v Z_v \\ X_h Y_h Z_h \end{bmatrix} \begin{bmatrix} u \\ v \\ h \end{bmatrix} = \begin{bmatrix} X \\ Y \\ Z \end{bmatrix} \quad \text{.....} \quad (34)$$

Expressions for Applied Loads and Turbulent Mixing

Bed Shear Stress

The bed shear stress is given by a modified form of Manning's Equation, as given by Christensen (1970). Any of 3 expressions can be used, depending on the instantaneous value of the depth/roughness height ratio ($\frac{d}{k}$). The expressions are as follows (given for the X-direction only):

$$\text{for } \frac{d}{k} < 4.32 \qquad \tau_x = \frac{\rho g}{L^2}\frac{|v|v_x}{d^{2/3}} \quad \text{where } L = \frac{6.46\sqrt{g}}{k^{1/3}} \quad \text{.....} \qquad (35)$$

$$\text{for } 4.32 < \frac{d}{k} < 276 \quad \tau_x = \frac{\rho g}{M^2}\frac{|v|v_x}{d^{1/3}} \quad \text{where } M = \frac{8.25\sqrt{g}}{k^{1/6}} \quad \text{.....} \qquad (36)$$

$$\text{for } \frac{d}{k} > 276 \qquad \tau_x = \frac{\rho g}{N^2}\frac{|v|v_x}{d^{1/6}} \quad \text{where } N = \frac{13.18\sqrt{g}}{k^{1/12}} \quad \text{.....} \qquad (37)$$

where:

τ_x = the bed shear in the X-direction

k = the roughness height

d = the local depth

v = the local velocity

g = the gravitational constant

ρ = the density of water

k is found as a function of Manning's n from the following expression:

$$k = \left(\frac{8.25\sqrt{g}\ n}{1.486} \right)^6 \quad \text{.....} \quad (38)$$

The Wind Stress

The wind stress is given by the following expression (given for the X-direction only):

$$\tau_{wx} = \rho_a C_w V_w^2 \cos\theta_w \quad \text{.....} \quad (39)$$

where:

τ_{wx} = the wind stress in the X-direction

ρ_a = the density of air

V_w = the wind velocity

θ_w = the direction from which the wind is blowing, measured counterclockwise from the positive X- axis.

C_w = the wind stress coefficient

For deep water, the wind stress coefficient is given by Wu (1980).

$$C_w = \frac{0.8 + 0.065 \times V_w}{1000} \quad \text{.....} \quad (40)$$

For shallow water, the wind stress is given by Teeter et. al., (2001)

$$C_w = \left(\frac{0.4}{16.11 - 0.5\ln(d) - 2.48\ln(V_w)} \right)^2 \times \left(1 - \frac{1.118}{\sqrt{V_{w1}}} e^{-.6(d_1 - 2)} \right) \quad \text{.....} \quad (41)$$

where:

d = the local water depth (in meters)

d_1 = the maximum of the local water depth (in meters) and 2 meters

V_{w1} = the maximum of the wind velocity (in m/s) and 5.063 m/s

Horizontal Turbulent Mixing and Diffusion

Horizontal Turbulent mixing can be specified directly, or it can be controlled by the method of Smagorinsky (1963). A descripttion of this method follows.

The Smagorinsky method of describing horizontal eddy viscosities and diffusion coefficients is a "tensorially invariant generalization of the mixing length type representation" (Speziale, 1998). The Smagorinsky description of the turbulent mixing terms in the Navier-Stokes Equations are given as follows. For the x-momentum equation

$$\rho h \frac{\partial}{\partial x}\left(2S\frac{\partial u}{\partial x}\right) + \rho h \frac{\partial}{\partial y}\left(S\left(\frac{\partial u}{\partial y} + \frac{\partial v}{\partial x}\right)\right) \quad \text{.....} \quad (42)$$

For the y momentum equation

$$\rho h \frac{\partial}{\partial y}\left(2S\frac{\partial v}{\partial y}\right) + \rho h \frac{\partial}{\partial x}\left(S\left(\frac{\partial u}{\partial y} + \frac{\partial v}{\partial x}\right)\right) \quad \text{.....} \quad (43)$$

where:

$$\text{.....} \quad S = kA\left[\left(\frac{\partial u}{\partial x}\right)^2 + \left(\frac{\partial v}{\partial y}\right)^2 + \frac{1}{2}\left(\frac{\partial u}{\partial y} + \frac{\partial v}{\partial x}\right)^2\right]^{\frac{1}{2}} \quad (44)$$

k = Smagorinsky coefficient, usually given a value ranging from approximately 0.005 for rivers to 0.05 for estuaries and lakes (Speziale, 1998; Thomas et al, 1995)

A = the surface area of the element

The Smagorinsky description of the turbulent diffusion terms in the advection-diffusion equation is given as follows:

$$h\frac{\partial}{\partial x}\left(2S\frac{\partial C}{\partial x}\right)+h\frac{\partial}{\partial y}\left(2S\frac{\partial C}{\partial y}\right) \quad (45)$$

In order to promote numerical stability, TABS-MDS provides a means of establishing minimum values of turbulent mixing and turbulent diffusion. These values are used in place of the Smagorinsky term (S) when they are found to exceed the value of that term. The minimum turbulent mixing value is given by the following equation:

$$S_{Emin} = TBMINF \times \rho\alpha\sqrt{A} \quad (46)$$

The minimum turbulent diffusion value is given by the following equation:

$$S_{Dmin} = TBMINFS \times \alpha\sqrt{A} \quad (47)$$

where

TBMINF = minimum turbulent mixing factor (default = 1.0)

TBMINFS = minimum diffusion factor (default = 1.0)

α = a coefficient, given as 5.00×10^{-3} ft/sec or 1.52×10^{-3} m/s, depending on the unit system being used in the simulation. This value is an arbitrary estimate of the minimum turbulent mixing needed to ensure model stability. It equals the value of eddy viscosity/diffusion which corresponds to a Peclet number of 40 and a velocity magnitude of 0.2 ft/sec.

Also, if $|V| < TBMINF \times V_{min}$, S_{Emin} is applied, regardless of the turbulent mixing as given by the Smagorinsky calculation. This is done to inhibit numerical instability in areas with both extremely small velocities and high velocity gradients.

Vertical Turbulent Mixing and Diffusion

Vertical turbulent mixing and diffusion are given by the method of Mellor-Yamada (1982) with a modification according to Hendersen-Sellers (1984).

The Mellor-Yamada expressions for vertical eddy viscosity and diffusion are given as follows:

$$E_{xz} = E_{yz} = \rho S_m l_m q \quad \text{.....} \quad (48)$$

$$D_z = S_h l_m q \quad \text{.....} \quad (49)$$

where:

$$l_m = 0.4(z-a)\left|1 - \frac{(z-a)}{h}\right|^{\frac{1}{2}} \quad \text{.....} \quad (50)$$

$$q = \left\{ b_1 l^2{}_m S_m \left[\left|\frac{\partial u}{\partial z}\right|^2 + \left|\frac{\partial v}{\partial z}\right|^2 \right] \right\}^{\frac{1}{2}} \quad \text{.....} \quad (51)$$

$S_m = 0.393$

$S_h = 0.494$

$b_1 = 16.6$

The Henderson-Sellers adjustment is a factor that accounts for the dampening affect on turbulence induced by stable stratification. The factor is expressed in terms of the Richardson Number:

$$R_i = \frac{-g(\partial\rho/\partial z)}{\rho\left[\left(\frac{\partial u}{\partial z}\right)^2 + \left(\frac{\partial v}{\partial z}\right)^2\right]} \quad \text{.....} \quad (52)$$

For vertical diffusion of momentum (i.e. vertical eddy viscosity) the expression is given as follows:

$$E_z = \frac{E_{zo}}{\left(1 + 0.74R_i\right)} \quad \text{.....} \quad (53)$$

Where E_z is the vertical eddy viscosity, and E_{zo} is the vertical eddy viscosity assuming no stratification influence on the turbulence (i.e. the value taken from Mellor-Yamada).

For vertical diffusion of salinity (i.e. vertical diffusion coefficient) the expression is given as follows:

$$D_z = \frac{D_{zo}}{\left(1 + 37R_i^2\right)} \quad \text{.....} \quad (54)$$

Where D_z is the vertical diffusion coefficient, and D_{zo} is the vertical diffusion coefficient assuming no stratification influence on the turbulence (i.e. the value taken from Mellor-Yamada).

References

Christensen, B. A. (1970) *Manning's n For Cast-In-Place Concrete Pipe; Discussions by Bent A. Christensen, and R. Sakthivadivel, S. Seetharaman and M.V. Somasundaram*, Journal of the Hydraulics Division, Proceedings of the American Society of Civil Engineers, Vol. 96, No. HY3.

Henderson-Sellers, B. (1984) *Engineering Limnology*, Pitman Advanced Publishing, Boston, pp 81-91.

King, I.P. (1988) *A Finite Element Model for Three Dimensional Hydrodynamic Systems*, Report prepared by Resource Management Associates, Lafayette California, for U.S. Army Corps of Engineers, Waterways Experiment Station, Vicksburg, Mississippi.

Mellor, G.L. and Yamada, T. (1982) *Development of a Turbulence Closure Model for Geophysical Fluid Problems*, Reviews of Geophysics and Space Physics, Vol20, No.4, pp 851-875.

Smagorinsky, J. (1963) *General Circulation Experiments with the Primitive Equations, I. The Basic Experiment*, Monthly Weather Review, 91, 99-164.

Speziale, Charles G. (1998) *Turbulence Modeling for Time-Dependent RANS and VLES: A Review*, AIAA Journal, Vol 36, No 2, pp 173-184.

Teeter, A. M., Johnson, B. H., Berger, C., Stelling, G., Scheffner, N. W., Garcia, M. H., Parchure, T. M.,(2001) *Hydrodynamic and Sediment Transport Modeling With Emphasis on Shallow-water, Vegetated Areas (Lakes, Reservoirs, Estuaries, and Lagoons)*. Hydrobiologia 444: 1-23.

Thomas, T.G., Williams, J.R.R. (1995) *Large Eddy Simulation of a Symmetric Trapezoidal Channel at a Reynolds Number of 430,000*, Journal of Hydraulic Research, Vol 33, No 6, pp 825-830.

Appendix B

Water Surface Elevation and Salinity Results

Observation Station Locations

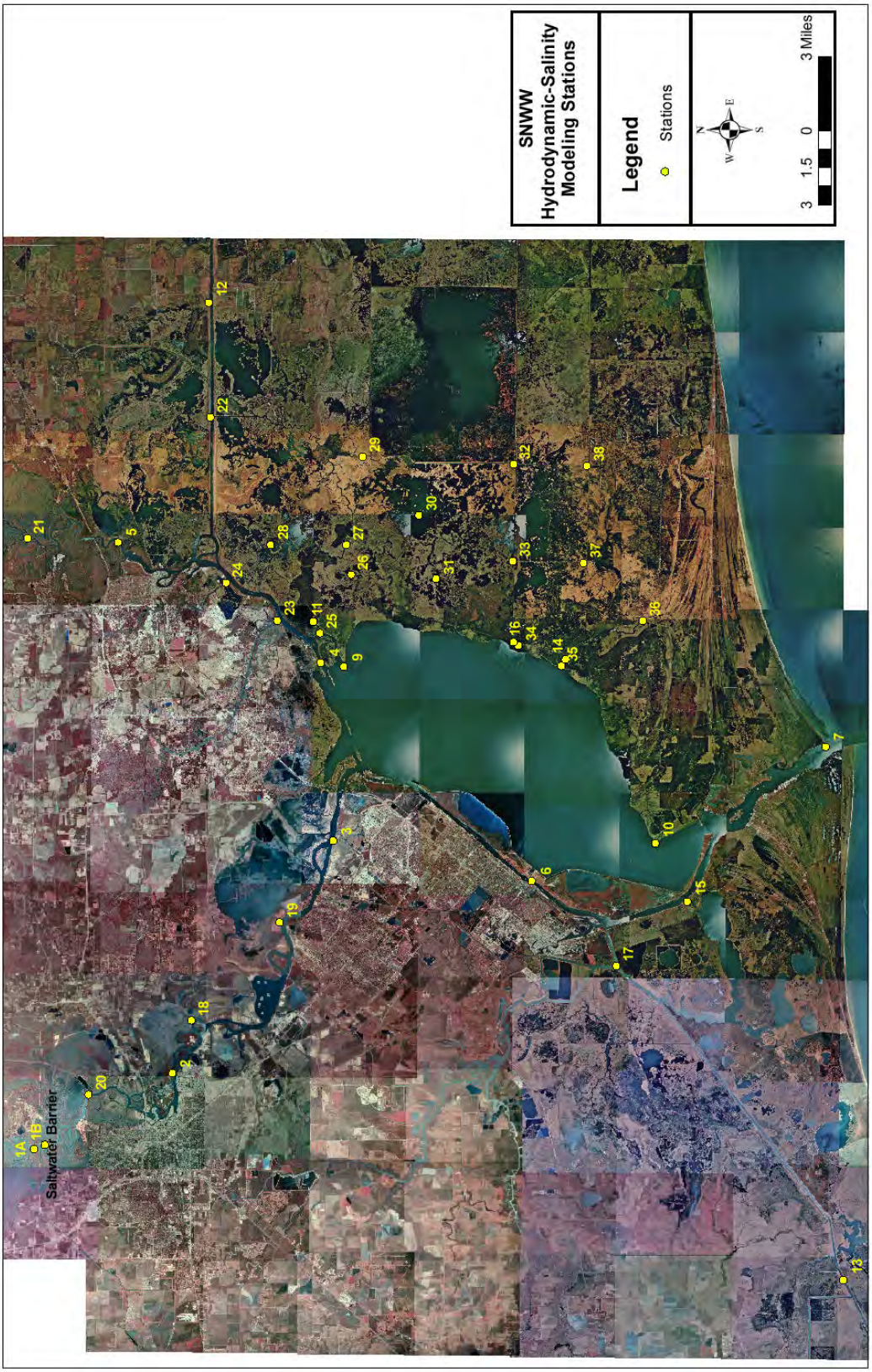

Water Surface Elevation Results

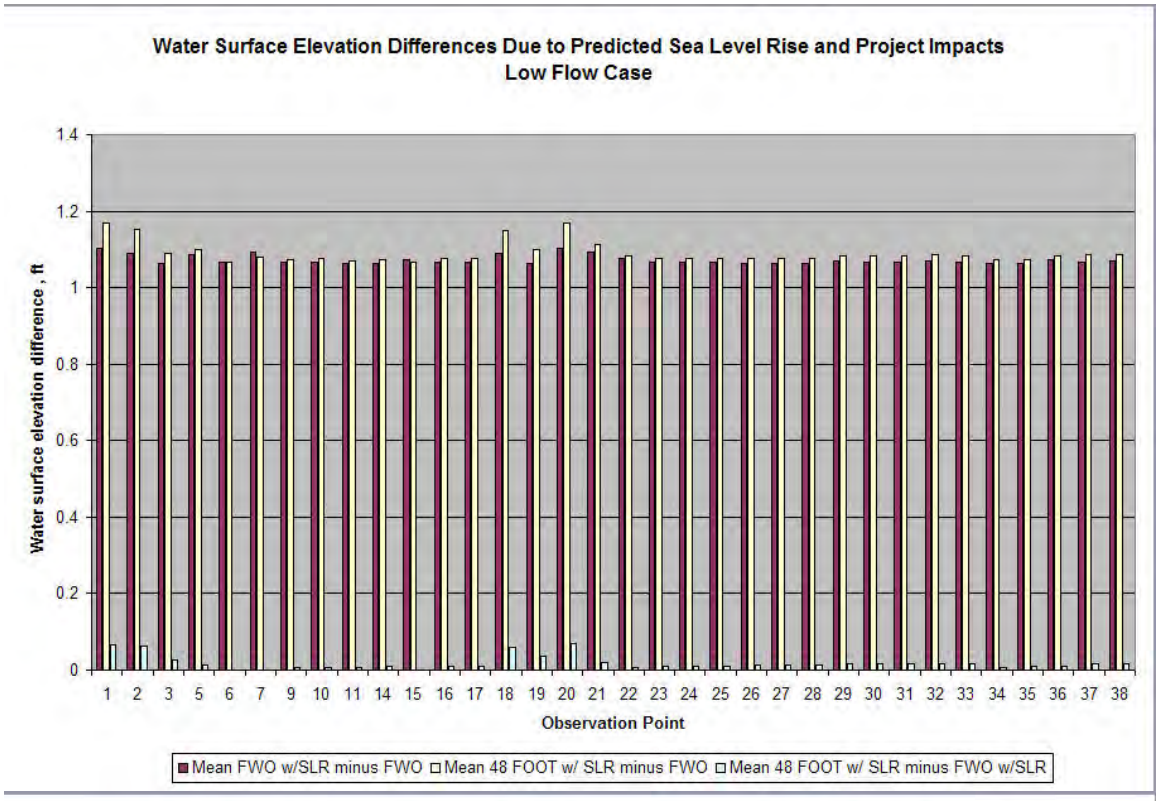

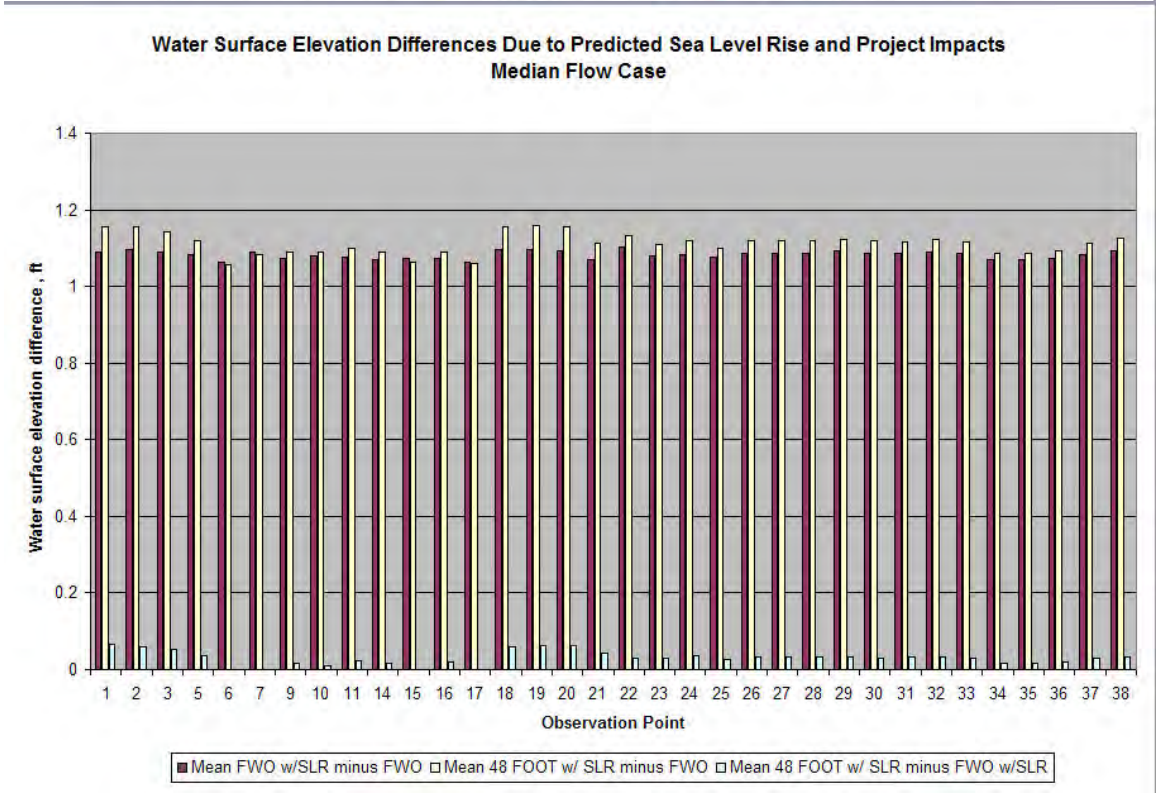

Base (with and without RSLR) and Plan Conditions

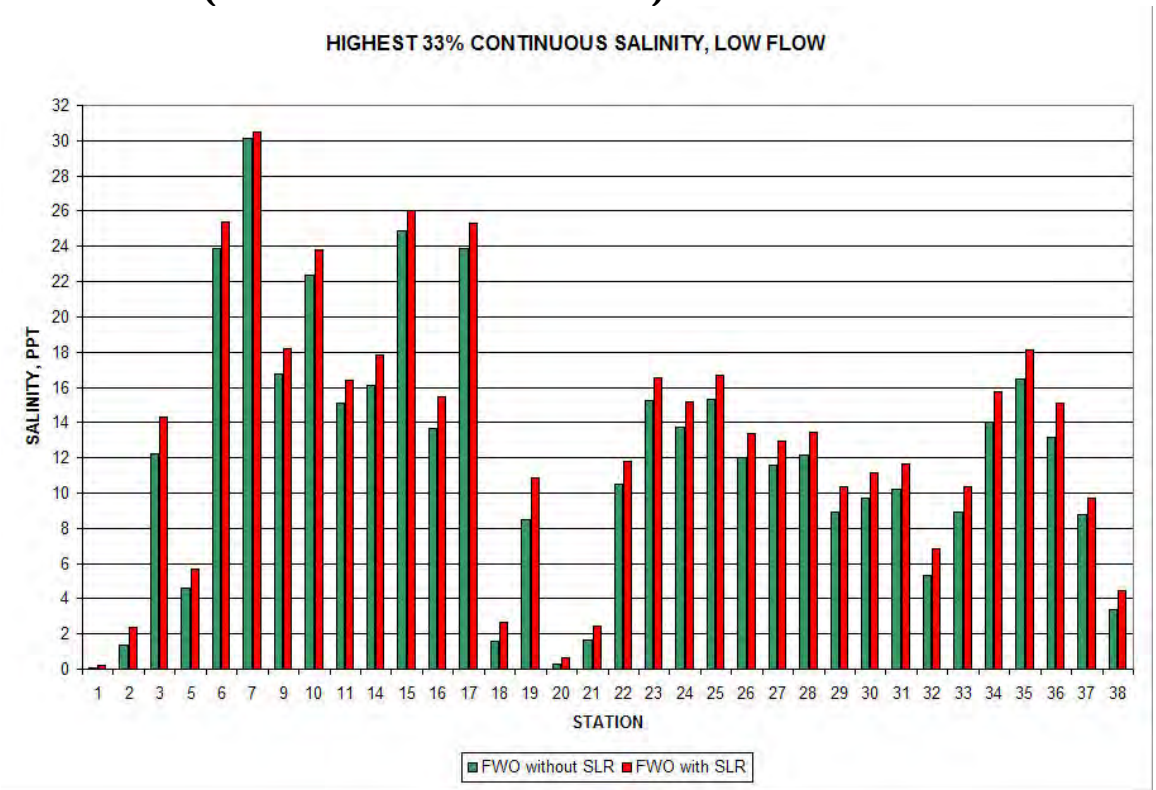

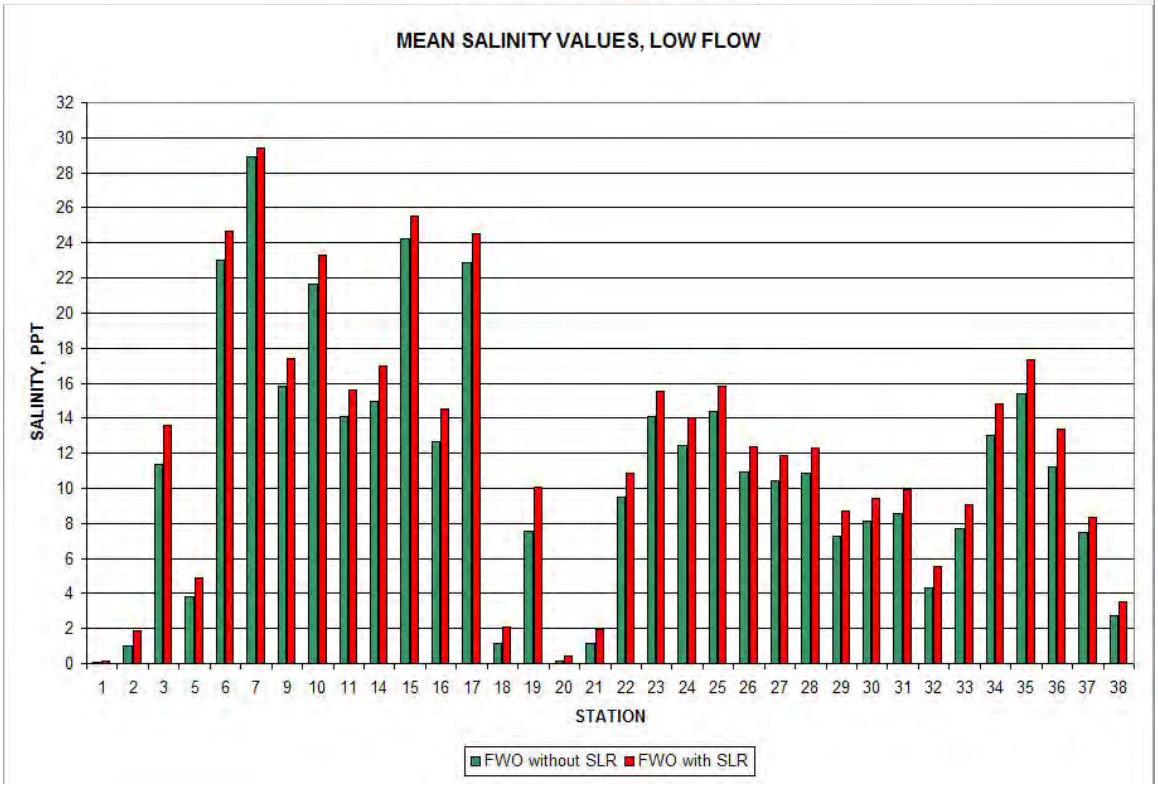

Base (with and without RSLR) and Plan Conditions

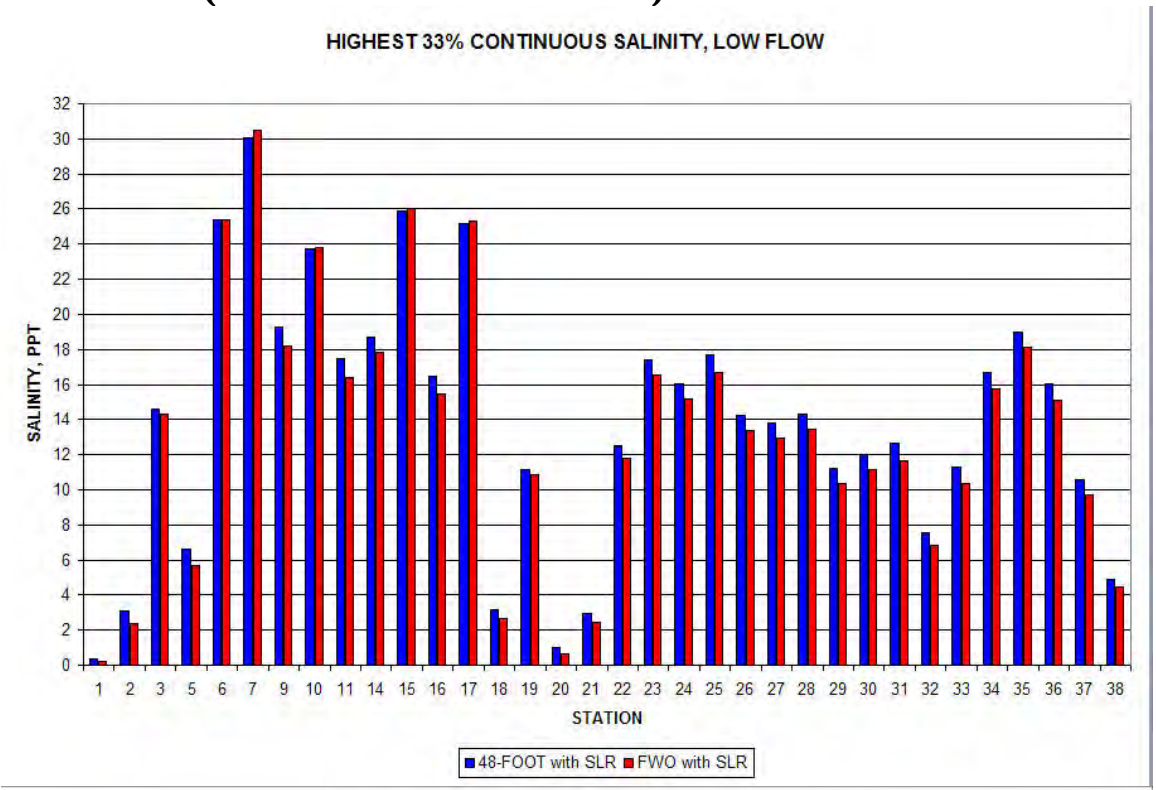

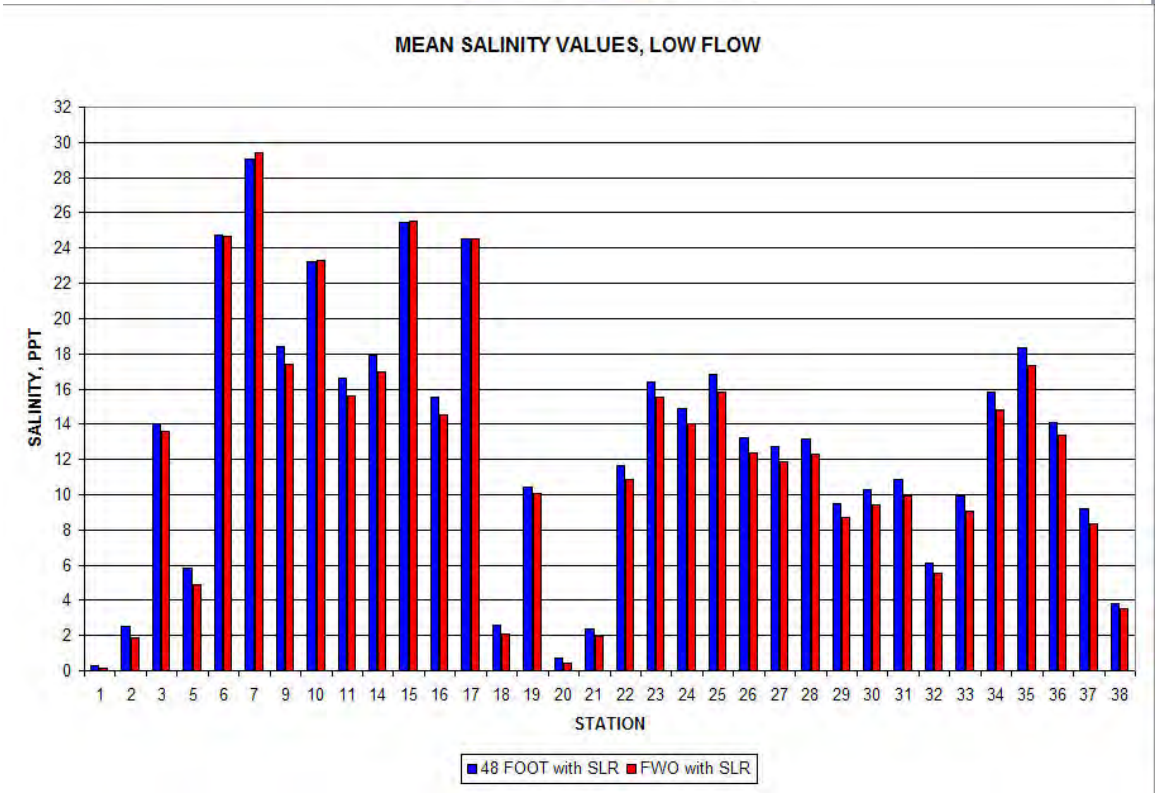

Base (with and without RLSR) and Plan Conditions

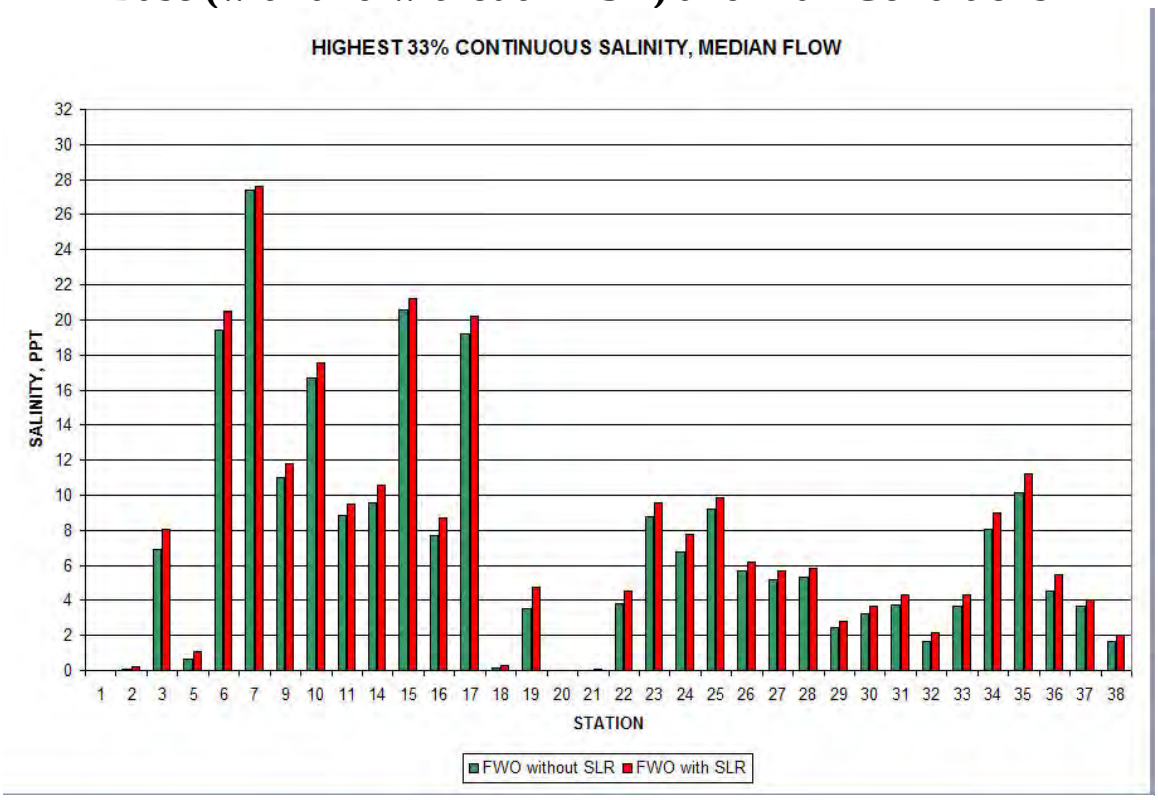

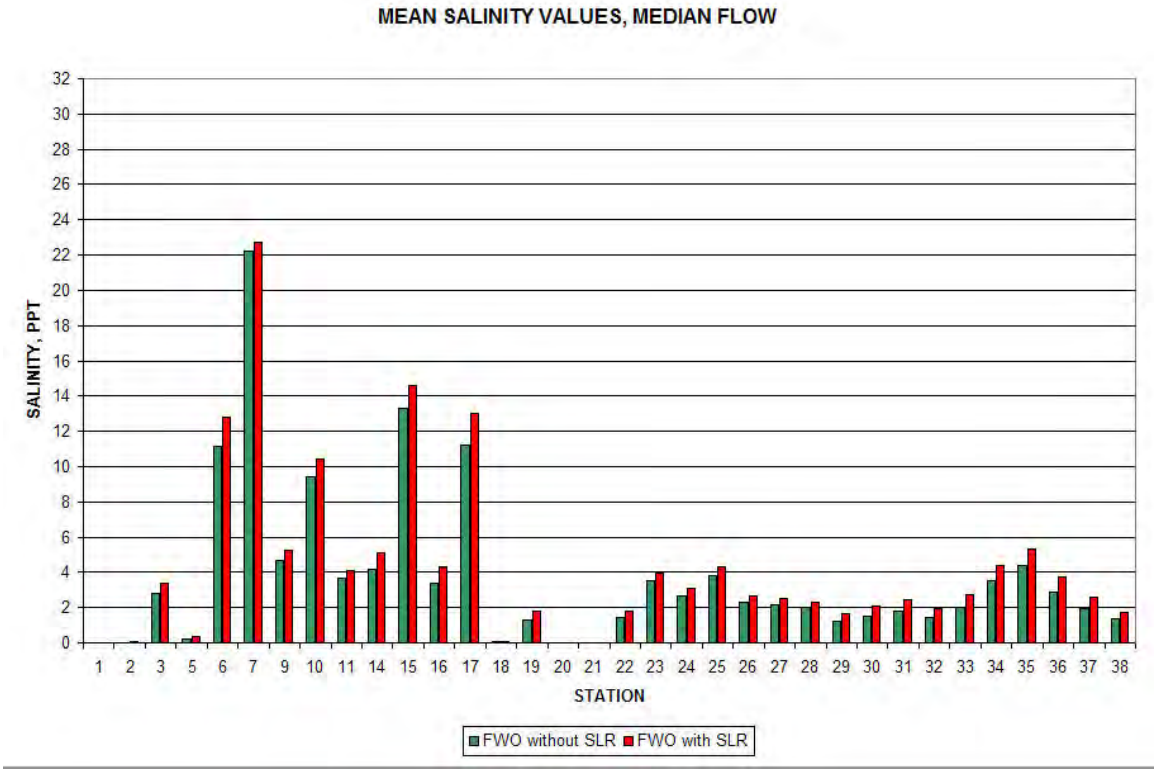

Base (with and without RSLR) and Plan Conditions

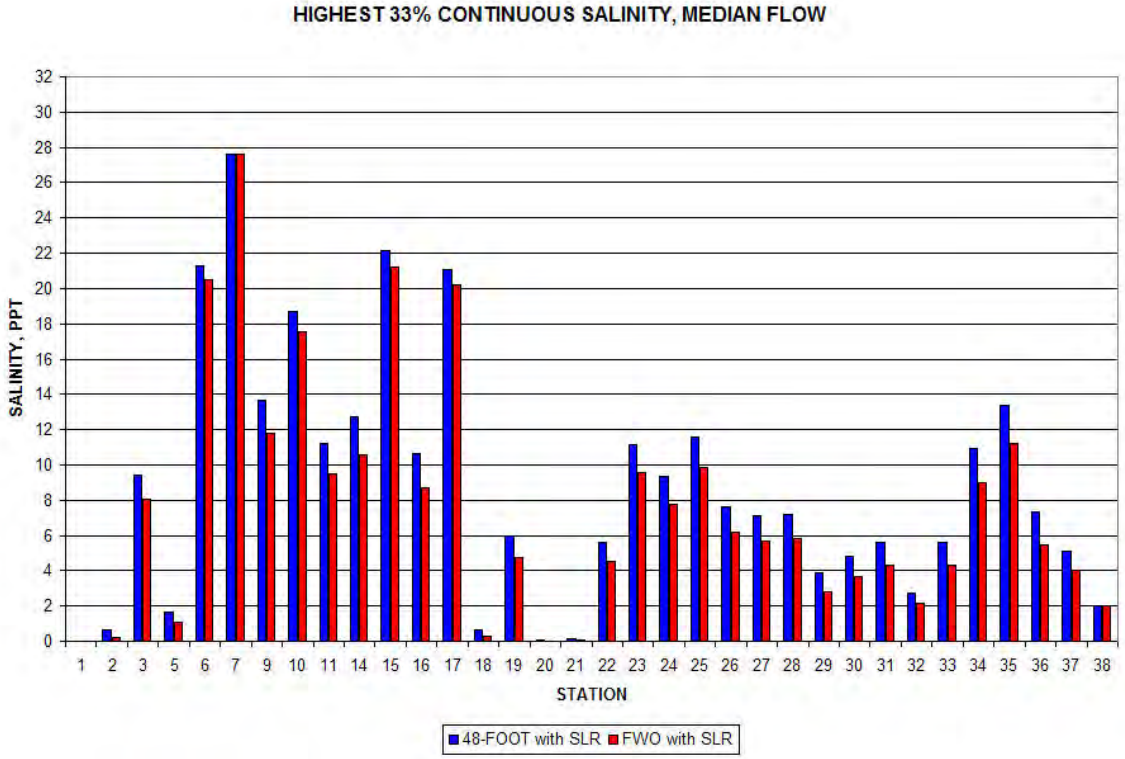

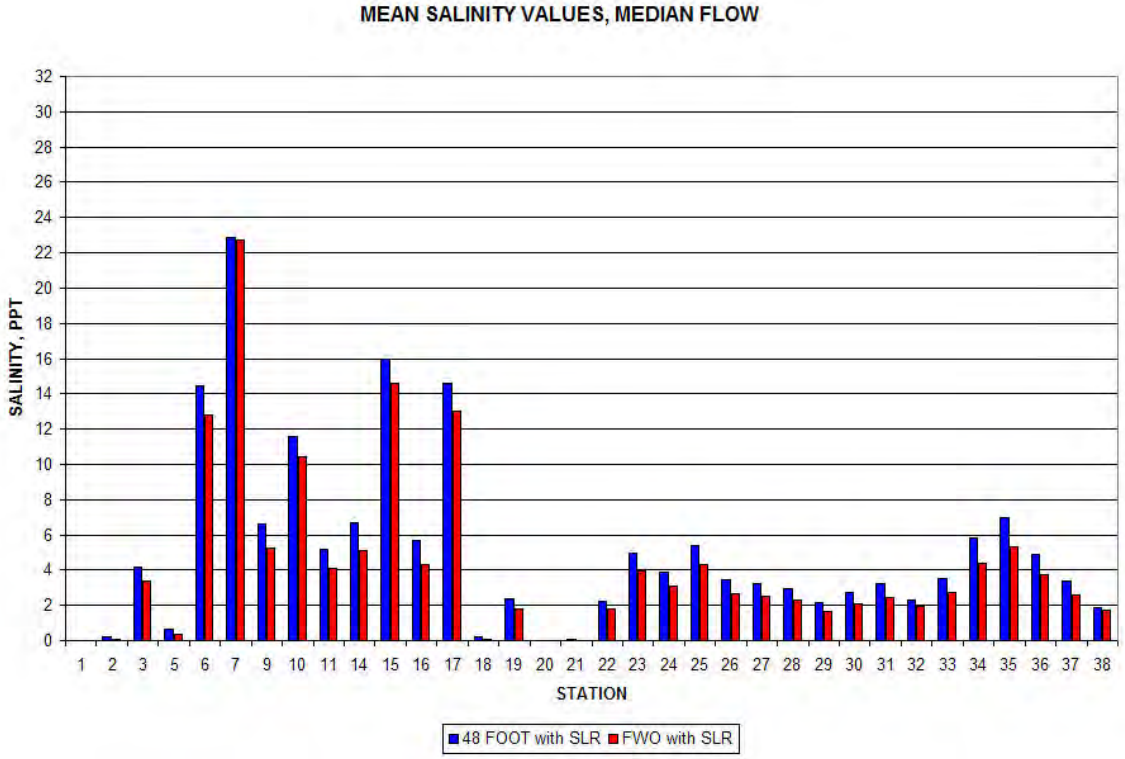

45 Foot Channel

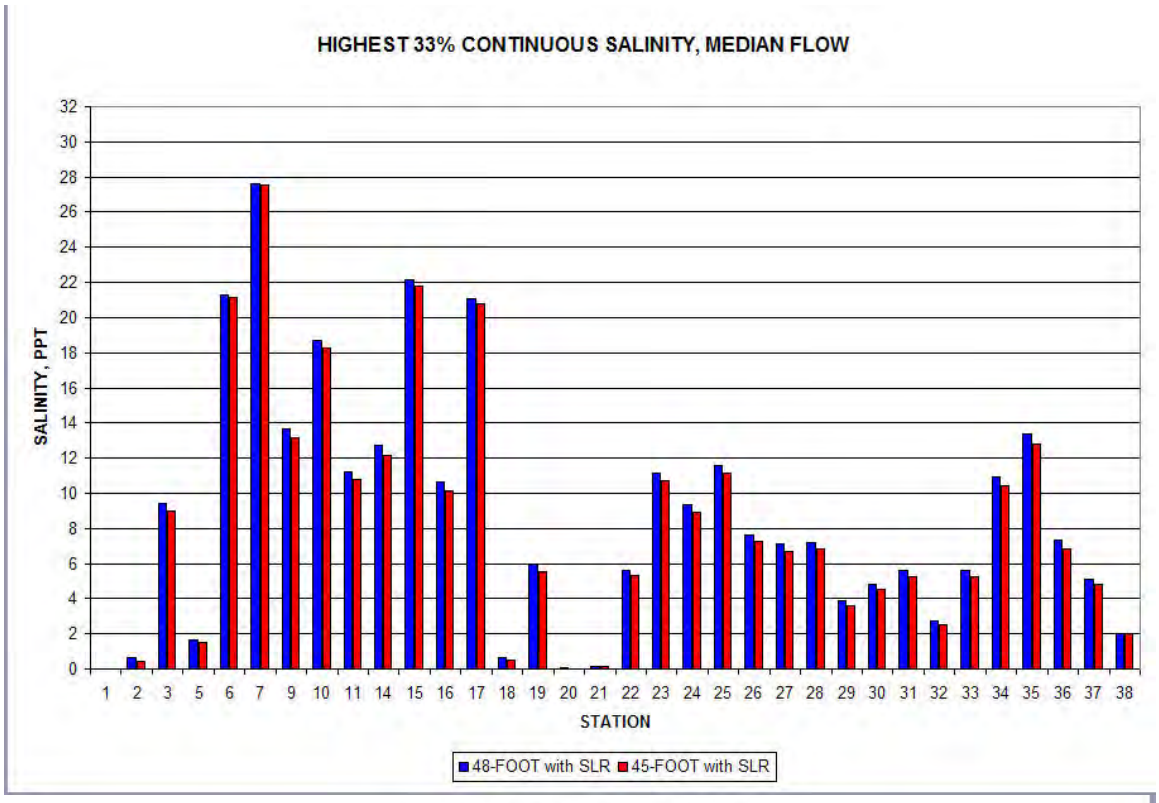

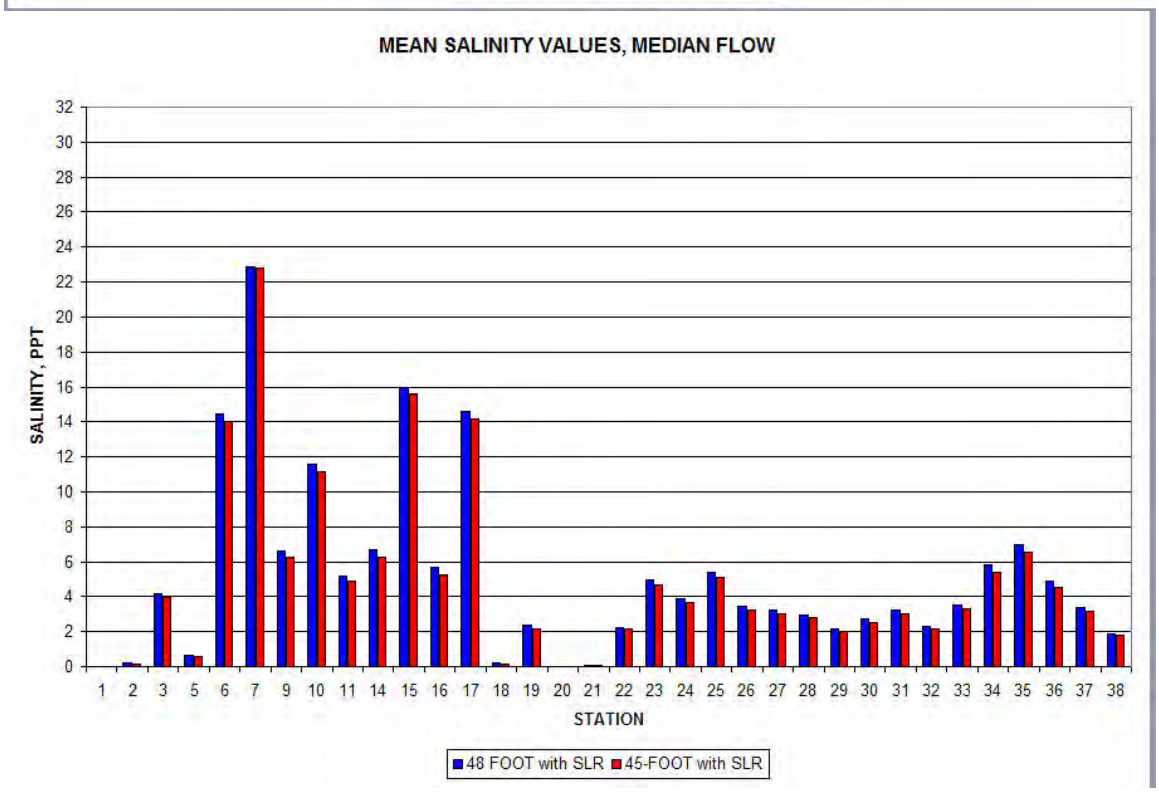

Mitigation Scenario

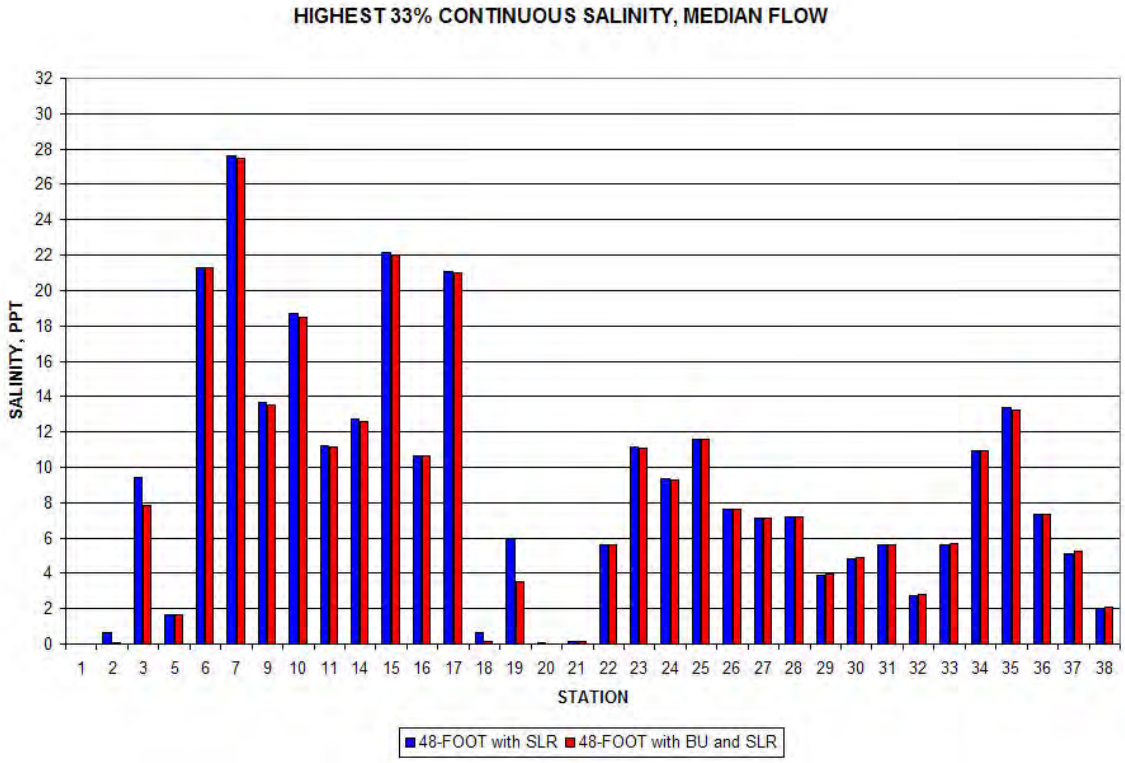

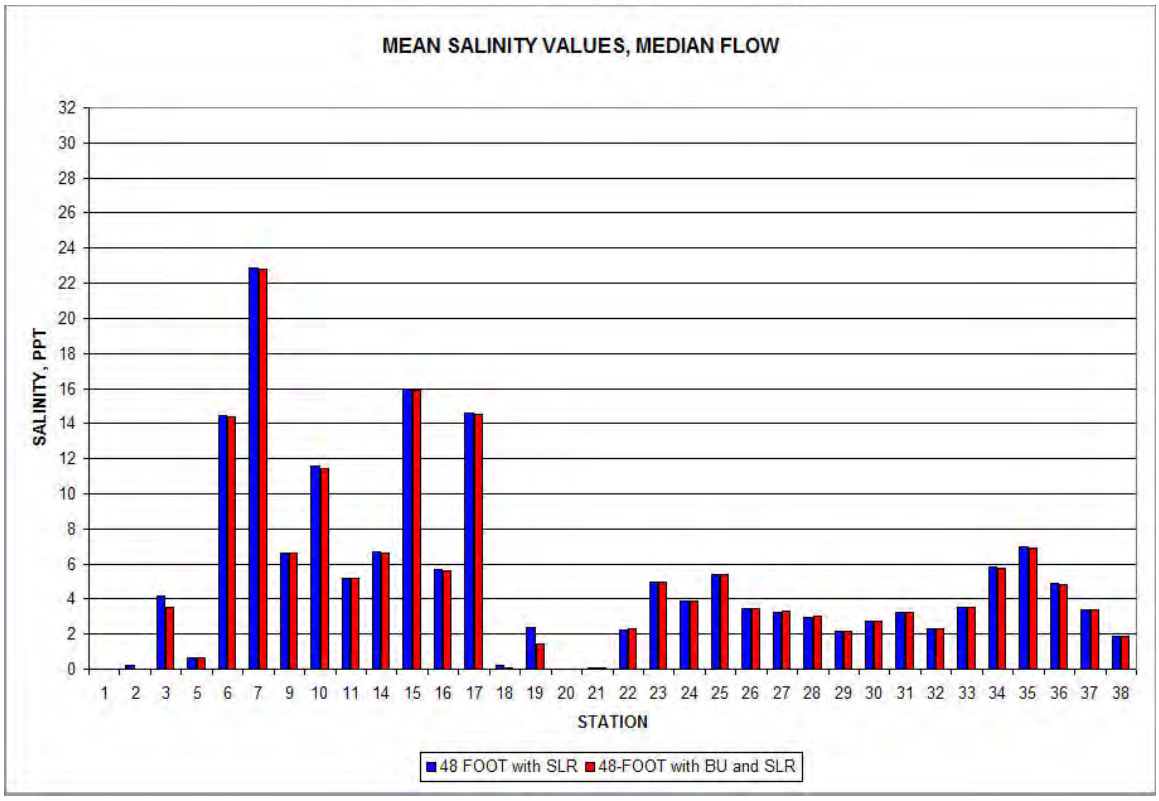

Appendix C

Dredging Analysis

For the original Sabine-Neches modeling work, the dredging analysis was performed according to the methods of Parchure (2005). Parchure employed several factors to determine the dredging potential for both existing channel conditions, and plan channel conditions. These factors are derived from model salinity and velocity data, general sediment and dredging data, and from experience. The analysis given for the original deepening and widening scenario is given below:

Dredging Requirements for the Original 48' Deepening and Widening Condition

Reach	Existing Dredging	Area Factor	Velocity Factor	Salinity Factor	Other Factors	Combined Factors	Estimated Dredging
NECHES RIVER CHANNEL (1)	1203310	1.06	1.05	1.05	1.2	1.36	1636502
SABINE-NECHES CANAL (2)	976551	1.06	1.05	1.1	1.15	1.36	1328109
PORT ARTHUR CANAL (3)	1694231	1.39	1.05	1.15	1.15	1.74	2947962
SABINE PASS CHANNEL (4)	768528	1.39	1.05	1.15	1.15	1.74	1337239
SABINE PASS JETTY CHANNEL (5)	223444	1.18	1.05	1	1.2	1.43	319524.9
SABINE PASS OUTER BAR (6)	1944987	1.17	1.93	1	1.2	2.3	4473470
SABINE BANK CHANNEL (7)	1249617	1.04	2	1	1.2	2.24	2799142
EXTENDED OUTER CHANNEL (8)	1249617	0.6	1	1	1	0.6	749770.2
TOTALS	8060668						15591719
% INCREASE	93.4%						

The new alternative to be analyzed is different that the old in 2 important respects:

- The influence of relative sea level rise must be considered
- The influence of channel widening must be omitted

A shear stress analysis was conducted to determine the potential impacts of relative sea level rise. it was determined that, although deepening the channel will slow the velocities, it will also enable a larger tidal prism to flush the estuary. The net result is that the changes in shear stress are small, and hence relative sea level rise is unlikely to have a significant impact on dredging requirements.

In order to remain consistent with the previous estimates of dredging requirements, it is necessary to repeat the same analysis, using the same methods as before with the omission of widening in the analysis. The values of the other factors are unchanged. The means to compute all of them are not available, and in any case it is unlikely that they would change significantly.

Repeating the analysis, with channel widening omitted, yields the following estimated dredging requirements for the 48’ channel condition.

Reach	Existing Dredging	Area Factor	Velocity Factor	Salinity Factor	Other Factors	Combined Factors	Estimated Dredging
NECHES RIVER CHANNEL (1)	1203310	1.06	1.05	1.05	1.2	1.36	1636502
SABINE-NECHES CANAL (2)	976551	1.06	1.05	1.1	1.15	1.36	1328109
PORT ARTHUR CANAL (3)	1694231	1.06	1.05	1.15	1.15	1.33	2248086
SABINE PASS CHANNEL (4)	768528	1.06	1.05	1.15	1.15	1.33	1019765
SABINE PASS JETTY CHANNEL (5)	223444	1.06	1.05	1	1.2	1.28	287030.9
SABINE PASS OUTER BAR (6)	1944987	1.06	1.93	1	1.2	2.08	4052887
SABINE BANK CHANNEL (7)	1249617	1.04	2	1	1.2	2.24	2799142
EXTENDED OUTER CHANNEL (8)	1249617	0.6	1	1	1	0.60	749770.2
TOTALS	8060668						14121292
% INCREASE	75.2%						